Determining Controlling Factors for Water Stratification in Flooded Underground Mines in an Analogue Model Mine

by

LESHEGO ESTHER MOLABA

Submitted in partial fulfilment of the requirements for the degree

MASTER OF APPLIED SCIENCES

in the

Department of Environmental, Water and Earth Sciences

FACULTY OF SCIENCE

TSHWANE UNIVERSITY OF TECHNOLOGY

Supervisor: Prof. Dr habil. Ch. Wolkersdorfer

Co-Supervisor: Dr M. Lupankwa

December 2022

Declaration

I hereby declare that the dissertation submitted for the degree MSc Applied Science: Geology, at Tshwane University of Technology, is my own original work and has not previously been submitted to any other institution of higher education. I further declare that all sources cited or quoted are indicated and acknowledged by means of a comprehensive list of references.

Parts of this thesis have been or will be published in either peer reviewed journals of the SCI or in conference proceedings.

Leshego Esther Molaba

Acknowledgements

I would like to express my sincere gratitude to my research supervisor Prof. Dr habil. Christian Wolkersdorfer, NRF mine water management, SARChI chair at the Tshwane University of Technology, Department of Environmental, Water and Earth Sciences, for affording me the opportunity to conduct this research work. His knowledge, support, enthusiasm, patience, constructive criticism and motivation carried me through to the end. Sincere gratitude to Dr Mlindelwa Lupankwa (co-supervisor), for his input and motivation.

Furthermore, warmest gratitude to the Tshwane University of Technology for affording me this opportunity and the National Research Foundation for providing funds for the study.

Heartfelt gratitude, to my colleagues, I can honestly say the laboratory would not have been as half as positive and inspiring without you in it. Thank you so much for your inspirational attitude and for always, providing a sense of sanity.

My family, “I am, because we are”.

Presentations and Publications

The work contained in this dissertation will be presented at conferences and published in journal articles as indicated.

Conference Output

- **Molaba, L.E.** & Wolkersdorfer, Ch. (2022): Investigating the Effects of Temperature on Density Stratification in a flooded Analogue Model Mine. Oral Presentation and Full Paper. Publication: Mine Water Association Congress; Christchurch, New Zealand

- Mugova, E., **Molaba, L.E**. & Wolkersdorfer, Ch. (2022): Predicting the Water Quality in Flooded Underground Mines–New Insights About the First Flush. Oral Presentation and Abstract Publication. In Bezuidenhout, J.: Navigating the Course. Water Institute of Southern Africa Conference, Sandton, South Africa (Sandton Convention Centre, 28–30 September 2022)

Journal Output

- **Molaba, L.E.** & Wolkersdorfer, Ch. (In preparation): Mine Flooding and Density Stratification in an Analogue Model Mine–Experimental Investigation towards *in situ* Mine Water Remediation. Paper Publication
- Mugova, E., **Molaba, L.E**. & Wolkersdorfer, Ch. (submitted): Understanding the Mechanisms and Implications of the First Flush Phenomenon in Mine Pools–Insights from Field Studies and Analogue Modelling. Paper Publication: peer reviewed articles

Extended Abstract

It is essential to understand the water chemistry in abandoned mine workings prior to pumping to alleviate bad quality of water pumped out of old flooded mines. Such practices can be effectively incorporated in water management and treatment plans to reduce related financial costs. It is imperative to understand *in situ* groundwater dynamics in order to implement remediation or treatment facilities.

The purpose of this study is to determine controlling factors for water stratification in flooded underground mines using a 4 × 6 m analogue model mine (Agricola Model Mine: AMM), constructed at Tshwane University of Technology's Arcadia campus. In this study, five experiments were conducted to provide the basis for discharge pumping to explain the first flush phenomenon and understand stratification build up and the mine flooding process. Experiments were conducted by flooding the AMM followed by injecting sodium fluorescein (Uranine) into the system.

Parameters such as temperature, flow rates and flow patterns were continuously monitored for all experiments. Furthermore, electrical conductivity was measured to monitor the stratification development at a) static conditions and b) stratification breakdown while increasing temperature using heating foils that represented a geothermal gradient, whereby heat was used as a proxy for energy. Stratification always occurs as a result of density differences; hence stratification was artificially initiated in the AMM using a layer of fresh tap water at the top and a 70 g L^{-1} NaCl solution at the bottom. This resulted in different electrical conductivities at varying levels of the shafts. Consequently, this resulted in a layered mine pool with higher mineralised water at the bottom and fresh tap water at the top. In the first two experiments, the AMM ran at steady state conditions. Thereafter, the temperature

was increased gradually from 19 to 44 °C in the following experiments, resulting in an increase in the average flow rate from 0.013 to 0.017 m s^{-1}. This further resulted in a stratification breakdown at different times proving that temperature is a paramount factor in stratification development and breakdown.

Mine water stratification is loosely defined as differentiation of water into horizontal strata of varying chemical and physical characteristics, whereby higher quality water usually dominates the upper zone of the mine and the lower zone contains lower quality water. Stratification might result due to the variation in turbidity as well as physical and chemical properties including temperature, viscosity, density and mineralisation (i.e. total dissolved solids [TDS]), respectively.

Water stratification in flooded underground mines is due to density variations controlled by temperature and the chemical composition of the mine water, the latter commonly identified as the sum parameter electrical conductivity or total dissolved solids. Therefore, density stratification might be used as an *in situ* remediation method where higher mineralised water stays in the deeper parts of the mine and only water with a lower mineralisation, thus better quality, is discharged. An increase in temperature has an effect on the stratification, thus increasing the flow velocity, causing convective flow and eventually resulting in stratification breakdown.

Contents

List of Figures

List of Tables

CHAPTER 1

1 Introduction

1.1 Background of the Study

Mining is the process of extracting metals and ore minerals of economic value from the crust of the Earth (Gabarrón *et al.*, 2019). It plays a critical role in the degradation of the environment, especially on ground and surface water quality (Northey *et al.*, 2019). Therefore, it is important to understand the environmental effects of mining activities, as this would play an essential role in drawing mine water management as well as mine closure plans. Legislation and guidelines have been adopted worldwide to address issues relating to current and future mine closures and post mining water management; regardless of this measure, old flooded underground mines remain an encumbrance to South Africa (Kgari *et al.*, 2016). Flooding of abandoned underground coal and gold mines plays a substantial role in discharging contaminated water into receiving water courses (Naicker *et al.*, 2003; Alhamed & Wohnlich, 2014; Sako *et al.*, 2016; Ali *et al.*, 2017).

The purpose of this study is to determine controlling factors for mine water stratification in flooded underground mines in an analogue (physical) model mine. Laboratory based experiments were performed using the Agricola Model Mine (AMM). The AMM is a physical representation of interconnected multiple mine shafts and drifts that may be isolated into single shafts by valves. This is a three-dimensional model depicting an existing structure. Mine water flooding models vary, therefore, understanding the release of potentially toxic elements from abandoned mines can be aided by modelling flows and contaminant distribution in flooded underground mines.

Hydrochemical stratification is a common occurrence that develops as a consequence of pumping cessation in abandoned flooded underground mine workings (Adams & Younger, 2001; Denimal *et al.*, 2005). Nuttall and Younger (2004) define stratification as layering of different water bodies with varying chemical composition. Wolkersdorfer (2008) further adds that mine water stratification as a function of the density.

Parameters including pH, temperature, Eh, electrical conductivity and the chemical composition of the concerned mine body water aids in the comprehension of stratification. Stratification stabilisation is not necessarily geothermal gradient dependent, however, density dependent, hence the mine water body can remain stratified over a long period, such in the case of the Oslavany coal mine in the Czech Republic that remained stable for a few years (Zeman *et al.*, 2008).

1.2 Motivation for the Study

Mine water in flooded underground mines may fractionate, resulting in stratification based on the physico-chemical properties of the water. Mugova and Wolkersdorfer (2019) emphasises that the upper part of the mine water is of better quality as compared to the water in the lower part. This phenomenon tends to mislead mine operators into thinking that the water quality is generally of a high quality when one takes water samples at the top layer and therefore concluding that the water in the overall system is of the same quality. It is therefore imperative to carry out more tests deeper into the system to gain knowledge on general characteristics of the water in the system before and after pumping.

Nuttall and Younger (2004) vaguely stated that stratification results from changes in the chemical structure, physical properties or turbidity in the water body; however, density difference is the principal controlling factor. Since then, no detailed work has been done to investigate these factors. Additionally, the geothermal gradient plays a role of a water heating mechanism in the lower sections of the mine. Convective mixing in the water then transfers this heat to the upper parts of the mine. This study will investigate the role of heating in the AMM model. To achieve the goal of delineating and predicting stratification development processes in abandoned flooded mines, an analogue mine model was constructed at Tshwane University of Technology. The development of the AMM sought to provide knowledge on stratification in South Africa. It will also serve as a basis to understanding stratification and it will be used to predict future stratification in the Witwatersrand gold mines and furthermore assist in planning better for future remediation procedures.

1.3 Problem Statement and Definitions

Stuart and Simpson (1961) seem to be the first to perform a study on stratification in flooded underground mines. Wolkersdorfer *et al.* (2016) point out that although studies on natural stratification in flooded underground mines date back as far as 1961, structured studies into the origin of stratification and whether it can be used as a passive remediation method in water treatment lacks literature. In certain instances, such as the mines in the German Freiberg/Saxony mining district, it was presumed that stratification can be used to exclude the release of contaminated mine water from abandoned shafts (Wolkersdorfer & Merkel, 2005). However no study has been conducted in this regard. The results obtained from this study will assist in the compilation of mine closure plans, environmental impact assessment reports and most importantly mine water management plans.

Wolkersdorfer *et al.* (2016) highlighted the lack of available data to prove whether all flooded underground mines are stratified and that the stratification is stable. Previous studies, such as those conducted by Wolkersdorfer *et al.* (2013) at Felsendome Rabenstein, Germany, and Wolkersdorfer and Hasche (2001) the German Straßberg mine highlight stratification complexities. Consequently, these studies raise the need for more work to be conducted to comprehend the parameters involved in flooded underground mine stratification. Physical and chemical properties of mine water play a critical role in stratification, however, optimum stabilisation and breakdown conditions are yet to be understood in these flooded underground mines.

1.4 Hypothesis

Water stratification in flooded underground mines is due to density differences of the fluid controlled by physical properties including but not limited to temperature, viscosity and pressure and can be used as an *in situ* remediation method.

Temperature variations play a role in mine water stratification breakdown.

1.5 Aim and Objectives

The aim of this research is to determine factors controlling water stratification in flooded underground mines using an analogue model mine to provide the basis for discharge pumping and understand stratification build up and the mine flooding process.

This aim is achieved through six objectives that this research study will adhere to for the optimal success of this research work. These objectives will be carried out in five experiments. However the fourth experiment will be divided into two sections, thus covering the fourth and fifth objectives. The fifth experiment will cover the last objective.

The first objective is to monitor the processes that transpire in the system at steady state condition in the Analogue Model Mine (AMM). Once the first objective is met, the second objective will be to monitor the temperature and velocity of the water injected with sodium fluorescein in the AMM at steady state conditions. The third objective will be to determine and monitor the processes that transpire in the system when the temperature is increased. The fourth objective is to monitor stabilisation of artificial density stratification in the AMM at steady state conditions. This will be followed by flushing the AMM with fresh tap water still at steady state conditions. The sixth objective is to monitor optimal breakdown conditions of density stratification in the AMM with an introduction of a heating system acting as the geothermal gradient.

CHAPTER 2

2 Literature Review

2.1 Introduction

This section comprises of the literature carried out on stratification in the past, mainly in flooded underground mines. Most of this work was carried out in Europe or northern America; there is no evidence in past literature showcasing work carried out in South Africa or Africa at large.

Ground water flow modelling in underground mines is difficult to simulate given the intricacy of the flow processes due to the variation in mine voids present in the system. Therefore, porous aquifers are easier to model, taking account the Darcy's laminar flow law (Wolkersdorfer, 2008; González-Quirós & Fernández-Álvarez, 2019). Flow models in flooded underground mines are critical tools in understanding and solving aspects that cannot be completely measured and observed at a given time. Models may aid in the prediction and control of the result to be expected (Diersch, 2013; Brown & Trott, 2014). It is therefore imperative that a numerical or analogue model is performed prior to the commencement of a hydrological study (Bredehoeft & Konikow, 2012).

A conceptual model serves as a framework to understanding and structuring of an analogue and numerical models, the former serves as a foundation for the designing of a numerical model (Anderson *et al.*, 2015). Conceptual models entail the following; physiochemical, physical properties (porosity, geothermal gradient, conductivity and recharge) and other factors pertaining to the actual system to be modelled (Diersch, 2013; Andrés *et al.*, 2017).

2.2 Water Stratification

2.2.1 Definition

Water stratification or layering occurs when water is differentiated into horizontal strata of varying chemical and physical characteristics (Nuttall & Younger, 2004; Rapantová *et al.*, 2013). In stratified mine systems, better quality water dominates the upper zone of the mine, whilst the lower zone contains lower quality water (Mugova & Wolkersdorfer, 2019). Stratification of mine water might result from the variation in turbidity, physical properties and chemical properties (e.g. sulfate, sodium concentration); however stratification occurs always as a result of density differences of the fluid (Henkel & Melchers, 2017). Due to the variation in density and temperature in a single stratum of water, stratification might be stable (long-lived) or unstable (short-lived). Gebhart *et al.* (1988) state that stratification stability is dependent on the difference in temperature and the density within an individual layer of water. Stratification is considered stable when high density differences and low temperature differences take effect in a stratified water (Wieber *et al.*, 2019). As water is a Newtonian fluid, pressure differences therefore are negligible. In stable stratification, the fluid density is directly proportional to the temperature and the electrical conductivity.

Water stratification is not only limited to flooded underground mines but occurs in lakes too. Stratified lakes consists of the following; the upper layer (epilimnion), the middle layer (thermocline or metalimnion) and lower most layer, hypolimnion (Boehrer & Schultze, 2008). This is however dependent on different seasons of the year, due to thermal influences. Furthermore, oceans too, have different water bodies thus implying that oceans show evidence of stratification (Ivey *et al.*, 2008).

The Richardson number (Ri) is used to create a distinction on different types of stratifications as it defines whether the water concerned will mix or not. Taylor (1931), with the aid of the perturbation theory, noted a critical Richardson number of 0.25 indicating that at lower numbers the stratified flow tends to be unstable (cited after Wolkersdorfer, 2008).

2.3 Factors Influencing Stratification Development, Stabilisation and Breakdown

2.3.1 Density Difference

High concentrations of different ions or molecules dissolved in mine water leads to elevated water density and hydrostatic pressure with an increase in depth across the system (Zeman *et al*., 2008). Chemical composition of water varies from mine to mine depending on the ore body extracted; coal mines commonly contain more sulfate with a low pH, whilst salt mines contain high chloride and sodium concentrations (Bozau *et al*., 2017).

Mineralisation efflorescent salts resulting from dissolving in mine water plays a paramount role in the chemistry of the water, by eventually producing different water bodies with different densities. The efflorescent salts will get washed down the shaft as water infiltrates from the top, thus resulting in a higher mineralised water body with higher electrical conductivities at the bottom and water with relatively good quality at the top (Mugova & Wolkersdorfer, 2022). Electrical conductivity is usually measured along a flooded column to delineate the different water bodies in a mine (Karakas *et al.*, 2003). Vertical temperature readings measured together with the conductivity, are usually employed in delineation of different water bodies that can be observed through temperature measurements (Wieber *et al.*, 2019; Mugova & Wolkersdorfer, 2022).

2.3.2 Hydrodynamics

Flooded mines comprise of shafts, inclines, adits, galleries and stopes, all known as mine voids. These mine voids are instrumental in the hydrodynamics of the enclosed fluid in the system (Wolkersdorfer, 2008). Darcy flow is the most prominent flow applied in hydrogeology and it describes the rate at which a fluid flows through a porous isotropic medium at a low velocity (Rubin, 1966; Dunne, 1990).

Flows in porous media that are not applicable to pipe flow are described by Darcy and Forchheimer. The flow occurs through open voids in flooded underground mines and are categorised as (1) laminar or turbulent Poiseuille flow, (2) laminar or turbulent convection flow, (3) almost no flow except for Brownian molecular forces or diffusion (after Wolkersdorfer, 2008). Generally, in porous media, turbulent flow is initiated at a Reynolds number exceeding 10 (Nuttall & Younger, 2004) but not greater than 100 (Wolkersdorfer, 2008). A precise critical Reynolds number cannot be stated with certainty given that the critical Reynolds number is dependent on the fluid in the system and the nature of the flow (Snyder & Castro, 2002). The transition from laminar flow to turbulent flow is observed at a critical Reynolds number of 2100 in smooth pipes, however it is different in porous media (Ryan & Johnson, 1959). The Reynolds number is expressed by equation 2.1 (Reynolds, 1883)

$$\mathrm{Re} = \frac{L \times V \times \rho}{\mu} \tag{2.1}$$

Table 2.1: Equation terms used in this section and their International System units

Symbol	**Description**	**SI unit**
L	Length	m
V	kinematic viscosity	$m^2\ s^{-1}$
ρ	Fluid density	$kg\ m^{-3}$
μ	Dynamic viscosity	$Ns\ m^{-2}$
g	Gravitational acceleration	$m\ s^{-2}$
β	Thermal Expansion coefficient	K^{-1}
ΔT	Temperature difference	K
C_p	Specific heat capacity	$kJ\ kg^{-1}\ K^{-1}$
k	Thermal diffusivity	–
Δh	Head difference between the shafts	m
h_1	Height of water column in shaft 1	m

Systems in longitudinal enclosures usually have free conductive flow, where the Rayleigh number (Ra) is larger than the critical Rayleigh number that is between 658 for two free surfaces and 1708 for no free surface (after Wolkersdorfer, 2008), furthermore, the transition from laminar to turbulent and from turbulent to laminar can be expressed by the Rayleigh number in the following equation:

$$\mathrm{Ra} = \frac{L^3 \times \rho^2 \times g \times \beta \times \Delta \mathrm{T} \times \mathrm{C_p}}{\mu \times k} \qquad 2.2$$

A flow in a system can be categorised as free flow or forced flow, where the former also known as natural flow is controlled by buoyancy. The difference in densities in a system, where fluid is the only driving force, defines the formation of free flow in a system. Forced flow develops when external forces cause the fluid to flow (after

Wolkersdorfer, 2008). Practically, free flow and forced flow may occur concurrently, resulting in mixed convective flow. Under convective flow conditions the Reynolds number is replaced by the Grashof number (Gr) (Sanders & Holman, 1972; Gebhart *et al.*, 1988).

$$\mathrm{Gr} = \frac{L^3 \times \rho^2 \times \beta \times \Delta \mathrm{T} \times g}{\mu^2} \qquad 2.3$$

The above mentioned flows may coexist over short distances or time. Channel flow within the voids, fracture and porous flow through the rock matrix occurs as soon as all the voids are filled with water (Norton & Knapp, 1977; Wolkersdorfer, 1996).

The rock–water interaction surface is paramount in ascertaining the chemical composition of the mine water, however these surfaces offer little to no hindrance to the flow within the voids in underground flooded mines (Jäger *et al.*, 1990). Forced flow occurs in interconnected mine shafts as a result of variation in water levels or pumping. These variations in water levels further perpetuate different densities in different shafts. When water levels in shafts finally equilibrate, water densities also equilibrate in all shafts. The variation in the water level of two interconnected shafts can be calculated using the water level h_1 and h_2 and the corresponding fluid densities using equation 12.4 (cited after Wolkersdorfer, 2008):

$$\Delta h = \rho_1 \times h_1 \times \frac{\left(1 - \frac{\rho_2}{\rho_1}\right)}{\rho_2} \qquad 2.4$$

Flow measurement is another method used to gain knowledge about the flow dynamics in flooded mines, resulting in the occurrence of stratified water bodies (v. Hünefeld-Mugova & Wolkersdorfer, 2018).

2.3.3 Temperature

The geothermal gradient plays a crucial role in the heating of mine water, further influencing the movement of water from the bottom to the shallower parts in the shafts (Mugova & Wolkersdorfer, 2019). Past literature states that the first systematic temperature profile measurements were conducted by Uerpmann (1980) at one meter intervals over a 300 m shaft column. He noticed the formation of convectional cells in the different water layers. Furthermore, with the aid of tracers, Uerpmann (1980) described the mixing of the different water bodies at the transitioning layer and the variation in flow velocities between the transitional layer and the convection zones. The same transitional layer referred to as a boundary layer by Uerpmann (1980) and Kories *et al.* (2004) is reported by Wolkersdorfer (2008) who calls it an intermediate layer.

When the mine water is heated, either from the galleries or shafts, mass and heat transfer occurs, thus resulting in the development of buoyancy driven convection cells in the system (Bau & Torrance, 1981a, 1981b; Bao *et al.*, 2018). Consequently, the system then acts as a thermosiphon (Wolkersdorfer, 1996). When water is heated from the sump, it moves up through the walls and back down in the middle of the shaft, thus forming both bigger convection cells and smaller ones, known as bales (Kories *et al.*, 2004; Mugova & Wolkersdorfer, 2022). Gradual heat transfer between different mine water bodies over time leads to a complete mixing of the water, thus resulting in stratification breakdown. However, if the energy is not enough, the stratification remains stable owing to the formed intermediate layer (Wolkersdorfer, 1996; Mugova & Wolkersdorfer, 2022).

2.3.4 Pumping

Water samples collected in the upper sections of the flooded mine are often misleading, giving a wrong impression of the overall chemistry of the water in the mine. A green light is given after running tests on the samples; pumps are then connected to pump out the water into discharge outlets. But bad quality water is eventually discharged. It is therefore important to understand all the dynamics pertaining to the water in the mine voids. As previously stated, usually, better quality water is found at the top of the column and poorer quality water at the bottom. It was shown that pumping of mine water may result in stratification breakdown (Elliot & Younger, 2014), which was the case at Frances Colliery in Scotland (Nuttall & Younger, 2004). It must be noted that this stratification breakdown is dependent on the depth of the pumps as pumping initiates turbulent flow in the system (Adams & Younger, 2001; Nuttall *et al.*, 2002).

2.4 Examples of known Cases of Density Stratification in the World

2.4.1 Introduction

There are numerous mine water stratification cases known worldwide. The occurrence of stratification is not only limited to flooded mines dealing with a specific type of ore. However, this can occur in many different mines mining different ores. It is this suite of flooded mines that has prompted a review of four mining scenarios dealing with different ores. These four scenarios cement the view that the AMM can be used as the basis to understanding mine flooding as well as stratification development and breakdown for mines dealing with different ore bodies. The four mining scenarios to be reviewed include those producing uranium, fluorspar, coal and salt. Extensive studies carried out in the German Niederschlema/Alberoda uranium and Straßberg fluorspar mine serve as two perfect examples of stratification cases for review. Additionally, the Frances colliery in Scotland serves as the third example in this review. General salt mines in Germany will be used as the fourth review case. The artificial density stratification experiments carried out in the AMM entails stratification development using a NaCl solution; hence salt mines were accounted for in this study. Therefore, it was pivotal to conduct a research on salt mines to serve as a basis to understanding the fundamentals of optimal conditions for stratification development and breakdown.

2.4.2 Niederschlema/Alberoda

The abandoned, German Niederschlema/Alberoda mine is an example of a flooded underground mine located close to Aue in the Erzgebirge (Ore Mountains). At this mine, uranium ore was extracted. However, with cessation of mining activities, the mine has seen flooding since 1991, with about 36 million m^3 of open mine voids (Wolkersdorfer, 1996).

The Niederschlema/Alberoda mine produced about 81 000 t of uranium between 1945 and 1991 (Wolkersdorfer, 2008). The uranium originates from uraninite, UO_2, vein deposits in the Aue granite, formed from contact and regional metamorphism from Devonian and Ordovician rocks (Meinrath *et al.*, 2003; Forster & Potsdam, 2005).

Wolkersdorfer (1996) conducted a study in Niederschlema/Alberoda, where a 500 m dipper was used in various temperature measurements ranging between 0.01 and 10 m intervals. These intervals were informed by the degree of stratification obtained from previous measurements. Additionally, electronic probes took readings at known depths to investigate the change in physico-chemical parameters and the cause of the rise in water level. Wolkersdorfer (2001) reported a multi tracer test conducted in the mine in 1995, where it was established that the water inside the mine was well mixed due to convective flow within the interconnected parts of the mine. *Lycopodium clavatum* spores of four different colours were injected at different but pre-defined depths in four shafts (Wolkersdorfer, 2008).

Density stratification was observed during the mine flooding, where higher temperatures were recorded in the deeper sections of the mine and lower temperatures at the shallow parts of the mine. Temperature and electrical conductivity decreased at lower water depths. According to Wolkersdorfer (2008), the situation remained stable up to the year 2004.

Shaft no 371 (Figure 2.1), one of the measuring locations, has three main levels connected to it at the time of measurement, namely: level 540 m, 990 m and 1080 m. At level 540, the temperature was constant, where else the temperature below the 540 m level increased steadily, with the drop in elevation. The whole shaft exhibited diffusive flow because in a convective flow scenario the temperature and electrical conductivities would be constant.

Wolkersdorfer (2008) further noted that stratification in the system broke down when the temperature difference was below the threshold value of about 5–6 K between the lower and upper stratification layers. The author also concluded that the fluctuation in temperature was indicative of turbulent conditions in the shaft.

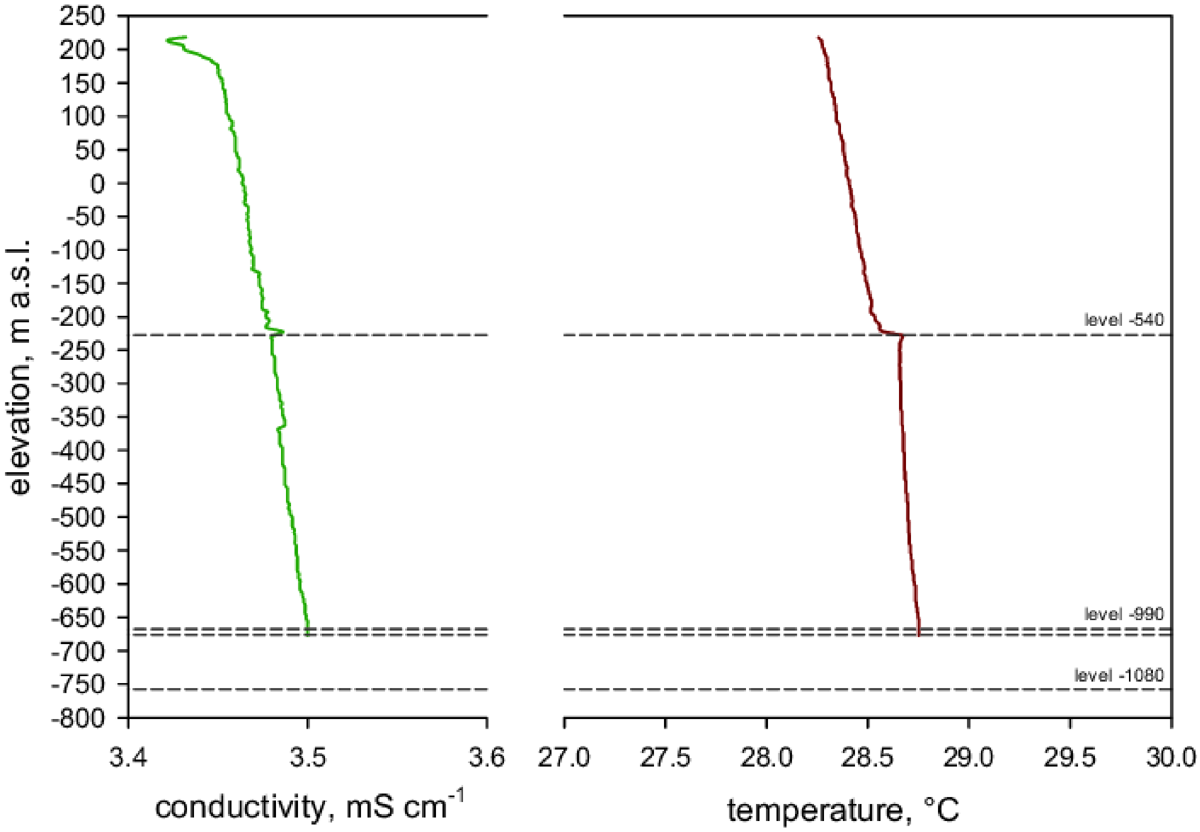

Figure 2.1: Electrical conductivity and temperature in shaft no 371, Niederschlema/Alberoda (from Wolkersdorfer, 2008)

2.4.3 Frances Colliery, Scotland

Frances colliery in Scotland is an abandoned underground coal mine, with evidence of stratified water bodies which resulted from the termination of the pumping system in 1995 (Adams & Younger, 2001; Nuttall & Younger, 2004; Elliot & Younger, 2007), leading to the flooding of the mine. Frances is a complex underground system interconnected to the Randolph and Michael mines, the two further connecting to the Belgonie and Wellesley mines (Figure 2.2a) (Nuttall & Younger, 2004).

According Nuttall and Younger (2004) and Elliot and Younger (2007), a pumping test was initiated to identify optimum pumping conditions for the given mine water levels. This pumping subsequently introduced disruption to the mine water stratification.

Younger (2000a) indicates the high sulfur content in the coal seam is indicative of acid mine drainage production, resulting from clastic marine sedimentary beds containing elevated amounts of pyrite.

Frances test pumping commenced on 7th August 2000 ending on 24th September 2000 leading to the dewatering of the mine to a water level of 3 m. According to Elliot and Younger (2007) and Nuttall and Younger (2004) and the water body in the mine had a distinct water stratification, where the top layer had good water quality which depreciated with an increase in depth. Parameters of interest used in measuring water quality at this mine were electrical conductivity, pH, Eh, temperature, alkalinity, anions and cations (Table 2.3). Through the presence of voids and an increase in the pumping rate, turbulent flow in the system could not be avoided (Nuttall *et al.*, 2002), thus resulting in vigorous water circulation leading to the mixing of the mine water. The highest Reynolds number of Re = 350 was recorded at the Lower Sandwell, followed by Lethemwell and Pit Bottom at Re = 242 and lastly the Lower Dysart at Re = 190 (Figure 2.2b). A high Reynolds number indicates that turbulent flow dominates in the system over laminar flow (Table 2.2).

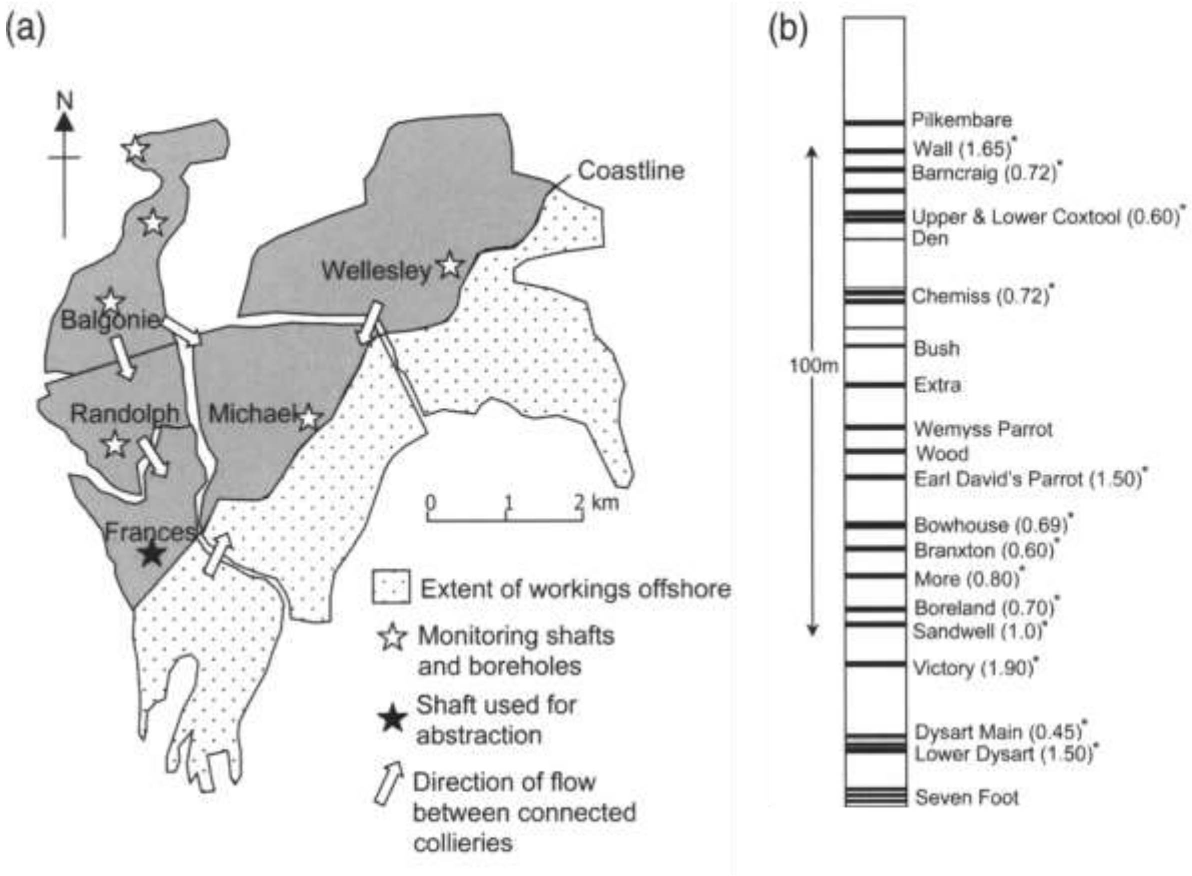

Figure 2.2: a) Map showing the location of the abandoned Frances colliery in relation to adjacent collieries b) a generalised stratigraphic column of the Frances colliery showing coal seams with their sulfur content. *Denotes the % sulfur content of the seam, whereby values greater than 0.5 represent a greater acid generating potential (from Sherwood, 1997)

Table 2.2: Level and depth positions below Ordanance Datum (bOD) and their respective Reynolds numbers (from Nuttall & Younger, 2004)

Name	**Depth (m bOD)**	**Reynolds number**	**Level**
Lower Sandwell	115.79	350	1
Dysart Main	Closed	Not applicable	Not applicable
Lower Dysart	188.94	190	2
Lethemwell	270.72	242	2
Pit Bottom	282.18	242	1

Table 2.3: Fe, pH and electrical conductivity measured at Frances colliery (from Nuttall & Younger, 2004)

Parameters	**Top layer**	**Deepest layer**
Fe	≤ 10 mg L^{-1}	≥ 599 mg L^{-1}
pH	7	5
Electrical conductivity	3000 µS cm^{-1}	20.300 µS cm^{-1}

Table 2.4: Variables measured in the Frances shaft at 70 m depth at specific day interval until day 48. The three days shown on the table were extracted to highlight ionic changes from the first through to the final day of pumping (from Nuttall & Younger, 2004)

Variable	**Pre Pumping**	**Day 1**	**Day 9**	**Day 48**
pH	6.30	5.22	4.99	4.80
Alkalinity (mg L^{-1} $CaCO_3$)	437.00	75.00	0.00	0.00
Conductivity (µS cm^{-1})	5557.00	25.55	27.61	26.50
Total Fe	6.50	406.70	546.80	596.60
Al (mg L^{-1})	Below detection	14.65	22.58	51.60
Mn (mg L^{-1})	3.41	24.96	26.75	24.90
SO_4 (mg L^{-1})	4975	4223	6755	6254
Cl (mg L^{-1})	14.93	13.06	18.32	18.28
Ca (mg L^{-1})	487.50	836.50	770.00	903.50
Na (mg L^{-1})	955.50	4316.00	51225.00	4935.50
K (mg L^{-1})	46.50	98.00	108.00	94.00
Mg (mg L^{-1})	182.00	896.50	873.50	930.00

Stratification at Frances colliery disintegrated due to the introduction of pumps leading to a decrease in pH and a general increase the main ions (Table 2.4). Introduction of pumps promoted circulation of water in the column resulting in turbulent flow thus concluding that stratification existed in the mine and disintegrated due to pumping. In the case of the Frances colliery test pumping, the effect of temperature on stratification is not well documented in the existing literature (Nuttall *et al.*, 2002; Nuttall & Younger, 2004; Elliot & Younger, 2007).

2.4.4 Straßberg Fluorspar Mine, Germany

Mining activities at the Straßberg fluorspar mine in Germany ceased in 1991, and the continuous pumping ceased as well resulting in flooding of the Straßerg Ü539 and Glasenbach shafts (Wolkersdorfer & Hasche, 2001). Over the life of mine, the Straßberg fluorspar mine was, among others, operated through shaft no 539 and the flour shaft all of which were gradually stratified (Wolkersdorfer, 2008). However the layering in the latter shafts was not as defined as in shaft no 539. Knowledge on the hydrodynamics of shafts is pivotal in forecasting future mine water variables for water remediation processing plants, hence tracer tests were performed at different shafts (Table 2.5).

Table 2.5: Points of different tracer injection, in six shafts depths and the quantities used (Wolkersdorfer, 2001)

Injection points	**Depth, m**	**Tracer type**	**Quantity**
No 539 shaft	92	microspheres blue	40 mL
No 530 shaft	20	microspheres orange	40 mL
Fluor shaft	247	microspheres red	40 mL
Fluor shaft	247	spores, malachite green	264.9 g
Fluor shaft	247	spores, saffron coloured	279.5 g
Glasebach shaft	4	microspheres green	40 mL

According to Wolkersdorfer (2001), between 2.5 days and 6 days post the lycopodium spore and microsphere tracer injection, residual tracer was detected at fluor shaft with a 6 % recovery rate. Peaks decreased 2 days post the injection, with the velocity ranging from 0.1 – 0.2 m min^{-1}. The tracer at Glasebach shaft peaked 10.5 days post the injection at a distance of 3.180 m and at 238 m, thus measuring 0.2 – 1.2 m min^{-1} in velocity.

Microspheres injected at shaft no 530 were discovered 13 days later at Glasebach shaft with a velocity of 0.3 m min^{-1} and a distance of 4.798 m. Others were, however, undetected therefore resulting in an inconclusive conclusion due to the shaft’s morphology.

Thus it is concluded that artificial tracer tests are useful in unravelling the hydrodynamics of flooded mines to predict and understand future scenarios. However, suitable tracers should be used given the specifications required (Wolkersdorfer & Hasche, 2001; Wolkersdorfer, 2008).

2.4.5 Salt Mines

Thermal stratification and chemical attributes are pivotal in understanding stratification development in salt mines. However, this concept is slightly different from coal and metal mines due to a higher mine water mineralisation and higher density differences (Wolkersdorfer, 2008). Salt mines play an important aspect in studying stratification. Furthermore, the results obtained from previous studies and the current study can be used as a background to understand stratification in both metal and coal mines as well.

According to Wolkersdorfer (2008), radioactive waste material from Germany's medicinal and nuclear programme was disposed in disused salt mines. Due to the country's strict policy on radioactive waste disposal, the need to understand the geological setup of waste storage sites became necessary. Thus, thorough studies into salt mines were conducted. Regardless of these intensive studies, there are gaps in literature and the little that exists is partly documented by Wolkersdorfer (2008). The author mentions that the first controlled and monitored mine flooding was the Hope salt mine located north of Hannover in Germany, where tracer tests, water investigations and monitoring programmes were conducted. Mining operations started in 1907 at the *Adolfsglück* shaft at a depth of 521.2 m and later in 1909, the Hope shaft at 628.5 m was commissioned. Rock salt, kieserite and anhydrite were amongst the salt varieties found in the salt dome, measuring 6 km in diameter and 4 km in depth.

Flooding studies at the Hope Mine began on the 12th March in 1994, after operations ceased in January 1984. During this study, the Hope mine shafts were filled with brine resulting from salt waste rock seepage brine. To observe flooding related processes unfold, 16 probes were installed to take measurements inside the mine. The mine was flooded with the Empelde NaCl brine solution with a volume of 1.6×10^6 m^3 and a density of 1.200 g cm^{-3}. Samples were constantly taken in the mine to monitor the brine solution development whilst the mine was being flooded.

According to Wolkersdorfer (2008), the main objective of the Hope mine flooding study was to explore heat and mass transport associated with flooded shafts and mine workings excluding backfilled galleries and the functioning of a newly constructed underground salt dam. It was therefore deduced from the Hope salt mine flooding experiment that three layers were observed, the top most stratum contained low concentrations of the originally injected brine or clean water, the intermediate stratum was saturated with NaCl solution at a density of 1.20 g cm^{-3} and the bottom most stratum had the highest NaCl concentration but the least $MgCl_2$ concentration, with the former at a density between 1.29 –1.30 g cm^{-3}. It was also concluded that the geothermal gradient and the chemical constituent of the surrounding rock are pivotal in the stratification of the mine (Wolkersdorfer, 2008). It was concluded that the mine setting with regards to its geometry has an effect too on the water stratification in the mine. The author further details how the homogenous strata showed evidence of convective flow whilst flow was absent amongst layers with temperature and density gradients. In that very same study, Wolkersdorfer (2008) adds that convective cells were formed adjacent to the two layers without any flow and the layer with convective flow.

As mentioned before, 14 measurements were taken at the Hope salt mine during the flooding process. Their measurements varied slightly, however, they all showed evidence of stratification. Shaft *Adolfsglück* was backfilled, therefore, it cannot be compared to the other shafts. Prior to the backfill, the stratification was more prominent, and post the backfill the mine had two distinct water bodies.

Peißen shaft with a depth of 477 m and a 5 m diameter was commissioned in 1900 and was flooded in a controlled manner from 1972 to 1974. It is located close to Bernburg in the Peißen syncline. Mining in this area began on the 31st January 1852, with its first potassium mine having been the Manteuffel shaft (Wolkersdorfer, 2008) in the Zechstein salt formation like all the mines in this area. Shaft measurements of the flooded shafts were taken to measure the following: density logs, chemical and temperature variables. These variables were further modelled using the KASOMO code.

The Braunschweig shaft near Beinrode, Desdemona shaft in Göttingen and lastly the Deutschland shaft located at the Ronnenberg salt mine were also investigated. However, there is still a gap in literature, therefore more work still needs to be conducted in relation to this study (Wolkersdorfer, 2008).

2.5 The use of Tracers in Hydrogeology

Tracer tests in flooded underground mines assist in identifying flow patterns and calculate the mine water's velocity over a greater distance (Wolkersdorfer, 2008). Divine and McDonnell (2005) define a tracer as an artificial substance injected purposefully into a system in low concentrations, to investigate and measure variables of concern in the system. Tracer tests aid in unravelling of velocity and flow direction of ground water. Additionally, tracer tests play a role in determining contaminants present, to predict future processes and other intricate hydrological processes (Davis *et al.*, 1980; Mugova & Wolkersdorfer, 2019). They are also utilised in water remediation schemes to comprehend the constituents of the water pumped out, to track contamination points in old flooded underground mines for pumping purposes (Wolkersdorfer, 2008; Jenk *et al.*, 2014). There are various types of tracers used differently according to their properties and optimum environment suited for each, for instance environmental and artificial tracers (Leibundgut *et al.*, 2009).

Sulforhodamine B and Uranine are referred to as organic dyes and are suitable for the experiments performed in this thesis. They have high fluorescence intensity (Table 2.6) and high solubility with minimal toxicity.

Table 2.6: Fluorescence intensity, detection limit and excitation/emission wavelength for Uranine and Sulforhodamine B (after Leibundgut *et al.*, 2009)

Dye	**Relative fluorescence intensity**	**Detection limit (mg m^{-3})**	**Excitation/Emission (nm)**
Uranine	100	0.001	491/516
Sulforhodamine B	7	0.03	561/586

2.6 General Reactor Models and First Flush

A mine can be considered as a reactor, where different reactions occur in the mine water body. For instance, efflorescent salts on the mine walls react with the infiltrated water and mine water. These salts and the different water qualities react within the system. However, when water percolates through the mine workings and gets flushed out, the parameters of the water body change with time. The concentration, electrical conductivity (EC) or other parameters will get affected and with time the concentrations/EC values will drop close to exponentially, thus the discharging water quality improves in the long run (Younger, 1997; Mack & Skousen, 2008; Cheong *et al.*, 2012). Firstly, it has to be estimated how long the discharge of usually poor mine water will last after the initial discharge. This initial water is usually characterized by high iron or sulfate concentrations, low pH values or an elevated mineralisation. Usually, discharged mine water reaches maximum concentrations of the potential contaminants which then gradually decrease – in the best case to natural background concentration (Younger, 2000b; Gzyl & Banks, 2007). This phenomenon is termed the “first flush” (Younger, 2000b; Merritt & Power, 2022). As such, the current research refers to a mine as a reactor. Various factors are responsible for the duration t_f of the first flush. These include the reduction of acidity, which is controlled by solution processes and buffering. In addition, the weathering rate of the acidic (secondary) efflorescent minerals, the volume and conductivity of the mine pools, hydraulic connections and the groundwater recharge rate are decisive factors (Younger, 2002).

A paper by the SARChI's research group is underway, describing the mine as a general reactor model explaining the first flush phenomenon. This section will provide different chemical processes, phases and different reactor models that can occur in various scenarios. It will further incorporate the first flush phenomenon in these reactions.

A typical chemical process entails breaking down or combining of raw material into a final product, basically producing an output from an input, taking into consideration all the contacts and kinetics involved in the process (Levenspiel, 1998). Further, chemical reactions are either a representation of a homogenous or heterogeneous system, the latter occurring in one phase whilst the former occurs in two or more phases. Constituents such as pressure, temperature and chemical composition are pivotal in accelerating a chemical reaction in a homogenous system whilst the reaction is intricate in a heterogeneous system where two phases are involved. Therefore, mass and heat transfer are pivotal constituents in defining the rate of a heterogeneous reaction (Levenspiel, 1998; Petkovska *et al.*, 2018), where the reaction rate is controlled by the energy it produces and the composition of the material concerned (Levenspiel, 1998).

Batch, plug flow and mixed flow reactors are ideal reactor types in which the composition is homogenous but changes over time. In these reactor types, the fluid moves through the reactor without initialising any mixing, whereby the fluid injected and ejected flows without mixing and in the mixed flow reactor, the fluid mixes homogenously, at the exit point aided by a stirrer, at the bottom (Zaldívar *et al.*, 2003; Balsamo & Montagnaro, 2018).

Chemical reaction rates may use any measure, corresponding to concentrations and pressure, thus resulting in the change of the constant K; however the order remains the same. According to Levenspiel (1998), elementary reactions entail the following; the molecule (A) and the rate constant (R):

$$2\,\mathrm{A} \rightarrow 2\,\mathrm{R} \qquad 2.5$$

The reaction is irreversible and bio-molecular containing a second order. Furthermore, Levenspiel (1998) suggests, it is paramount to specify the nature of constituents in the reaction in a more complex situation. A reaction that varies in its kinetics is referred to as a non-elementary reaction, thus resulting in a number of series postulated to define the kinetics involved (Levenspiel, 1998). In some instances, the rate equation is temperature and composition dependent, taking into account the Arrhenius law. However, in experiment 4 of this research, the effect of the first flush in the AMM started from a steady state condition and the application of heat did not take place. Subsequently, temperature was irrelevant for the experiment.

Brusseau (1996) and Paul *et al.* (2011) describe the “perfectly mixed flow reactor” (PMFR) for flooded underground mines. Thereby the flooded mine is considered as a “well mixed defined water reservoir” (Paul *et al.*, 2011), where dissolution and dilution processes by inflowing water take place. If the element peak concentration (c_0), the hydraulic residence time (T) (flooded mine volume divided by mean inflow rate) and the time after peak concentration (t) are given, the theoretical dilution curve

(TDC) can be calculated. It is possible to calculate this curve after the peak of the first flush (Eq. 2.6).

$$c(t) = c_0 \times e^{\frac{-t}{T}} \qquad 2.6$$

With $c(t)$ concentration at time t after the peak concentration, c_0 peak concentration, t time after the peak concentration and T hydraulic residence time.

Since according to Paul *et al.* (2011), the water flowing into the mine is already mineralized, $+c2$ (inflow concentration) can be added to the equation 2. Three different types can be derived from the calculated TDC curves; in type A, only dilution of the mine water occurs, no other processes take place. Measured data are similar to the calculated TDC curve. If the measured data is above the calculated TDC curve, further dissolution processes are taking place in the mine or the inflowing water is of poorer quality. In this case it is type B. For type C, the measured values are below the calculated TDC curve and precipitation reactions need to be considered or the water flow behaves differently. For the three former uranium mines Schlema-Alberoda, Pöhla and Königstein in Saxony, Germany, the TDC curves for the parameters arsenic and uranium concentration were calculated and evaluated. For the Schlema-Alberoda mine, the TDC curves matched the measured values widely, which is why Paul *et al.* (2011) assume that this mine acts like a PMFR. In Pöhla and Königstein, the simple TDC-concept could not be applied sufficiently, because further geochemical and hydraulic processes are not included enough in the TDC-equation.

Whether the TDC concept can also be transferred to the first flush curves, which were determined by depth profile measurements, shall be evaluated with data from the Schlema-Alberoda mine, as well as from the other mines studied in this article. In equation 2 the concentrations were replaced by the electrical conductivity, since the electrical conductivity is directly proportional to TDS (total dissolved solids), which is the sum of the cat- and anions (Eq. 2.7).

$$\mathrm{EC}(t) = EC_0 \times e^{\frac{-t}{T}} \qquad 2.7$$

With EC(t) electrical conductivity at time t after the peak concentration, EC_0 peak electrical conductivity, t time after the peak electrical conductivity and T hydraulic residence time.

Redox reactions occur for example, when the geosphere interacts with the atmosphere. This can result in a reducing and basic environment or acidic and oxidising (Demchak *et al.*, 2004; Gzyl & Banks, 2007). Mining surge increased mineral reaction deep in the geosphere where marcasite or pyrite disintegrate releasing dissolved sulfate, iron and protons leading to acid mine water drainage (Demchak *et al.*, 2004). Stopping the dewatering stoppage in abandoned mines leads to an increase in water levels, therefore, flooding the mine (Nuttall & Younger, 2004; Wolkersdorfer, 2008; Nordstrom, 2009).

In retrospect, the initial pumped water is often acidic and has elevated concentrations of sulfate and metals, potentially harmful to the environment. Cairney and Frost (1975) and Banks *et al.* (1997) describe acid mine drainage in the Mainforth colliery, county Durham, UK in the middle of the 20th century. Gzyl and Banks (2007) denominated this occurrence and the subsequent quality improvement as “first flush”. Frost (1979) explained that iron concentrations decrease exponentially over time post the first flush peak, thus resulting in a 350 days half-life of the iron concentration. Consequently, the iron concentration reduced over time resulting in the equalisation of the background concentration. Gzyl and Banks (2007) further reiterate that efflorescent salt producing minerals, the electrical conductivity and volume of the mine water bodies, the rate of mine water recharge and other hydraulic connections are paramount controlling factors of the first flush.

Younger (1997) summarised that “the iron concentration of uncontrolled mine water discharges falls by 50% in each subsequent period equal to that taken for the abandoned workings to fill with water after the pumps were withdrawn” i.e. an exponential decay and determined an empirical equation for the duration of the first flush through empirical investigations at 80 individual discharges from abandoned coal workings (Younger, 2000b). The duration t_f of the first flush is approximately four times the flooding period.

The following equation is utilised to calculate the duration of the first flush (Younger, 1997).

$$t_f = (3.95 \pm 1.2)\ t_r \qquad 2.8$$

Where t_f is the duration of the first flush and t_r is the rebound time. Rebound time takes the following into consideration: the volume of the voids, weathering rate of acid forming minerals, volume of the mine voids and ground water recharge.

Three different empirical models were developed to constitute the first flush phenomena in mine water. Gzyl and Banks (2007) created a single phase model that was later known as the G&B model which models the exponential drop in the mine water quality over a long period to background concentration and it is explained as follows:

$$C = C_v \times \exp(m \times t) + C_b \qquad 2.9$$

Where C_v is initial concentration at time 0, t is time, m is the slope of the curve and C_b is the background concentration, which is normally 90 % less of C_v.

Perry and Rauch (2013) and Merritt and Power (2022) established another model similar to that of Gzyl and Banks (2007) known as the P&R model, where they demonstrated that the mine water quality constantly drops to beyond background concentration:

$$C = C_v \times \exp(m \times t) \qquad 2.10$$

Merritt and Power (2022) and Perry and Rauch (2013) further proposed a new two phased model known as the P&R dual phase model. Modelling the drop in concentration slopes at different time periods, where phase one indicates an initial steep drop in concentration. The following phase indicates an effectively slower drop over a long period, as explained below:

$$C_{v1} \times \exp(m_1 \times t) \text{ when } t < t_{transition} \qquad 2.11$$

and

$$C_{v1,2} \times \exp(m_2 \times t) \text{ when } t \geq t_{transition} \qquad 2.12$$

Where C_{v1} is the initial peak concentration, C_{v2} is the second concentration, transitioning from the first slope to the second slope, m_1 is the initial steep slope, m_2 is the shallow long tern slope, t is the time and $t_{ransition}$ is the change from the first slope to the slower decay slope.

Merritt and Power (2022) collected historical data from a stratified Sydney, Nova Scotia, Canada coal field, which showed evidence of the first flush. Two different water body models were investigated; a shallow model with 600 mg L^{-1} and deep model with 3300 mg L^{-1} of sulfate and iron concentrations. From the historical data, it was deduced that the upper water body takes a longer time to improve, whilst the lower body takes a shorter time to improve.

CHAPTER 3

3 Methodology

3.1 Introduction

This chapter gives a brief description of the different components and instruments used in the construction of the Analogue Model Mine (AMM). The experimental layout comprises of five experiments entailing the following: the activity, duration and the aim of each experiment. Furthermore, a description of sample acquisition procedure for each experiment is given.

Immense research on mine water stratification dynamics have been conducted in Europe, mainly in Germany, France, Britain, Poland and the Czech Republic (Denimal *et al.*, 2005; Wolkersdorfer, 2008; Luo *et al.*, 2012; Wieber *et al.*, 2019) and almost none documented in South Africa. Other laboratory based stratification investigations were conducted by using boreholes, analogue and numerical modelling (Berthold & Börner, 2008; Mugova & Wolkersdorfer, 2022). However, these were still conducted outside South Africa, in Germany.

3.2 Components of the Agricola Model Mine

The AMM is named after Georgius Agricola, the author of *De Re Metallica Libris XII*, first ever book on mining (Hoover & Hoover, 1950). The AMM (Figure 3.1 and Figure 3.2) was constructed at Tshwane University of Technology’s Arcadia campus’ mine water laboratory. It is 4 × 6 m in size and consists of four shafts (shaft #1–#4) that can be isolated with valve systems and four working levels, ranging from 65 cm to 305 cm depths and can hold a maximum of 153 L of water.

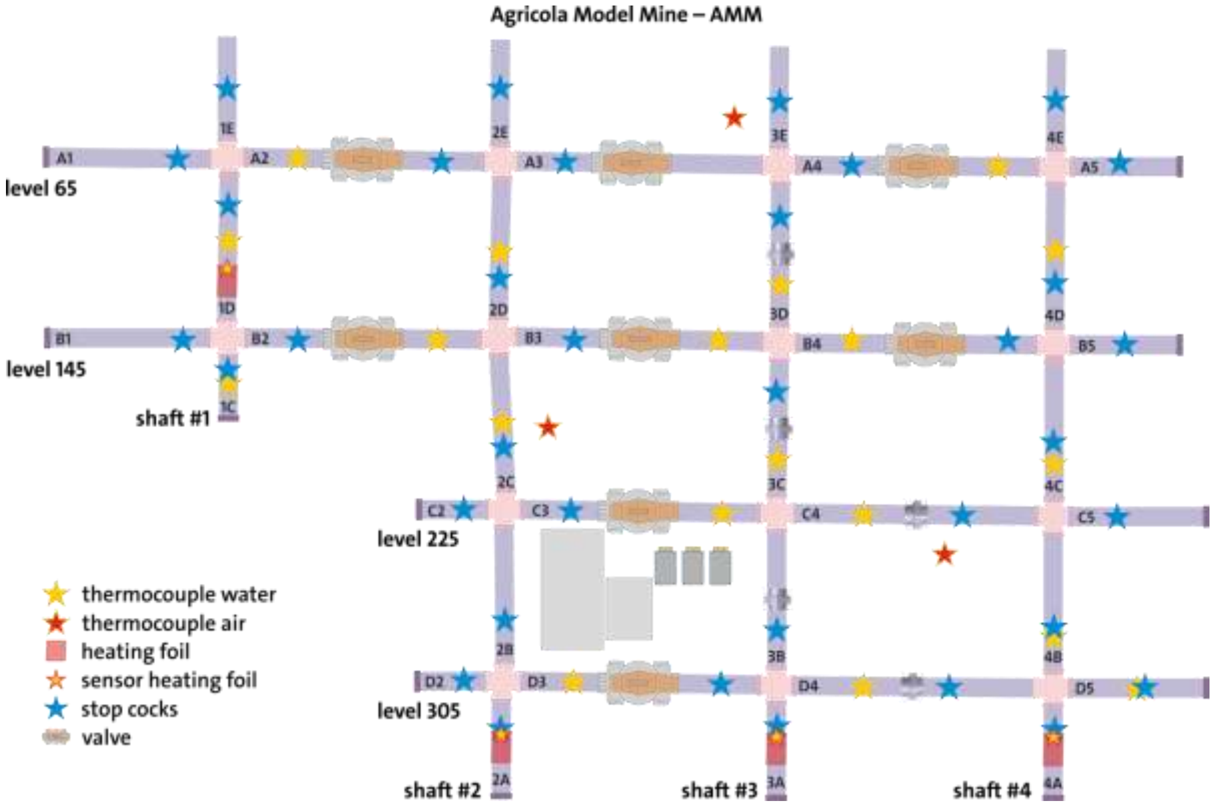

Figure 3.1: Schematic representation of the Agricola Mine Model (AMM) at Tshwane University of Technology. Each column, shaft, is labelled with a number, 1 to 4 and each row, level, is labelled with a letter, A to D. Thus each section is labelled accordingly for identification purposes. Some sections can be entirely isolated from each other by valves (e.g. within sections A2 or A3)

These shafts and working levels were constructed with transparent PVC tubes mounted to the wall using wooden planks and plastic straps. PVC tubes were insulated with 80 × 25 mm polystyrene foiled sections (Insul-pro, South Africa) to isolate the system from external heat fluctuations. Polystyrene foil insulation has a low *k* factor and the PVC temperature limits range between -110 °C and 74 °C. Furthermore, it is resistant to weak and strong alkalis, weak and certain strong acids, alcohol, saline and fresh water. Hence, it was a preferred choice to use for the experiments ran for this research study.

Figure 3.2: Photograph of the insulated AMM showing some levels with already installed isolator valves

Eight temperature controlled 12 V, 137 × 320 mm large heating foils (Conrad Electronics, Germany; H-Tronig TSM 125 temperature controller, Germany), with a switch on/switch off temperature (minimum/maximum) regulator with a maximum surface temperature of 60 °C are mounted outside the tubes at sections 1C, 2A, 3A, 4A to simulate a geothermal gradient. Twenty thermocouples are placed inside the tubes at each section to monitor the *in situ* fluid temperature while flowing through the AMM. Furthermore, three thermocouples are placed outside the AMM to measure the ambient air temperature. This brings the number of thermocouples used at any given time to 23. The measured temperature was logged using Huato S220-T8 data loggers (Shenzhen HUATO System, China) mounted to the wall between sections 2B and 3B (Figure 3.1 and Figure 3.3).

K-type thermocouples usually measure temperatures ranging from –200 to 1350 °C, whereby the positive end consists of chromel and the negative is alumel. The manufacturer stated that the K-type thermocouple has an accuracy of roughly 2.2 °C/0.75 %. To correct the measurements taken from the temperature data logger for any drift, water samples were drawn from each sampling point and measured using a temperature probe. Subsequently, the differences were obtained by subtracting or adding the logger measurements from the samples collected from the AMM. This correction occasionally proved a temperature discrepancy higher than manufacture’s statement (Table 3.1).

Figure 3.3: Huato temperature loggers with 23 K-type thermocouples, 20 to measure the *in situ* water temperature and three to measure the ambient air temperature

The model also holds a battery charged energy supply to backup power outages. Top inlet pipes (sections 1–4E) are used to flood the mine, and the lower outlet pipes (sections 1C and 2–4A) are used to release the water from the system at the end of the experiments.

Additionally, the shafts can be either flooded individually by manipulating the valves or they can be flooded simultaneously. Ports (consisting of a stop cock and a lure lock) are attached to the model on every section and used as a pathway to inject tracers into the AMM or take water samples.

Injection of tracer dyes and microspheres in flooded shafts aids in measuring the flow velocity, thus giving indication of the flow dynamics in the column

(Wolkersdorfer, 1996). Sodium fluorescein (Uranine) dye was used for experiment 2, 3, 4 and 5. In addition to Uranine, Sulforhodamine B was used in experiment 4 and was injected into the AMM and analysed fluorometrically (Cary Eclipse Fluorescence Spectrofluorimeter; Agilent, Australia) to monitor the water distribution and flow within the AMM.

Seven Uranine standards, 0, 25, 50, 100, 250, 500 and 1000 μg L^{-1}, were prepared and used to acquire a calibration curve (Figure 3.4) suitable for the type of tracer used. Excitation and emission wavelengths of 492 and 515 nm, respectively, were used to calibrate the spectrofluorimeter. These wavelengths were obtained from pre scanning of the standard with the highest concentration (1000 μg L^{-1}). A five nm slit width was used for both wavelengths, with a photomultiplier (PMT) voltage of 480 V.

Table 3.1: The data shown below is the difference between the temperature measured by the K-type thermocouples and the one measured using a probe from extracted solution. Recorded temperatures used to adjust the measured temperatures for the calibration of the temperature logger

Logger name	Correction, K
1C	-0.60
1D	0.70
A2	1.90
B2	1.70
2B	1.90
2C	0.40
2D	0.50
D3	0.90
C3	2.00
B3	-5.60
3C	2.00
3D	3.00
D4	0.60
C4	-3.70
B4	-1.00
D5	1.40
4B	-0.70
4C	1.80
4D	-1.80
A4	0.40

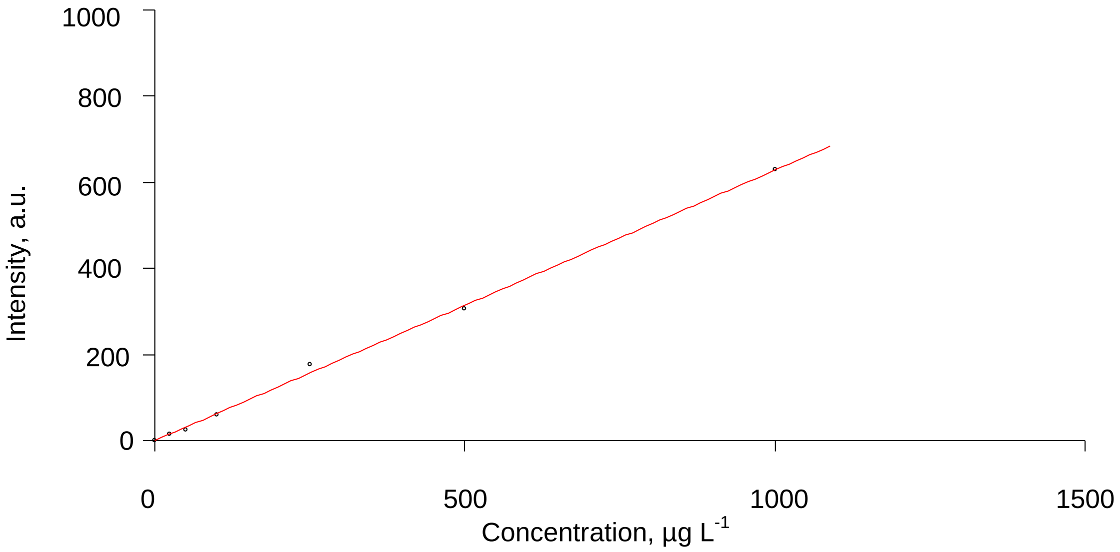

Figure 3.4: Uranine dye calibration curve for the 7 standards prepared. The intensity (a.u.) is plotted against concentration (µg L^{-1}) to produce optimum analysing conditions for the spectrofluorimeter

Eight Sulforhodamine B samples with concentrations of 0, 50,100, 250, 500, 750 1000 and 1500 µg L^{-1} were analysed using the spectrofluorimeter at excitation and emission wavelengths of 566 and 587 nm, respectively (Figure 3.5). A 5 nm slit width was used for both wavelengths with a PMT voltage of 505 V.

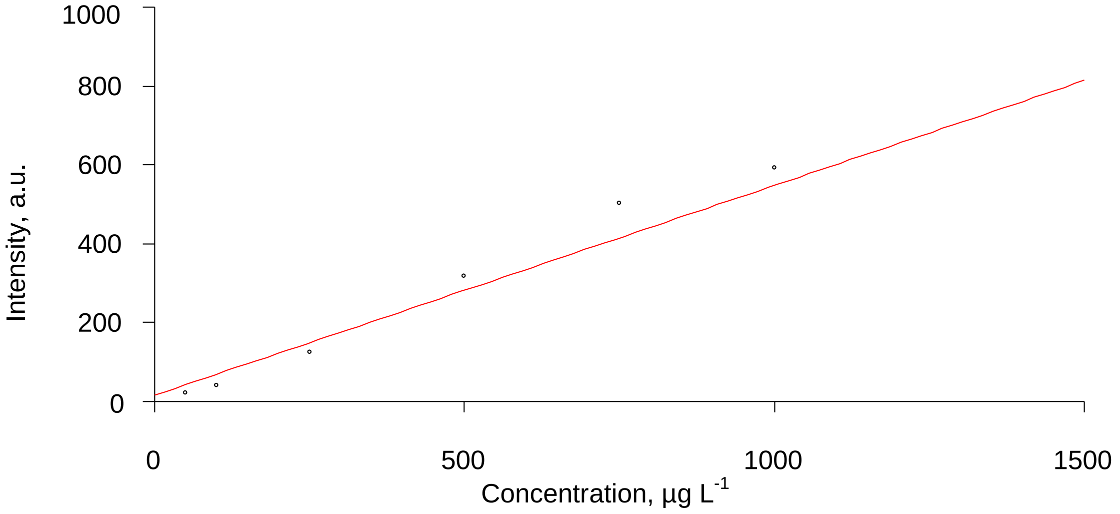

Figure 3.5: Sulforhodamine B calibration curve for the eight standards prepared, with the intensity (a.u.) plotted against the concentration (µg L^{-1}) to produce optimum analysing conditions for the spectrofluorimeter

The flow of the water in the system was measured continuously using Portaflow portable ultrasonic flow meters (Portaflow 220 and Portaflow 330; GF Piping Systems, Switzerland) at each level and section. Additionally, the relevant dimensionless hydraulic numbers were calculated to compare the AMM to real world scenarios. Two measuring points were identified for the positioning of the two rails each comprising of 2 transducers, recording the flow measurement. One rail is positioned horizontally to measure the horizontal flow between section C4 and C5. The other one is positioned vertically to measure the vertical flow at section 2B. The second flow meter measuring the horizontal flow was only introduced at the commencement of experiment 5.

CTD divers (Van Essen, Netherlands) were used to measure electrical conductivity and temperature inside the AMM, with one barodiver used to measure the ambient pressure located above shaft 3. The divers are made of zirconium oxide, making it corrosion proof.

3.3 Experimental Design

Five experiments were conducted throughout the duration of this study and at the end of each experiment the data was evaluated to verify if the objective of each experiment was achieved (Table 3.2). The objectives will be detailed below, with each experiment. At the beginning of each experiment, the AMM was flooded from the top water inlet pipes of each mine shaft with tap water and letting it stand for the duration of each experiment. Subsequently, the model was drained and flooded thrice with tap water at the end of each experiment in preparation for the experiment to follow.

Table 3.2: Activity layout and the objectives, as well as the duration for each experiment conducted during the research work. Experiment 1A could not be finished due to the Covid-19 Lockdown

Experiment	**Objective**	**Start Date**	**End Date**
1A	System Monitoring	2020-02-19	-
1B		2020-10-28	2020-11-25
2A	Tracer Addition	2021-01-13	2021-02-11
2B		2021-03-09	2021-03-31
3A	Application of Geothermal Gradient	2021-05-25	2021-05-25
3B		2021-05-03	2021-05-03
3C		2021-06-08	2021-06-08
3D		2021-06-09	2021-06-09
3E		2021-06-17	2021-06-17
4	Stratification Development	2021-06-24	2021-07-19
	First Flush	2021-07-20	2021-07-21
5	Stratification Breakdown	2021-07-26	2021-10-26

Experiment one comprises of experiments 1A and 1B and the objective was to monitor the processes that transpire in the system at steady state conditions, therefore, serving as a control.

Experiment 1A commenced on the 19th February 2020 and ended abruptly due to the commencement of the Covid 19 pandemic lockdown. On the 28th of October 2020 experiment 1B continued by flooding the AMM and the system was monitored at steady state condition, to give a clear comprehension and general behaviour of the AMM.

After the AMM was flooded at all working levels and shafts, 31 mg, resulting in 200 µg L^{-1} concentration of Uranine at the beginning of experiment 2 and 3 was injected at sampling point 2A. The injection of the tracer was carried out after the AMM was flooded and standing for a 24-hour period to let the water settle.

Experiment two comprises of experiment 2A and 2B and the objective was to monitor the tracer distribution in the AMM at steady state condition and to measure the flow rate of the water in the AMM. Experiment 2A commenced on the 13th January 2021 and stopped due to an incorrect calibration of the spectrofluorimeter. Initially, the Uranine samples were run at a PMT voltage of 490 V which results in a smaller sample range of 100 µg L^{-1} instead of 480 V that gives a bigger range of sample concentration of 1000 µg L^{-1}. The second successful attempt commenced on the 9th March 2021 and similar flooding and tracer injection processes were followed as in experiment 2A.

The objective of experiment 3 was to understand the processes that transpire in the shafts when the temperature was increased from the model's ambient temperature, whereby heat was used as a proxy for energy. Experiment 3 comprises of experiment 3A, 3B, 3C, 3D and 3E with similar flooding procedure followed in experiments 1 and 2 was followed and thereafter, samples of water were drawn from each sampling port immediately after the tracer injection.

Experiment 3A commenced on the 25th May 2021 and ran for a day where the water in the flooded AMM was heated. This was archived by switching on the heating foils to simulate a geothermal gradient. The temperature ranged between 30/32 °C (switch on/switch off temperature). Experiment 3B running at temperatures between 28/30 °C commenced on the 3rd of June 2021 and a day later, the experiment stopped after a malfunctioning of the heating foils. Experiment 3C commenced on the 8th June running at temperatures between 28/30 °C; yet the results were not satisfactory. The tracer dispersed too quickly, therefore failing to give a clear steady distribution/dispersion in the AMM due to the high temperatures set on the heating foils.

To improve the results obtained in experiment 3C, experiment 3D commenced on the 9th June 2021, with reduced temperatures ranging between 26 and 28 °C. To further improve the measurements obtained in experiment 3D, also a shorter sampling interval was introduced, as it was observed in the subsequent experiments that the dispersion rate was high. Experiment 3E commenced on the 17th June 2021 at a reduced temperature ranging between 23/25 °C to suit the sampling interval. A clear tracer build up was observed across the AMM.

Experiment 4 comprises of two sections, with the following objectives: first to determine the stabilisation of the artificial density stratification in the AMM at steady state conditions. The objective for the second segment of the experiment was to monitor the first flush effect in the AMM. The experiment commenced on the 24th June 2021.

At the commencement of experiment 4, the lower half of the AMM, levels 225 and 305 were filled with 93 L of fresh water. Post the flooding of the AMM, fresh water samples were collected and analysed using the spectrofluorimeter. Electrical conductivity was measured by lowering a CDT diver (Van Essen Instrument, Netherlands) in each shaft. One baro-diver (Van Essen Instrument, Netherlands) was installed outside the AMM to measure the atmospheric pressure.

60 L of brine with a concentration of 70 g L^{-1} of sodium chloride and sodium fluorescein dye (Uranine) with a mass of 31 mg, resulting in a concentration of 517 µg/L was pumped into shafts #2, #3 and #4 simultaneously from the top. This was achieved by lowering tubes inside to the bottom of the 3 shafts and the solution was

pumped at 0.33 L min^{-1} using a peristaltic pump (Heidolph, Germany) at the lowest speed of 50 rpm. To add in the 60 L of brine solution, three shafts, 2, 3 and 4, were initially filled by pumping in 2.7 L of the solution into each shaft to get the solution to the same level (305). The remaining 51.9 L were pumped into the AMM through shaft 3. Calibration of the peristaltic pump showed that a setting of 50 rpm equals a pump rate of 0.33 L min^{-1}. We chose the 100 mS cm^{-1} because pre – experiments showed it was not possible to fill the AMM with lower EC water and artificially create stratification. Only later we developed a new method to induce artificial stratification and will be detailed in future papers to be published.

Flooding resulted in a stratified system in the AMM. A highly mineralised layer with a density of 1.065 g cm^{-3} was observed from the bottom of the AMM to level 225. From level 225 to the shaft collars, the freshwater layer with a density of 0.998 g cm^{-3} dominated. Thirty six verification samples were collected at each sampling port and were fluometrically analysed for Uranine dispersion and diffusion between the two layers.

On the 1st July 2021, seven days post the commencement of experiment 4, the upper half of the system containing fresh water was injected with Sulforhodomine B with a mass of 31 mg at sampling ports A2, A3, B4 and B5 at 15:00. Thereafter, daily measurements of both Uranine and Sulforhodomine B were taken to monitor the processes that transpired in the AMM. This was in preparation for the second part of the experiment, with the objective to monitor the effects of the first flush in the AMM. Once all observations were made from measuring of the Sulforhodamine B and Uranine tracers, the fresh tap water layer containing Sulforhodamine B dye was flushed with tap water at sampling port A1 at a pumping rate of 0.33 L min^{-1}. The water discharged continuously at the discharge outlet above sampling port 3E. This experiment commenced on the 20th July 2021 and lasted for duration of 860 min.

After the flushing experiment stopped, experiment 4 was carried over to experiment 5. It commenced on 26th July 2021. Irrespective of the flushing of the AMM, the water body in the model was still stratified, and the lower half of the AMM, levels 225 and 305, contained sodium chloride solution and Uranine dye from experiment 4. The upper half of the system contained tap water containing small concentrations of Sulforhodomine B from the first flush experiment. The objective of experiment 5 was to determine the breakdown conditions of the density stratification in the model. To achieve this objective, stratification was degraded by slowly increasing the temperature at shafts #2, #3 and #4 from 19 °C to 44 °C (Figure 3.6). Electrical conductivity readings for shafts #1, #2, #3 and 4 were taken in addition to the tracer concentrations. Tracer distribution in the AMM was measured by analysing for both Uranine and Sulforhodamine B.

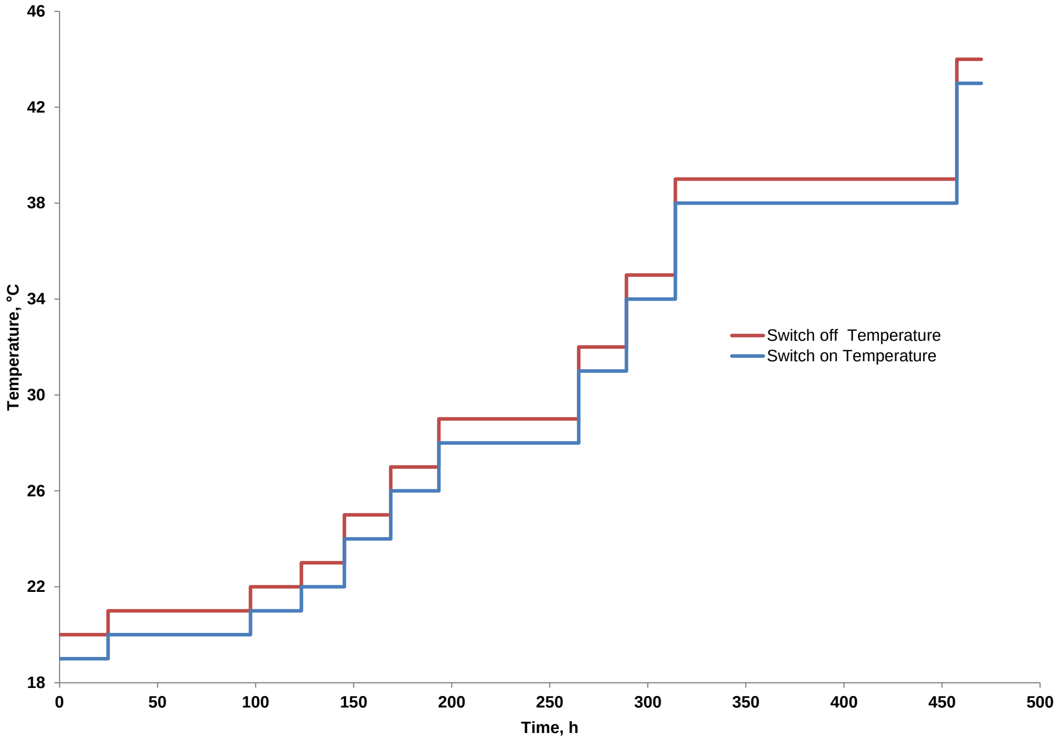

Figure 3.6: Temperature increase in the AMM caused by heating foils over the remainder of the experiment

3.4 Sampling

Ambient and *in situ* water temperature together with flow measurements were logged daily for the duration of all the experiments. Prior to the commencement of each experiment, water samples were taken at each sampling port to analyse for tracer cross contamination. Since no tracer was injected for experiment 1, it was therefore unnecessary to collect tracer samples. However, 36 samples for experiment 2 were taken daily at all measuring ports post the injection of Uranine.

Uranine samples were taken immediately after the tracer was injected and every three hours thereafter during the running of experiment 3A, 3B and 3C. For experiment 3D, samples were collected immediately after the tracer injection. Furthermore, samples were taken again at 35, 52, 92, 107, 127, 142, 162, 227, 347 min, 527 and at 1667 minutes the following day. At every sampling period, all 36 samples were collected.

Uranine measurements were taken immediately after the injection at 0 minutes and thereafter every 15 minutes at all 36 measuring ports to monitor the rapid distribution in the AMM for experiment 3E. Samples were collected at 0, 15, 30, 45, 60, 75, 90, 105, 120, 135, 150, 165, 195, 315 and at 495 minutes at all sampling ports.

Sampling for experiment 4 began on the 24th June 2021 and the first set of samples was collected at 0 hours post the flooding of fresh tap water in the AMM. Thereafter, another set of 36 samples were collected immediately, after pumping the sodium chloride solution containing Uranine in the AMM. Over the succeeding days, a set of 36 samples were taken at the sampling ports.

For the first flush experiment, samples were collected every hour and analysed for both Uranine and Sulforhodamine B. Furthermore, 119 samples were collected every 10 minutes at the discharge point to measure the development of the Sulforhodamine B concentration in the model.

Sampling for Uranine and Sulforhodamine B in experiment 5 commenced on the 26th July 2021, where five sets of 36 samples were collected (Table 3.3). Additionally, four sets of 36 samples were collected 23 hours post the start of the experiment at different intervals. 71 hours later the sampling intervals were reduced to 3 sets and the same sampling procedure continued until 167 hours.

Stratified layers remained stable thus far. At 191 to 431 hours the sampling intervals were reduced to 2 sets and only one sample was taken 24 hours later (the following day). Because sampling port A1 broke, no samples were collected after 23 hours post the start of the experiment until 217 hours when it was fixed.

Due to a low rate of stratification disintegration, no samples were taken between 502 and 694 hours of the running of the experiment. The objective was to observe the processes that transpire in the AMM over a longer time frame when heated. Sampling then commenced 694 hours later and the sampling interval was reduced to twice a week on Tuesday and Friday. For experiment 5, electrical conductivity was measured daily in each shaft along with the collection of Uranine and Sulforhodamine B samples.

Table 3.3: Sampling intervals for Uranine and Sulforhodamine B in experiment

Time	Hours	Time	Hours	Time	Hours
2021-07-26 10:45	0	2021-08-02 16:00	173	2021-10-05 12:00	1705
2021-07-26 13:00	2	2021-08-03 10:00	191	2021-10-12 10:00	1871
2021-07-26 14:00	3	2021-08-03 15:00	196	2021-10-19 10:00	2039
2021-07-26 15:00	4	2021-08-04 11:30	217	2021-10-26 09:00	2206
2021-07-26 16:00	5	2021-08-04 15:00	220		
2021-07-27 09:45	23	2021-08-10 11:15	361		
2021-07-27 14:30	28	2021-08-10 15:30	365		
2021-07-27 15:30	29	2021-08-11 10:15	384		
2021-07-27 16:15	30	2021-08-11 15:15	389		
2021-07-28 10:00	47	2021-08-12 10:15	408		
2021-07-28 12:00	49	2021-08-13 10:00	431		
2021-07-28 14:00	51	2021-08-24 07:30	693		
2021-07-28 16:00	53	2021-08-27 08:30	766		
2021-07-29 10:00	71	2021-08-31 10:00	863		
2021-07-29 13:00	74	2021-09-03 10:00	935		
2021-07-29 16:00	77	2021-09-07 10:00	1031		
2021-07-30 10:45	96	2021-09-10 10:30	1104		
2021-07-30 14:00	99	2021-09-17 14:30	1276		
2021-07-30 15:30	101	2021-09-23 10:00	1415		
2021-08-02 10:00	167	2021-09-28 10:00	1535		
2021-08-02 14:00	171	2021-10-01 11:00	1608		

CHAPTER 4

4 Results and Discussion

4.1 Introduction

This section describes the outcomes of the five experiments conducted to achieve the aim of this research work and it gives a detailed discussion of each experiment. Flow rate, temperature and tracer distribution are the parameters that were measured and will be discussed for all the experiments conducted. Electrical conductivity and temperature for experiment 5 in the AMM were measured with the aid of Van Essen CTD divers.

Each subsection heading represents experiments 1, 2, 3, 4 and 5. Supporting raw data are available on an online archive (www.wolkersdorfer.info/ThesisMolaba), and the folders are labelled according to each individual experiment. The data online comprise of flow rate, temperature, Uranine and Sulforhodamine B results and videos showing the distribution thereof.

Different statistical approaches were performed on the results obtained from the different data sets. A normality test was performed using the Krustal-Wallis one way analysis of variance with the software tool Sigma Plot, with the *p* value set to <0.050. A value of $p < 0.001$ was obtained from the Turkey test, thus implying that there is a statistically significant difference, when data from different temperature sensors were compared. This was done for the temperature readings at given frequencies (F) for all the experiments. Therefore, this proves that the data obtained from the different temperature sensors during one experiment are statistically significantly different.

4.2 System Monitoring at Steady State Condition in the AMM

4.2.1 Experiment 1: Flow Measurements in the AMM

An average flow rate of 0.013 m s^{-1} was measured in the AMM and remained constant throughout the duration of experiment 1. This is shown by the running average coloured in dark blue (Figure 4.1). There were minor fluctuations in the measurements with a minimum recorded flow rate of 0.006 m s^{-1} at instantaneous time of 1.0 and 8.6 min. Furthermore, there were other occasional flow fluctuations of 0.007 m s^{-1} at 8.57 and 23.48 min, 0.008 m s^{-1} at 1, 1.93 and 1.95 min, 0.009 m s^{-1} at 0.57 and 0.58 min, 0.011 m s^{-1} at 0.90 and 0.92 min and 0.12 m s^{-1} at 0.55 min and 0.6 min. The maximum flow measured in this experiment was 0.014 m s^{-1}. Pavelyev *et al.* (2003), Nuttall and Younger (2004) and Wolkersdorfer (2008) stated that turbulent flow occurs at Reynolds number between 10 and 100 for porous media but at a critical Reynolds number of approximately 2000 in pipes. An average flow rate in the AMM was 0.013 m s^{-1}, thus resulting in a Reynolds number of 61, and this is indicative of laminar flow, given that the AMM is made up of pipes. Fluctuations in the system were related to data and signal processing between the transducers and the data logger positioned at section 2B, measuring the vertical water flow rate in the AMM. The individual 0.001 m s^{-1} flow rate fluctuations shown on the graph result predominantly from the A/D converter (analogue to digital converter).

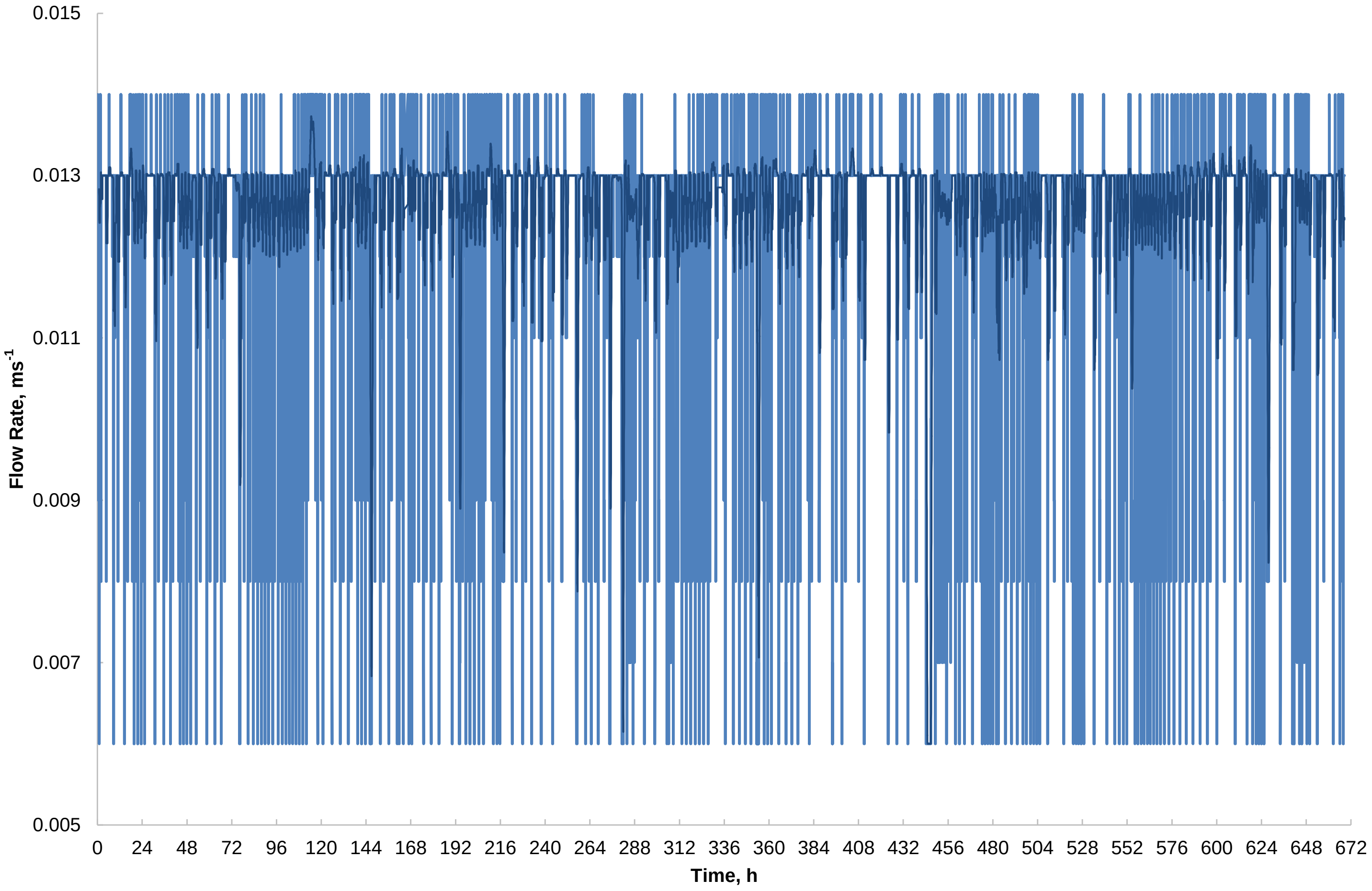

Figure 4.1: Flow rate in the AMM plotted against time showing a relatively constant flow at 0.013 m s^{-1} with occasional fluctuations throughout the 28 day experiment period. Dark line is the running average

4.2.2 Experiment 1: Temperature Measurements

Three thermocouples AT1, AT2 and AT3 measuring ambient temperature averaged 23.0 °C, 23.3 °C and 22.9 °C, respectively, (Table 4.1) with a standard deviation of 0.2 K. This implies that the room air temperature is ever so slightly warming upwards to the middle section and becomes colder at the top.

Shaft #1 is equipped with 2 thermocouples located at sections 1C and 1D measuring *in situ* water temperature averaged 22.8 and 21.4 °C, respectively (Table 4.2). There is an upward temperature decrease in the AMM in this particular shaft. This corresponds with lower room air temperature, with an average of 22.9 °C at section AT3, located at the upper level of the AMM.

Table 4.1: Statistical values, depicting the minimum, maximum and average values for the room air temperatures in °C

Thermocouple	AT1 (Top)	AT2 (Middle)	AT3 (Lower)
Min	21.5	21.6	21.4
Max	25.5	26.3	25.6
Ave	23.0	23.3	22.9
Std dev	0.9	1.0	0.9
Std dev %	3.8	4.1	3.9

There are 3 thermocouples located on shaft #2 at sections 2D, 2C and 2B with temperatures averaging 21.2, 20.4 and 20.1 °C, respectively. Sections 2C and 2B show similar temperatures with a general vertical temperature increase. The temperature in the shaft varies slightly with the room air temperature.

Shaft 3 is equipped with two thermocouples located at sections 3D and 3C with average temperatures of 18.0 °C and 20.1 °C, respectively. There was a general vertical temperature decrease within the shaft.

Three thermocouples are installed in shaft #4, located at sections 4D, 4C and 4B with average temperatures of 19.8 °C, 16.1 °C and 18.5 °C, respectively. This shows a vertical temperature fluctuation within the shaft. Temperature readings in sections of all four shafts (1D, 1C, 2D, 2C, 2B, 3D, 3C, 4D, 4C and 4B) showed a similar trend and were comparable to the ambient temperature at locations AT1, AT2 and AT3 (Figure 4.2).

Three thermocouples were installed in the lowermost levels 305, at sections D3, D4 and D5, and recorded average temperatures of 20.7 °C, 20.2 °C and 20.4 °C, respectively, with a standard deviation of 0.2 K.

Level 225 had two thermocouples, C3 and C4 with temperatures averaging 20.4 °C and 23.4 °C, respectively, with a standard deviation of 1.5 K. Section C4 showed the second highest maximum temperature in the AMM.

The uppermost level 145 contains three thermocouples, B2, B3 and B4, that gave average temperatures of 19.8 °C, 24.0 °C and 21.3 °C, respectively, with a standard deviation of 1.6 K. Thermocouple B3 recorded the highest maximum *in situ* temperature in the model. Level 65 had two installed thermocouples located at A2 and A4 with temperatures averaging 19.7 °C and 17.4 °C, respectively.

Temperatures from the ambient air measurements were comparable to those of the *in situ* water temperature (Figure 4.2). Temperatures showed a fluctuating system defined by an initial drop followed by a marked increase roughly 200 hours into the experiment accompanied by another drop 100 hours (a total of 300 h) later. As the experiment approached 400 hours, another increase in temperature occurs; this was also followed by a decrease towards 600 hours. Before the experiment came to a conclusion at 672 hours, a final temperature increase appeared. Conclusively, the room temperature was pivotal in controlling the *in situ water* temperature as demonstrated by the similar trends of the ambient temperature.

The objective of experiment 1 was to monitor the processes that transpire in the AMM at steady state condition. In summary, the 672 hour experiment had a Reynolds number of 62 thus indicating an overall laminar flow, though the fluctuations of the measured parameters might suggest turbulences. Monitored *in situ* temperatures mirrored those of the ambient room temperature.

Table 4.2: Temperatures in shafts #1, #2, #3 and #4, and to levels 65, 145, 225 and 305 in the AMM showing the number of samples, average, minimum, maximum, standard deviation (S.D) and standard deviation % (S.D %) from the different thermocouples in °C

	No. of samples		**Min**	**Max**	**Ave**	**S.D**	**S.D%**		**Min**	**Max**	**Ave**	**S.D**	**S.D%**		**Min**	**Max**	**Ave**	**S.D**	**S.D%**		**Min**	**Max**	**Ave**	**S.D**	**S.D%**
Shafts	239304	1D	18.4	28.3	21.4	1.3	6.1	2D	19.1	32.4	21.2	1.1	5.2	3D	16.2	27.7	18.0	1.0	5.6	4D	12.8	26.9	19.8	1.3	6.6
		1C	20.3	28.4	22.8	1.2	5.3	2C	16.4	31.9	20.4	1.6	7.8	3C	18.4	30.5	20.1	1.0	5.0	4C	13.3	23.2	16.1	1.4	8.7
								2B	17.7	28.2	20.1	1.1	5.5							4B	16.7	24.5	18.5	1.1	6.0
Levels		A2	16.8	27.1	19.7	1.4	7.1							A4	14.7	28.7	17.4	1.3	7.5						
		B2	17.5	30.9	20.0	1.3	6.5	B3	21.4	37.4	24.0	1.3	5.4	B4	19.6	29.3	21.3	1.1	5.2						
								C3	19.0	26.8	20.4	0.9	4.4	C4	21.4	33.4	23.5	1.2	5.1						
								D3	18.6	32.1	20.7	1.0	4.8	D4	18.3	30.0	20.2	0.9	4.5	D5	18.6	26.1	20.4	1.0	4.9

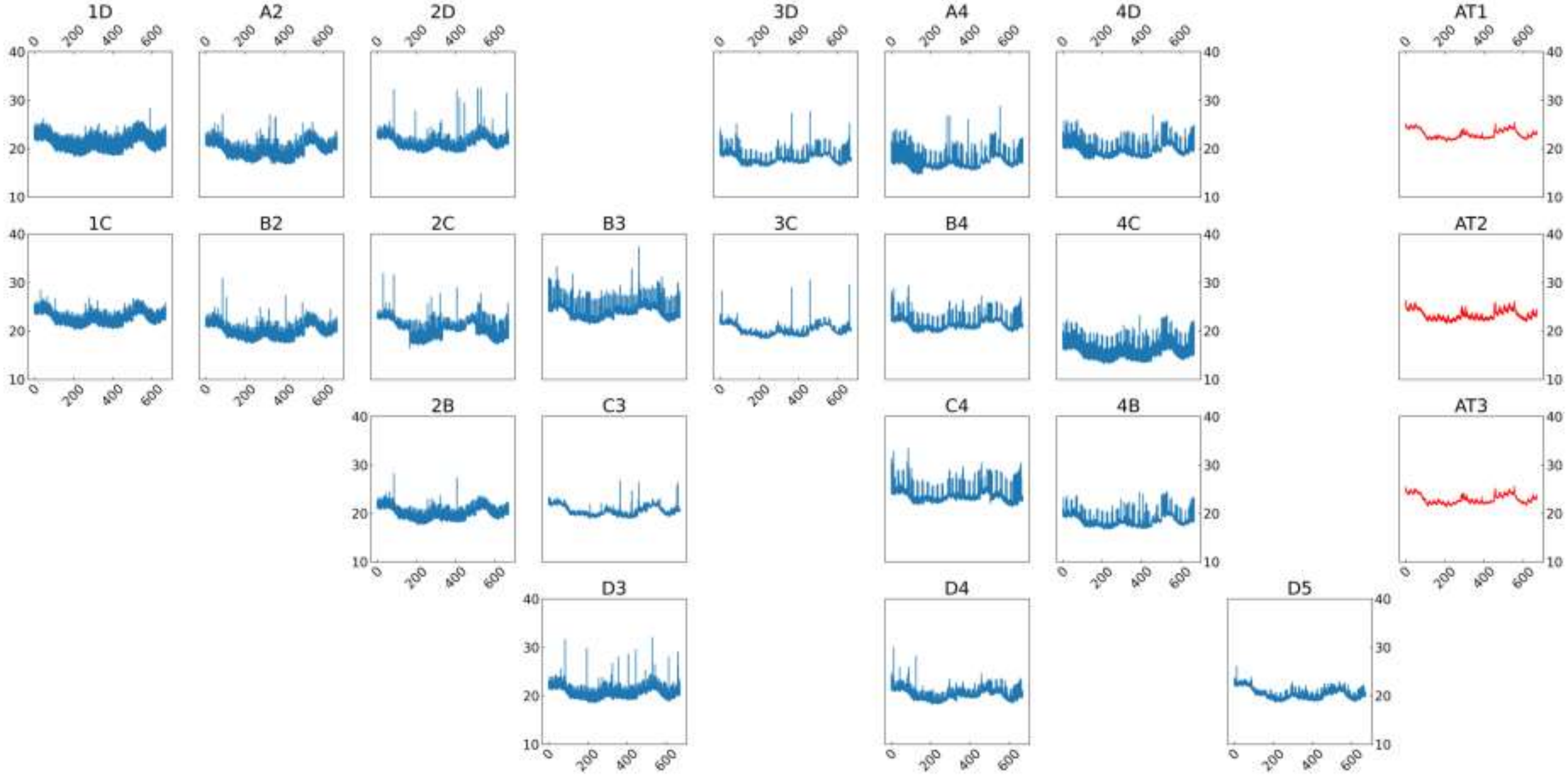

Figure 4.2: Temperature measured against time in hours for experiment 1; the blue represents the temperature inside the model and the red is the ambient air temperature in °C

4.3 Monitoring Tracer Distribution at Steady State Condition in the AMM

4.3.1 Experiment 2: Flow Measurement

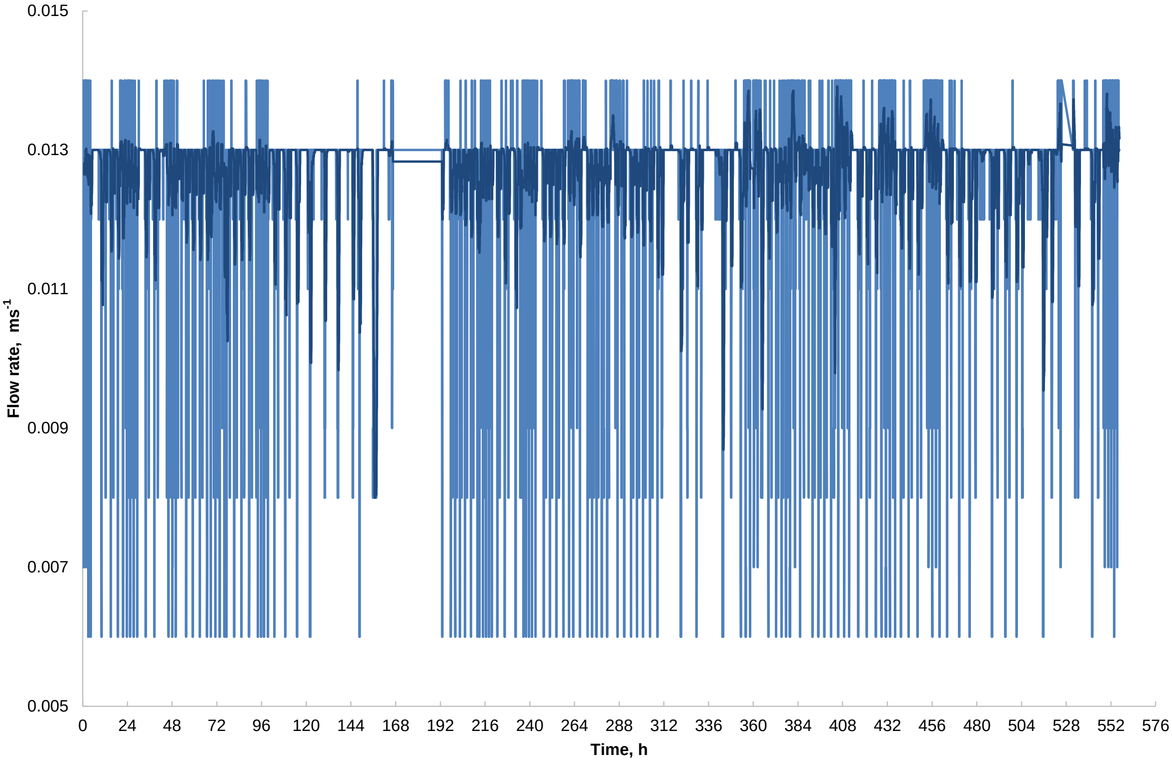

Figure 4.3: Flow rate measured in the AMM, plotted against time

In experiment 2, a relative constant average flow of 0.013 m s^{-1} existed in the AMM shown by the running average (Figure 4.3). A minimum flow rate of 0.006 m s^{-1} and a maximum flow rate of 0.014 m s^{-1} prevailed through the duration of the experiment. The flow rate of 0.013 m s^{-1} results in a Reynolds number of 61. At the maximum flow rate, the Reynolds number was 66, having no effect on the overall characteristics of the flow. It remained close to 60 and therefore indicates a laminar flow in the AMM. These findings are similar to the results obtained in the previous experiment, as they were based on similar conditions. Fluctuations in the AMM were related to data and signal processing between the transducers and the data logger positioned at section 2B to measure the vertical water flow.

4.3.2 Experiment 2: Temperature Measurement

Three thermocouples AT1, AT2 and AT3, were used to measure the ambient air temperature in experiment 2. Thermocouple AT2 recorded a slightly higher average temperature of 23.5 °C, followed by AT1 and AT3, both recording equal average temperatures of 23.0 °C (Table 4.3.)

Table 4.3: Statistical values for the thermocouples measuring ambient temperature throughout the duration of the experiment. The data depicts the minimum, maximum and average temperatures in °C

Thermocouple	**AT1 (Top)**	**AT2 (Middle)**	**AT3 (Lower)**
Min	21.2	21.4	20.9
Max	25.6	27.0	25.9
Ave	23.0	23.5	23.0
Std dev	1.0	1.1	1.0
Std dev %	4.3	4.5	4.3

In experiment 2, section 1D had an average of 21.4 °C and section 1C of 22.8 °C in shaft #1 (Table 4.4). This indicated the presence of warmer water conditions at the bottom of shaft #1 as compared to the temperature of the water at section 1C. A similar trend was observed in shaft #2, equipped with three thermocouples, 2D, 2C and 2B. In this instance, the middle section, 2C, had the lowest average of 19.9 °C, followed by section 2B located below section 2C averaging 20.2 °C. A higher average temperature of 21.4 °C was observed at section 2D, located above section 2C.

The lowest temperatures were recorded in shaft #3. Section 3C with an average of 19.7 °C and section 3D with 18.0 °C. The two sections show a vertical temperature decrease. In shaft #4, the temperatures in sections 4D, 4C and 4B were 24.3 °C, 20.7 °C and 24.3 °C, respectively. There was a general vertical temperature increase towards the top of the shaft.

In the lowermost level of the AMM (305) sections D3 averaged 20.6 °C, D4 averaged 9.8 °C and D5 averaged 20.6 °C. Sections D3 and D5 had similar temperatures, as compared to D4, with the lowest temperature within level 305. Level 225 had temperatures in section C3 averaging 20.5 °C and C4 averaging 20.3 °C. Level 145, at sections B2, B3 and B4 had temperatures averaging 19.8 °C, 23.0 °C and 21.9 °C, respectively. Section B3 recorded the highest temperature within this level. Level 65, at section A2 had temperatures averaging 20.0 °C and 18.2 °C at section A4.

Temperature in the AMM ranged between 19.0 °C and 20.0 °C with the highest average temperature in section B3 in both the shafts and levels. A comparable average temperature trend was observed between the ambient and *in situ* water measurements (Figure 4.4).

At the beginning of the experiment, the ambient and *in situ* average temperatures increased. As the experiment advanced, the temperature generally decreased and followed an average temperature increase 450 hours later. This was followed by a drop towards the 600 hour mark. Close to the end of the experiment, the temperature was rising again. The *in situ* water temperature is thus controlled by the ambient air temperature.

Table 4.4: Temperature variations in shaft #1, #2, #3 and #4, and levels 65, 145, 225 and 305 in the AMM showing the number of samples, average, minimum, standard deviation (S.D), standard deviation percentage (S.D%) and maximum temperature measurements in °C

	No. of samples		**Min**	**Max**	**Ave**	**S.D**	**S.D%**		**Min**	**Max**	**Ave**	**S.D**	**S.D%**		**Min**	**Max**	**Ave**	**S.D**	**S.D%**		**Min**	**Max**	**Ave**	**S.D**	**S.D%**
Shafts	33161	1D	18.9	25.9	21.4	1.1	5.1	2D	19.2	29.7	21.4	0.9	4.2	3D	14.6	123.8	18.0	1.0	5.6	4D	18.9	27.2	24.3	1.1	4.5
		1C	20.6	26.8	22.9	1.0	4.4	2C	15.6	25.9	19.9	1.2	6.0	3C	18.1	23.3	19.7	0.8	4.1	4C	15.3	23.6	20.7	1.1	5.3
								2B	18.2	23.8	20.2	0.8	4.0							4B	17.5	26.2	20.3	1.2	5.9
Levels		A2	17.5	24.7	20.0	1.0	5.0							A4	14.8	26.3	18.2	1.7	9.3						
		B2	17.4	24.5	19.8	1.0	5.1	B3	19.6	32.9	23.0	1.2	5.2	B4	19.5	26.2	21.9	0.9	4.1						
								C3	18.3	24.7	20.5	0.9	4.4	C4	13.6	31.5	20.3	3.0	14.8						
								D3	18.4	29.7	20.6	0.9	4.4	D4	13.6	31.5	19.8	1.0	5.1	D5	18.7	23.6	20.6	0.9	4.4

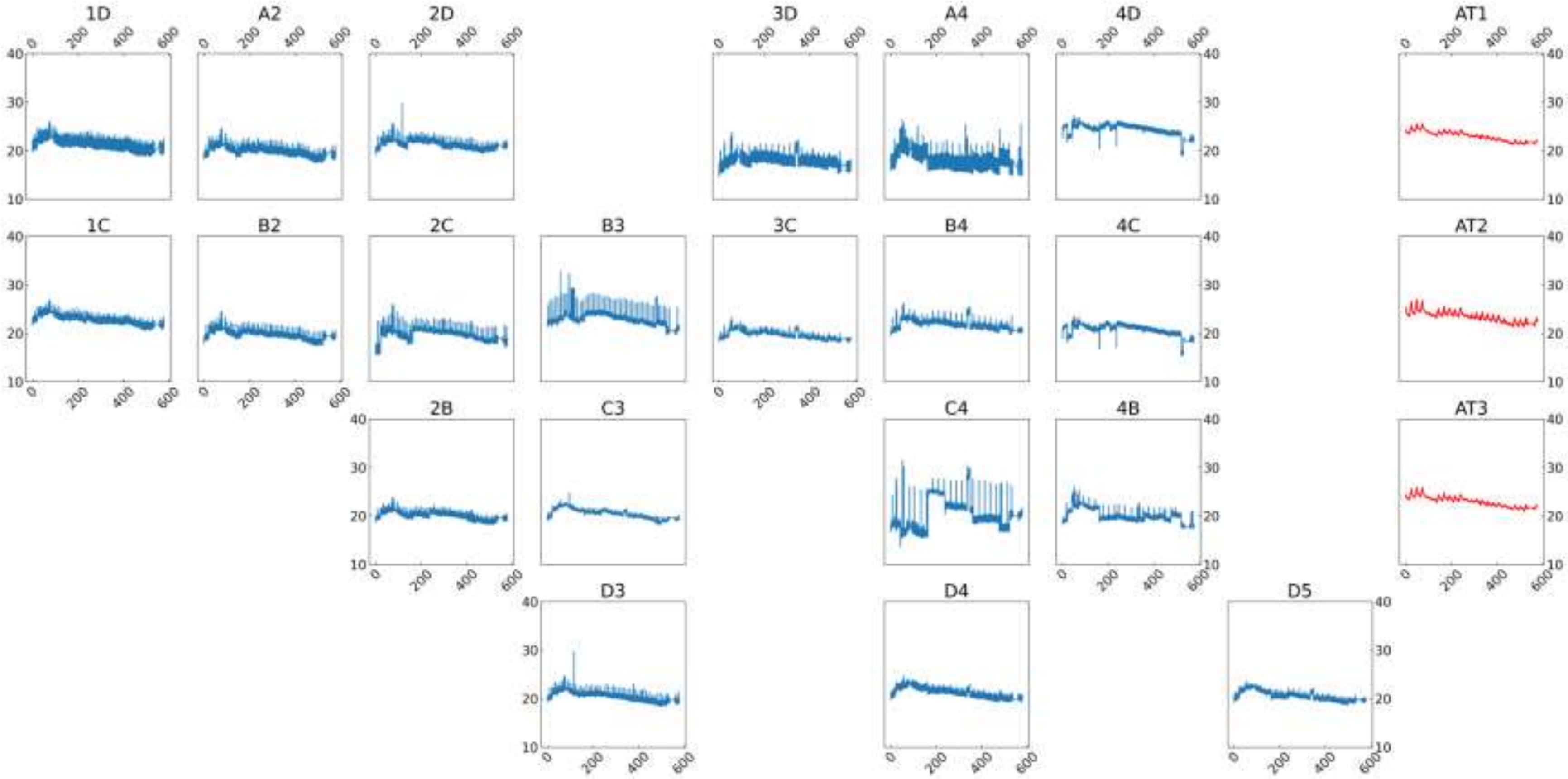

Figure 4.4: Temperature measured against time in hours for experiment 2; the blue represents the temperature inside the model and the red is the ambient air temperature in °C

4.3.3 Experiment 2: Uranine Distribution

At the beginning of the Uranine dispersion experiment, blind samples were taken from the AMM sampling ports to analyse for potential background contamination. These samples were analysed for Uranine, and a 0 µg L^{-1} concentration was recorded for all 36 samples (Figure 4.5a). Therefore, the Uranine tracer with a mass of 31 mg was injected into the AMM through sampling port 2A.

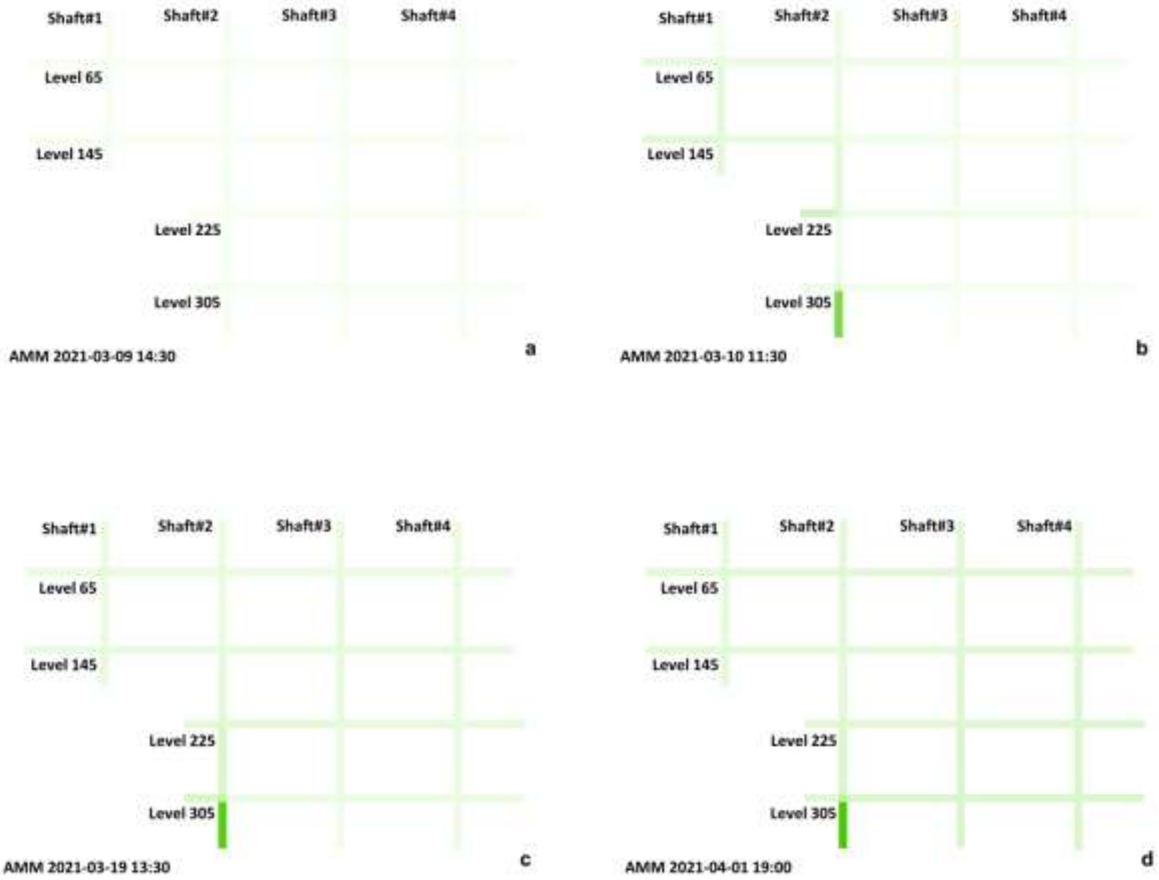

Figure 4.5: Uranine dye distribution in the AMM (a. prior to the commencement of the experiment, b. on the day of the tracer injection (0 h), c. at 218 h, post tracer injection, d. last day of the experiment (535 h))

A gentle build-up of the tracer from low concentrations was observed (Figure 4.7). On the day the tracer was injected, 36 samples were taken immediately after injection and then analysed. The results show that the tracer had diffused to all sections except for sections 4A, 3A, D5 and 4B (Figure 4.5).

Subsequently, the tracer moved only to the upper parts of the AMM. At 22 hours the tracer was detectable in all AMM sections except section 4A. At 51 h, all AMM sections had detectable Uranine tracer concentrations. The highest concentrations were in sections 2A, D2, 2B and C2 with concentrations above 100 µg L^{-1}.

Section 2A was the tracer injection point and had the highest concentration throughout the experiment possibly resulting from tracer within the sampling port after injection or a slow flow around it. 317 hours into the experiment, the tracer had spread throughout the AMM (Figure 4.5c) and was detected at concentrations higher than 50 µg L^{-1} except in the lower sections 4A (44 µg L^{-1}) and 3A (34 µg L^{-1}).

At the end of the experiment (535.5 hours) the tracer had dispersed across all the sections of the AMM, and the tracer concentration had progressively increased to values above 100 µg L^{-1}, except in section 1C (98 µg L^{-1}) where it remained slightly below 100 µg L^{-1}.

From the beginning of the experiment, there was an exponential drop in the dispersion of the Uranine (Figure 4.6) from the point of injection. The tracer was moving from the point of high concentration to a low concentration. Furthermore, the spark lines of experiment 2 indicate that at the end of the experiment, the tracer had reached equilibrium across the AMM (Figure 4.7).

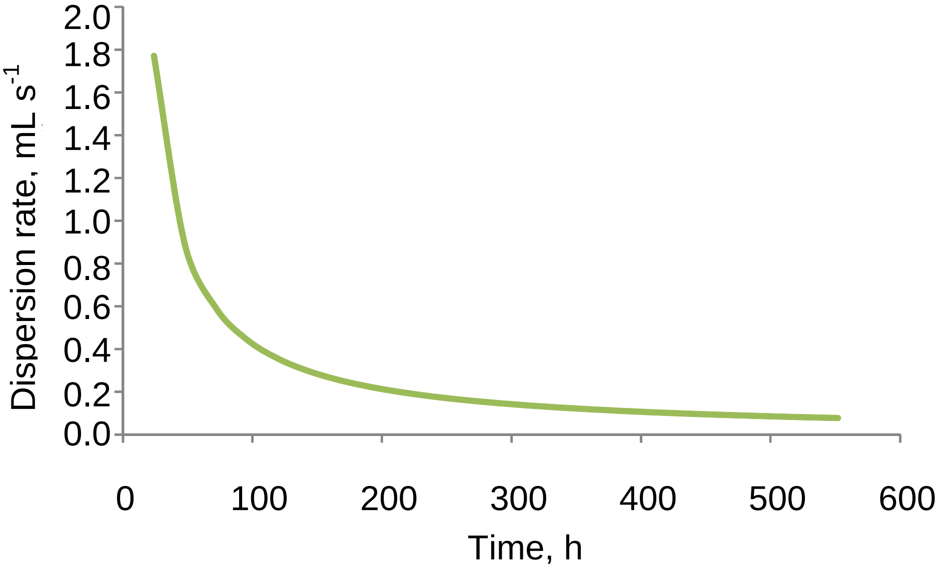

Figure 4.6: Uranine dispersion over the 552 h duration of the experiment

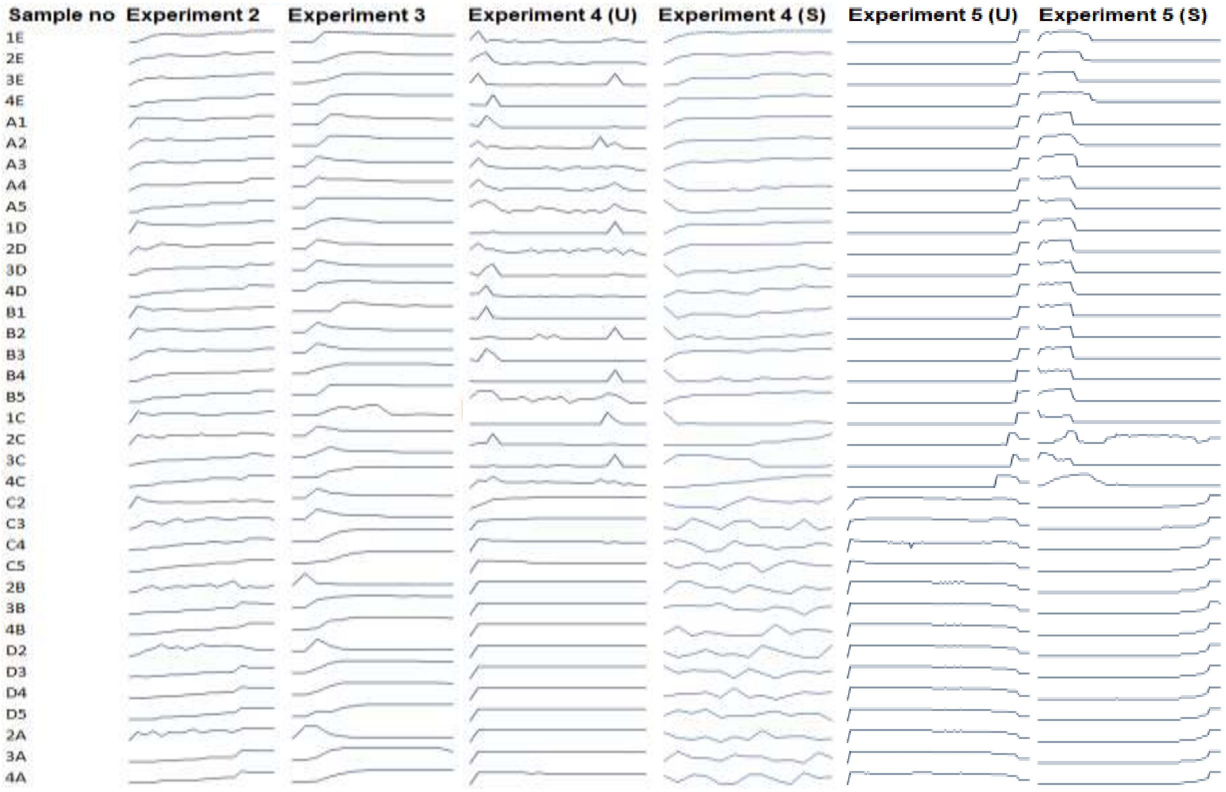

Figure 4.7: Sparklines of the Uranine (U) distribution in experiments 2, 3, 4 and 5 measuring the dispersion rate and Sulforhodamine B (S) distribution introduced in the flushing experiment (4) with small traces extending to experiment 5 in the AMM

4.4 Applying Thermal Gradient to the Analogue Mine Model

4.4.1 Experiment 3: Flow Measurement

An average flow rate of 0.013 m s^{-1} was measured in experiment 3 (Figure 4.8), with a minimum flow rate of 0.012 m s^{-1}. This experiment ran for 384 min, and there were flow measurement fluctuations in the beginning due to the temperature increase in the AMM. Regardless of the temperature increase, the flow rate remained at 0.013 m s^{-1}, similar to the first 2 experiments, running at steady state conditions. The same Reynolds number as in the previous experiments was calculated, thus indicating laminar flow, regardless of obstacles found in the shafts and galleries.

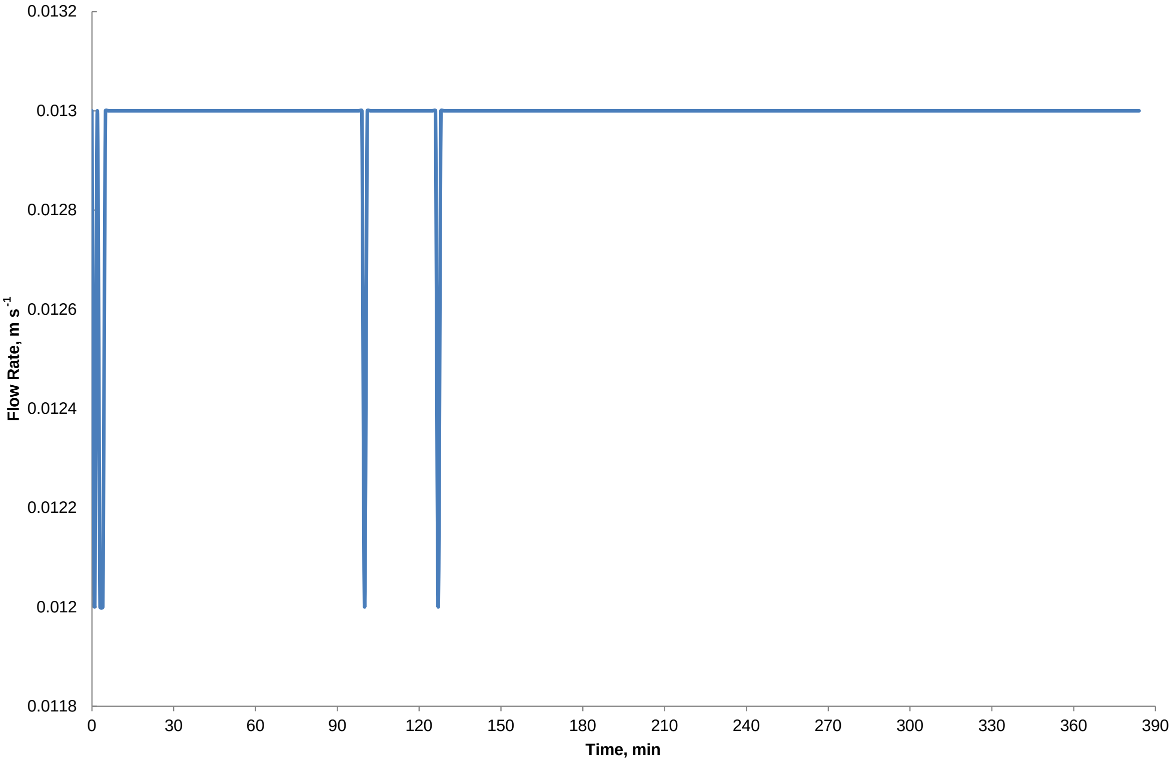

Figure 4.8: Flow rate plotted against time for experiment 3 in the AMM

4.4.2 Experiment 3: Temperature Measurement

Temperatures at locations, AT1, AT2 and AT3 showed different ambient air temperature averages. Location AT2, showed the highest average of 19.3 °C, followed by AT1 (19.2 °C) and AT3 (18.4 °C) (Table 4.5). A general temperature increase existed with room height.

Table 4.5: Statistical values, depicting the minimum, maximum and average values for the room air temperatures in °C

Thermocouple	AT1 (Top)	AT2 (Middle)	AT3 (Lower)
Min	17.9	18.0	17.6
Max	20.2	20.3	18.9
Ave	19.2	19.3	18.4
Std dev	0.6	0.4	0.3
Std dev %	3.3	2.0	1.5

During experiment 3, eight external heat sources (heating foils) were installed at sections 1D, 2A, 3A and 4A of the AMM. One of these heating foils was placed on section 1D thus raising *in situ* water temperature from that point. Shaft #1, section 1C had an average temperature of 18.7 °C and 20.3 °C at section 1D. The raised temperature measured by section 1D results from the heating foil positioned there. Thus, the *in situ* water temperature was warmer at the bottom and colder at the top (Table 4.6). The warm water sank down to section 1C and rising up to the top of the AMM thus forming a convection loop between levels 145 and 65. This observation was similar to that of Bau and Torrance (1981b) or Solodov *et al.* (2002) in their experiments.

Section 2B had the lowest average of the 2 sections, showing 18.6 °C. Section 2C had an average of 20.4 °C, whilst 2D had an average temperature of 20.2 °C; the two shafts showed similar temperatures. Thus the temperature in shaft 2 was increasing upwards, implying that warm water was circulating upward due to the heating foil located at 2A, forming a convective loop between levels 305 and 225 and the upper levels. A development of a convective loop was absent from the interconnected shafts (#1 and #2), very likely due to the variation in the position of the heating foils on each shaft.

An average temperature of 17.8 °C at section 3C and 15.5 °C at section 3D in shaft 3 developed. The lower section comprises of warmer water due to the location of the heating foil at section 3A. Temperature cooled with height towards section 3D. The presence of only 2 thermocouples in shaft #2 makes it difficult to identify a clear temperature distinction in the shaft. Shaft #4 had the lowest average temperature at section 4B (17.7 °C), followed by 4D (18.3 °C) and 4C (18.8 °C). The *in situ* water temperatures in the shaft are almost similar. Although section 4B is located closer to the heat source, the temperature is low due to the influence of the cold water from section D5.

At the beginning of the experiment, the ambient air temperature had a minimum of 18.0 °C, which was higher than the *in situ* water temperatures, which varied between 11.0 and 18.0 °C (Figure 4.9). Regardless of the heating foils being set up to a minimum of 23.0 °C and maximum of 25.0 °C, the *in situ* water temperature never reached 25.0 °C, which could be due to the effect of the room's ambient temperature. However, the maximum temperature varied from 19.0 °C to 23.0 °C. There is a clear indication of an increase in temperature in the AMM, further there is a slight increase in the ambient room temperature from 18.0 °C to 20.0 °C. The temperature fluctuations are due to the data logger sensor's A/D converters and noise.

Table 4.6: Temperature variation in shaft #1, #2, #3 and #4, and levels 65, 145, 225 and 305 in the AMM showing the number of samples, average, minimum, maximum, standard deviation (S.D) and standard deviation % (S.D%) and temperature measurements in °C

	No. of samples		**Min**	**Max**	**Ave**	**S.D**	**S.D%**		**Min**	**Max**	**Ave**	**S.D**	**S.D%**		**Min**	**Max**	**Ave**	**S.D**	**S.D%**		**Min**	**Max**	**Ave**	**S.D**	**S.D%**
Shafts	582	1D	16.1	23.0	20.3	1.3	6.4	2D	16.3	21.9	20.2	1.3	6.4	3D	10.8	18.80	15.5	1.8	11.6	4D	13.7	21.0	18.3	1.5	8.2
		1C	17.6	20.2	18.7	0.5	2.7	2C	16.6	22.0	20.4	1.4	6.9	3C	13.6	19.50	17.8	1.4	7.9	4C	15.4	20.6	18.8	1.2	6.4
								2B	13.6	21.9	18.6	1.9	10.2							4B	13.3	19.9	17.7	1.1	6.2
Levels		A2	14.8	21.0	18.8	1.3	6.9							A4	10.2	21.3	15.9	2.4	15.1						
		B2	14.4	20.5	18.0	1.4	7.8	B3	16.4	21.9	20.1	1.2	6.0	B4	15.0	21.4	19.2	1.3	6.8						
								C3	14.7	20.1	18.3	1.4	7.7	C4	13.0	22.1	19.0	2.2	11.6						
								D3	14.9	21.6	19.2	1.5	7.8	D4	14.9	21.8	19.4	1.4	7.2	D5	15.2	21.5	19.4	1.3	6.7

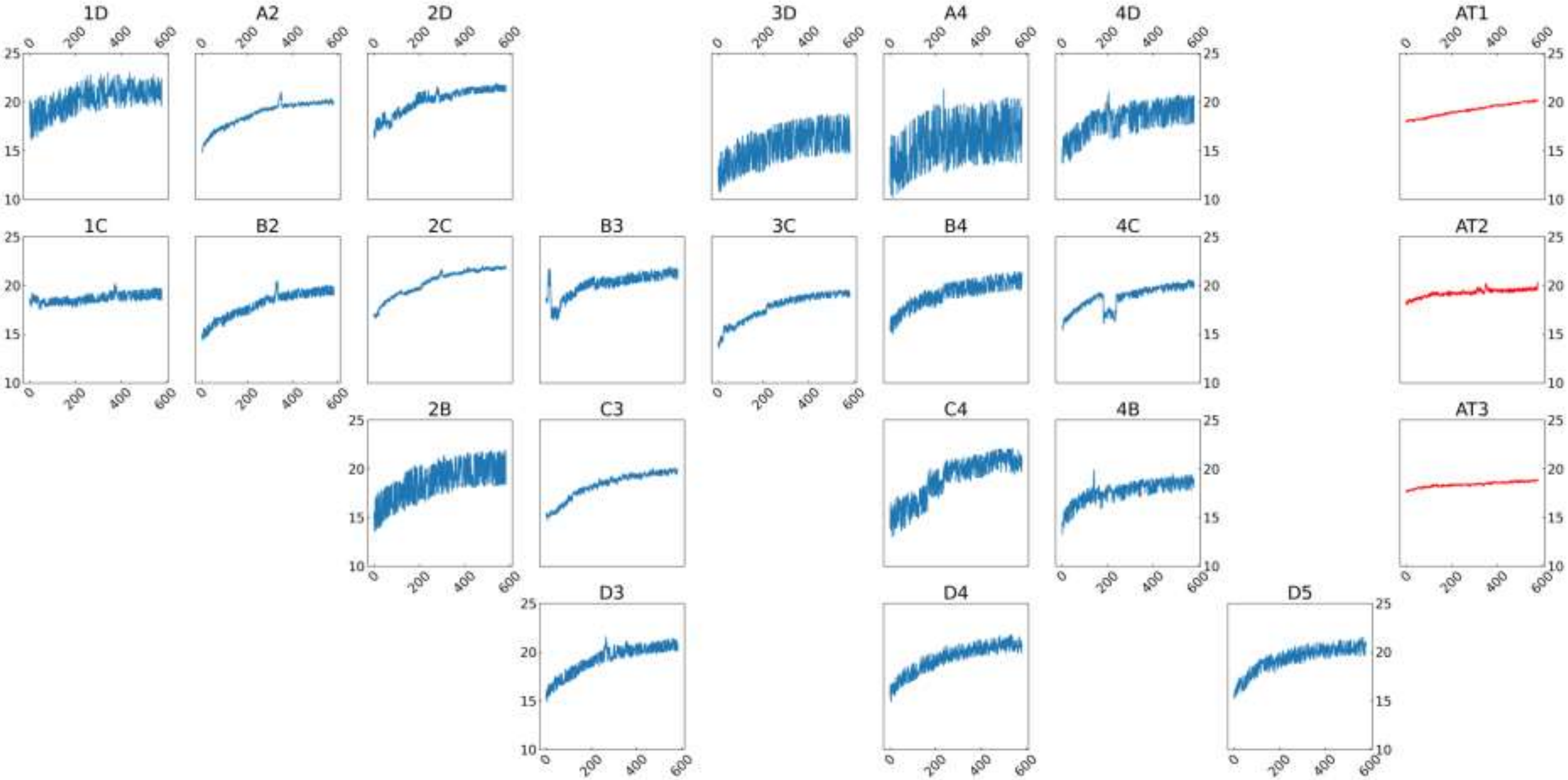

Figure 4.9: Temperature measured against time in hours for experiment 3; the blue represents the temperature inside the model and the red is the ambient air temperature in °C

4.4.3 Experiment 3: Sodium Fluorescein Measurement

Thirty six water samples were collected from the AMM a day before the experiment to examine for background Uranine concentration. All the analysed samples had a concentration of 0 µg L^{-1}; therefore no Uranine from the previous experiment stayed in the AMM (Figure 4.10a). Another set of 36 samples were collected immediately after the Uranine was injected.

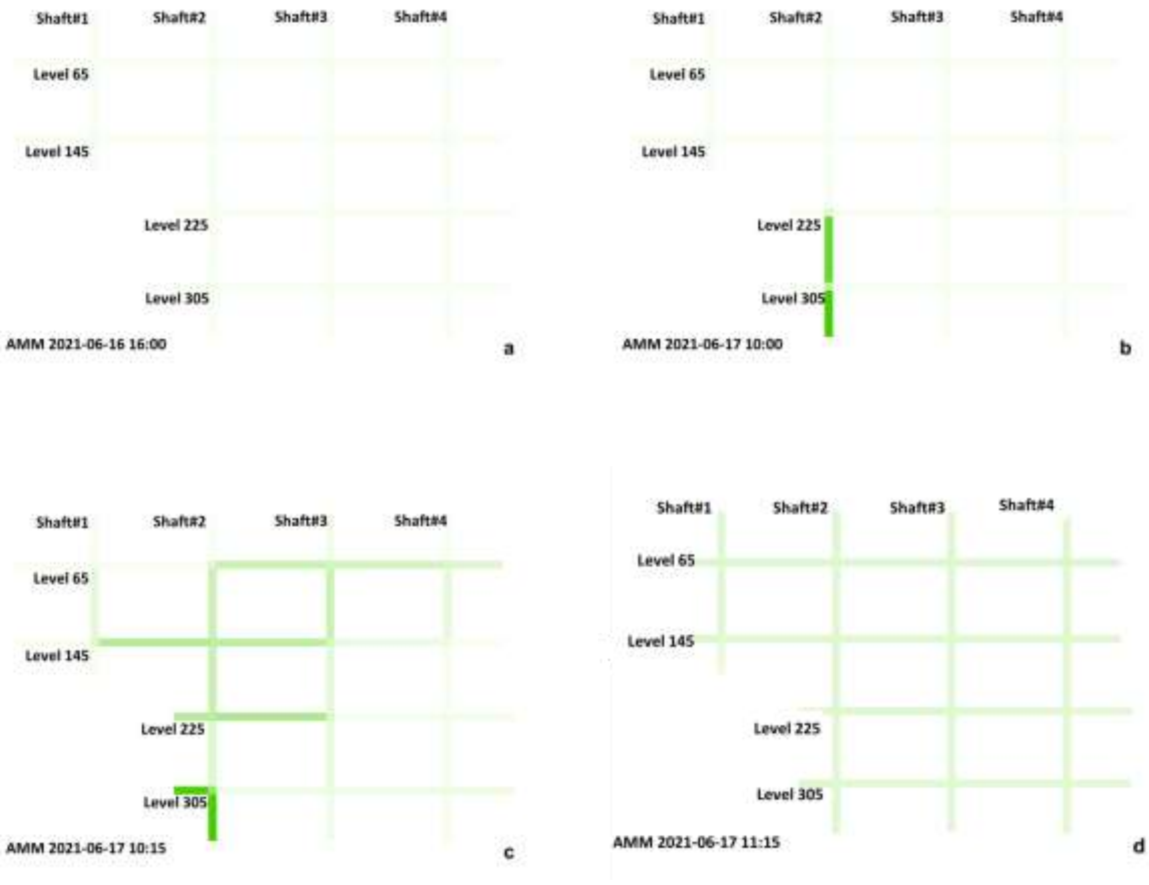

Figure 4.10: Uranine dye distribution in the AMM (a. prior to the commencement of the experiment, b. on the day of the tracer injection, c. 15 min post the tracer injection, d. 75 min post the tracer injection)

At the point of injection (2A), the concentration was above 1000 µg L^{-1}, on section 2B, located above the injection point, the concentration was 814 µg L^{-1} and 11 µg L^{-1}

at 1C. At all other sections, the concentration remained at 0 µg L^{-1} (Figure 4.10b). The tracer had dispersed to most parts of the AMM 15 min later. However, it had higher concentrations at the following sections, 2A (1000 µg L^{-1}), D2 (994 µg L^{-1}), C2 (384 µg L^{-1}), C3 (424 µg L^{-1}), 2C (264 µg L^{-1}), B2 (387 µg L^{-1}), B3 (338 µg L^{-1}), 3C (264 µg L^{-1}), 2D (256 µg L^{-1}), 3D (261 µg L^{-1}), A3 (269 µg L^{-1}), A4 (200 µg L^{-1}) and A5 (134 µg L^{-1}) (Figure 4.10c). The Uranine concentrations remained at 0 µg L^{-1} at sections 1E, A1, A2 and B1.

After 60 minutes, the tracer had equalised throughout the AMM, with the concentration being roughly 100 µg L^{-1}, except for section 1C where it remained at 51 µg L^{-1}. Verification samples were taken 75 min later, to compare the Uranine concentration with the previously obtained results at 60 minutes. All over the model, the results from the two sampling periods were comparable with an exception of section 1C, where the Uranine concentration had risen to 74 µg L^{-1} (Figure 4.10d). The last samples were taken 360 min post the commencement of the experiment, where the concentration had equalised throughout the AMM, with 1C as an exception.

The dispersion rate for experiment 3 was faster (Figure 4.11) than in experiment 2. Within minutes, the Uranine solution had reached equilibrium in all the sections of the AMM. The elevated dispersion rates in experiment 3 are driven by heating from the heating foils. The temperature increase was not enough to initiate flow rate changes; however, it was enough to accelerate the tracer dispersion. A 42.5 cm^3 s^{-1} dispersion rate was calculated 60 minutes post the injection. The dispersion rate is 54 times higher than in experiment 2 running at steady state condition.

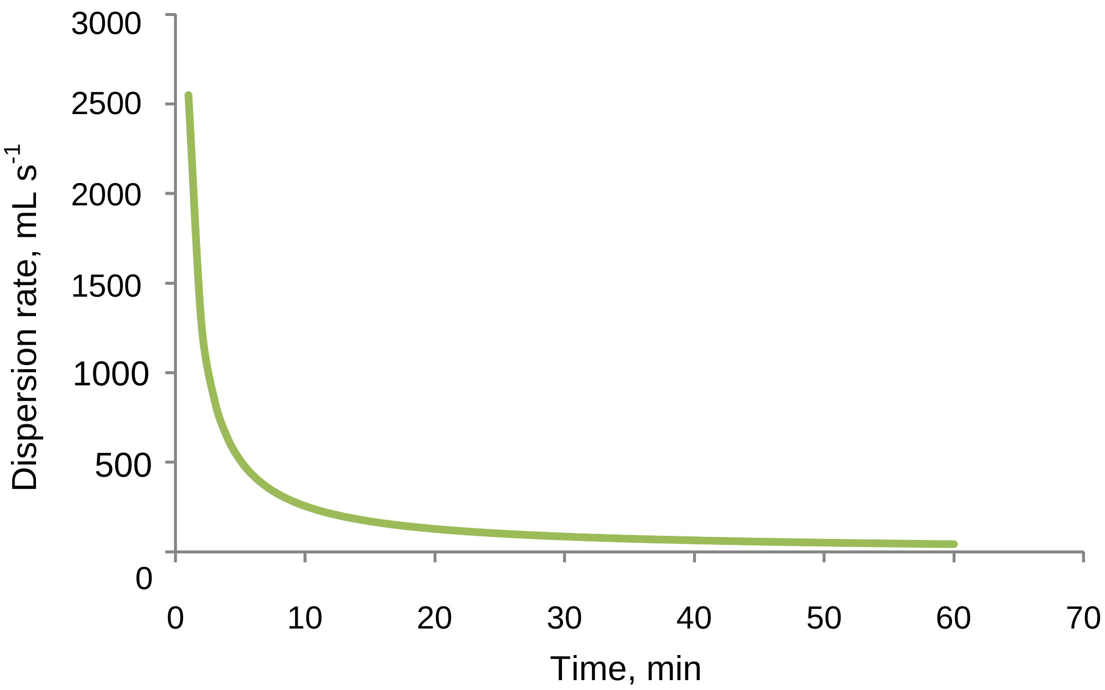

Figure 4.11: Uranine dispersion over the duration of the experiment in minutes

4.5 Stratification Development at Steady State Condition and the Effect of the First Flush in the Analogue Model Mine

4.5.1 Experiment 4: Flow Measurement

Experiment 4 is concluded in two processes where the first part is run at steady state condition. The second part involves flushing the AMM from this steady state condition.

An average flow rate of 0.013 m s^{-1} was recorded during the experiment as observed in the previous experiments (Figure 4.10). A minimum flow rate of 0.006 m s^{-1} and a maximum of 0.014 m s^{-1} were measured. These measurements represent the AMM operating at steady state condition; hence the results are similar to those in experiments 1 and 2.

Furthermore, the average flow resulted in a Re = 61 with a maximum Reynolds number of Re = 66. This implies that the flow remained laminar throughout.

Fluctuations in the results were predominantly due to the data and signal processing between the transducers and the data logger, positioned at section 2B.

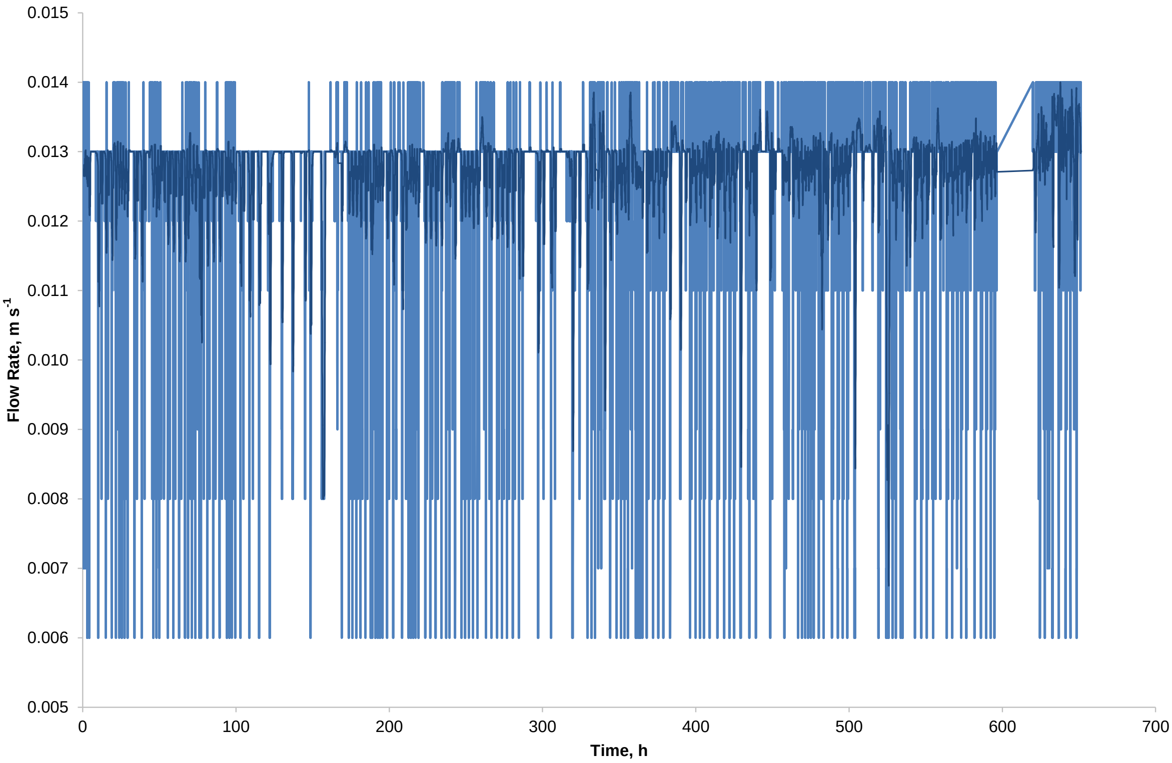

Figure 4.12: Flow rate in the AMM plotted against time for experiment 4

4.5.2 Experiment 4: Temperature Measurement

Experiment 4 took place during the colder winter season. Thermocouple AT1 showed an average temperature of 17.9 °C, AT2 averaged 17.7 °C and AT2 averaged 17.4 °C (Table 4.7). The ambient air temperature was therefore increasing from the bottom to the upper level of the AMM.

During the experiment, section 1C had an average temperature of 17.7 °C, whilst section 1D measured 16.3 °C (Table 4.8). Therefore, the temperature was decreasing from the bottom to the top of shaft #1. In shaft #2 the temperature was showing a general increase from section 2B (14.6 °C), to 2C (16.7 °C) and increasing at 2D (16.0 °C).

Table 4.7: Statistical values, depicting the minimum, maximum and average values for the room air temperatures

Thermocouple	AT1(Top)	AT2 (Middle)	AT3 (Lower)
Min	15.0	14.9	14.9
Max	20.0	22.8	20.4
Ave	17.9	17.7	17.4
Std dev	1.1	1.3	1.0
Std dev %	6.1	7.3	5.7

Furthermore, the temperature was decreasing from section 3C at an average temperature of 14.0 °C to 12.8 °C at 3D in shaft #3. A similar trend that was observed in shaft #2, was observed in shaft 4, the average temperature at section 4B was 14.2 °C, then increased to 15.2 °C at section 4C and then decreased to 14.9 °C (4D). The variations in temperature were due to the constant flushing of the AMM. The lower sections containing brine solution had a more stable temperature whilst the tap water temperature fluctuated.

A similar trend was observed at all the levels in the shaft, where the temperature decreases from the left to the right (shaft #1 to shaft #4) of the AMM. At the lowest level (305), the average *in situ* water temperature increased from D3 (14.9 °C) to D4 (15.4 °C) and decreased to 14.4 °C. At level 225, the average temperature increased from C3 (14.6 °C) to 15.3 °C at C4. Furthermore, the average temperature decreased from B3 (18.2 °C) to B4 (15.7 °C) on level 145. At level 65, the average temperature decreased from A2 (14.8 °C) to A4 (11.9 °C). The room seems to have been colder from the left to the right of the AMM.

The minimum *in situ* water temperature in the AMM ranges between 8.1 °C and 14.0 °C, and the maximum temperature between 16.1 °C and 27.8 °C (Figure 4.13).

The ambient air temperature measured a minimum of 14.9 °C and maximum of 20.8 °C, with a decrease in temperature towards the end of the experiment. Additionally, the temperature in the AMM started to rise before the cessation of the experiment with a similar trend in all sections except at section 4C.

Table 4.8: Temperature variation in shafts #1, #2, #3 and #4, and levels 65, 145, 225 and 305 in the AMM showing the number of samples, average, minimum, maximum, standard deviation (S.D) and standard deviation % (S.D %) in °C

	No. of samples		**Min**	**Max**	**Ave**	**S.D**	**S.D%**		**Min**	**Max**	**Ave**	**S.D**	**S.D%**		**Min**	**Max**	**Ave**	**S.D**	**S.D%**		**Min**	**Max**	**Ave**	**S.D**	**S.D%**
Shafts	40020	1D	13.4	27.8	16.3	1.0	6.1	2D	13.2	24.3	16.0	0.9	5.6	3D	8.1	16.2	12.8	1.1	8.6	4D	10.5	20.1	14.9	1.2	8.1
		1C	14.0	22.9	17.7	1.0	5.6	2C	13.5	21.3	16.7	0.9	5.4	3C	10.5	16.1	14.0	0.8	5.7	4C	8.6	17.2	15.2	1.2	7.9
								2B	10.7	20.8	14.6	1.0	6.8							4B	9.8	21.3	14.2	1.0	7.0
Levels		A2	10.9	19.1	14.8	1.1	7.4							A4	8.2	18.5	11.9	1.1	9.2						
		B2	11.10	23.20	14.51	1.0	6.9	B3	13.5	24.2	18.2	1.4	7.7	B4	11.2	20.0	15.7	1.0	6.4						
								C3	11.3	19.8	14.6	0.9	6.2	C4	11.9	23.9	15.3	1.4	9.2						
								D3	12.4	24.2	14.9	0.8	5.4	D4	9.9	18.6	15.4	0.9	5.8	D5	10.8	17.2	14.4	0.9	6.3

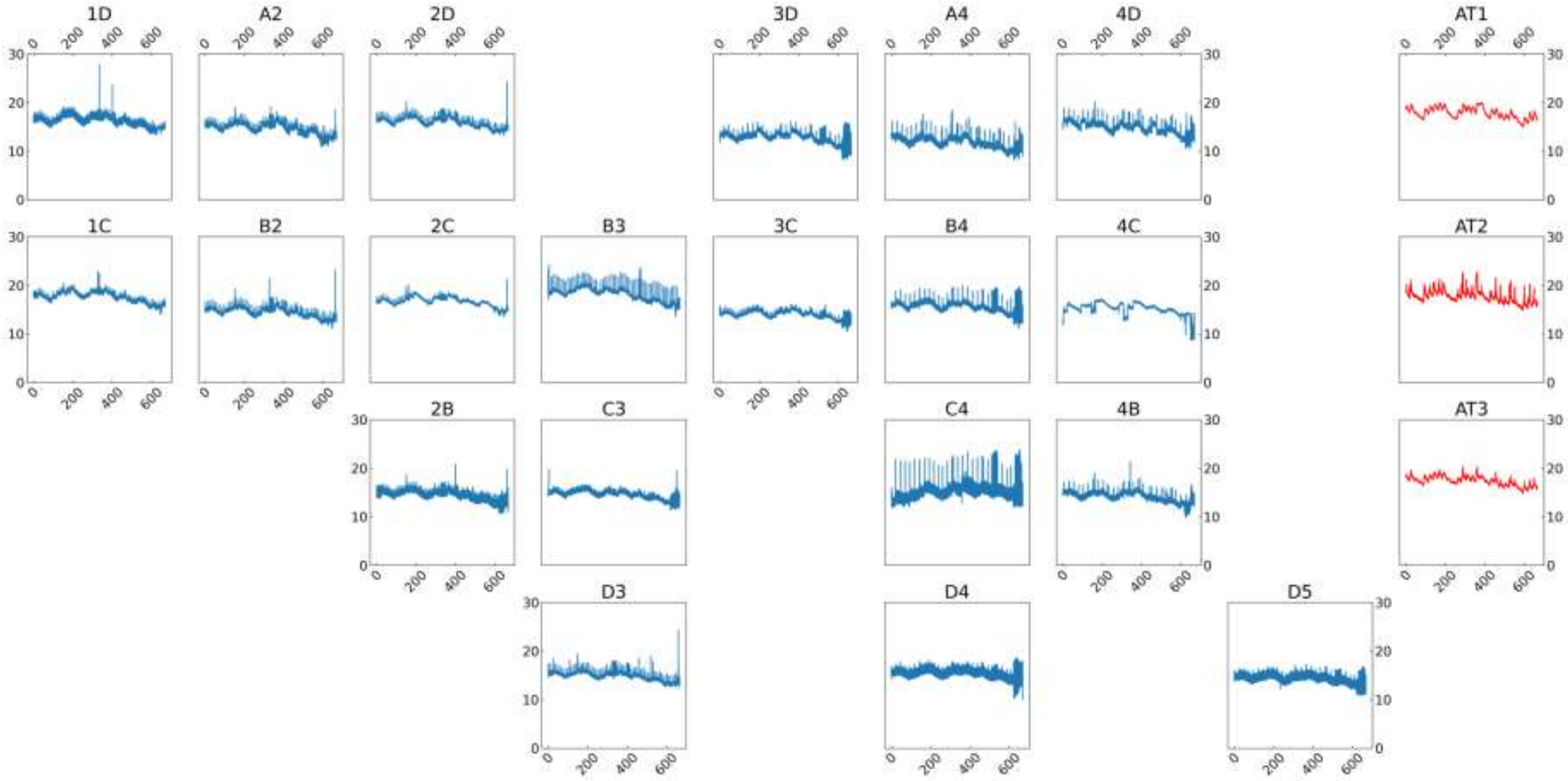

Figure 4.13: Temperature measured against time in hours for experiment 4; the blue represents the temperature inside the model and the red is the ambient air temperature in °C

4.5.3 Experiment 4: Artificial Density Stratification

At the commencement of experiment 4, the AMM was flooded with tap water to level 225 (CF layer). Water samples were taken at all sampling ports of the AMM, up to level 225 to analyse for background Uranine dye prior to the flooding of the AMM with sodium chloride solution containing Uranine (WM layer) (Figure 4.14a). This was carried out to perform quality control, to ensure that no Uranine contamination from the previous experiment existed. In all the sections, the Uranine concentrations ranged between 0.04 and 0.07 µg L^{-1} (Figure 4.13), showing that a small amount of Uranine remained from the previous experiment. This could be neglected, taking into consideration that the subsequent Uranine concentrations remained substantially above these background concentrations.

When the experiment began, the AMM system was flooded with tap water followed by Uranine containing saline solution. This was done to create an artificial stratification with tap water at the top and saline solution in the lower parts. A total number of 36 samples were taken 300 minutes post the flooding of the AMM. The results showed that the AMM maintained the two stratified layers, below and above level 225 (Figure 4.14b). The artificial stratification remained stable days after the commencement of the experiment (Figure 4.14c) conducted at steady state conditions.

Throughout the duration of the experiment, negligible Uranine concentrations were recorded for the upper tap water containing layer and those of the highly mineralised layer maintained roughly at 500 µg L^{-1}. The intermediate layer, between the CF layer and WM layer, namely: C2–C5 had an average Uranine concentration of over 400 µg L^{-1}.

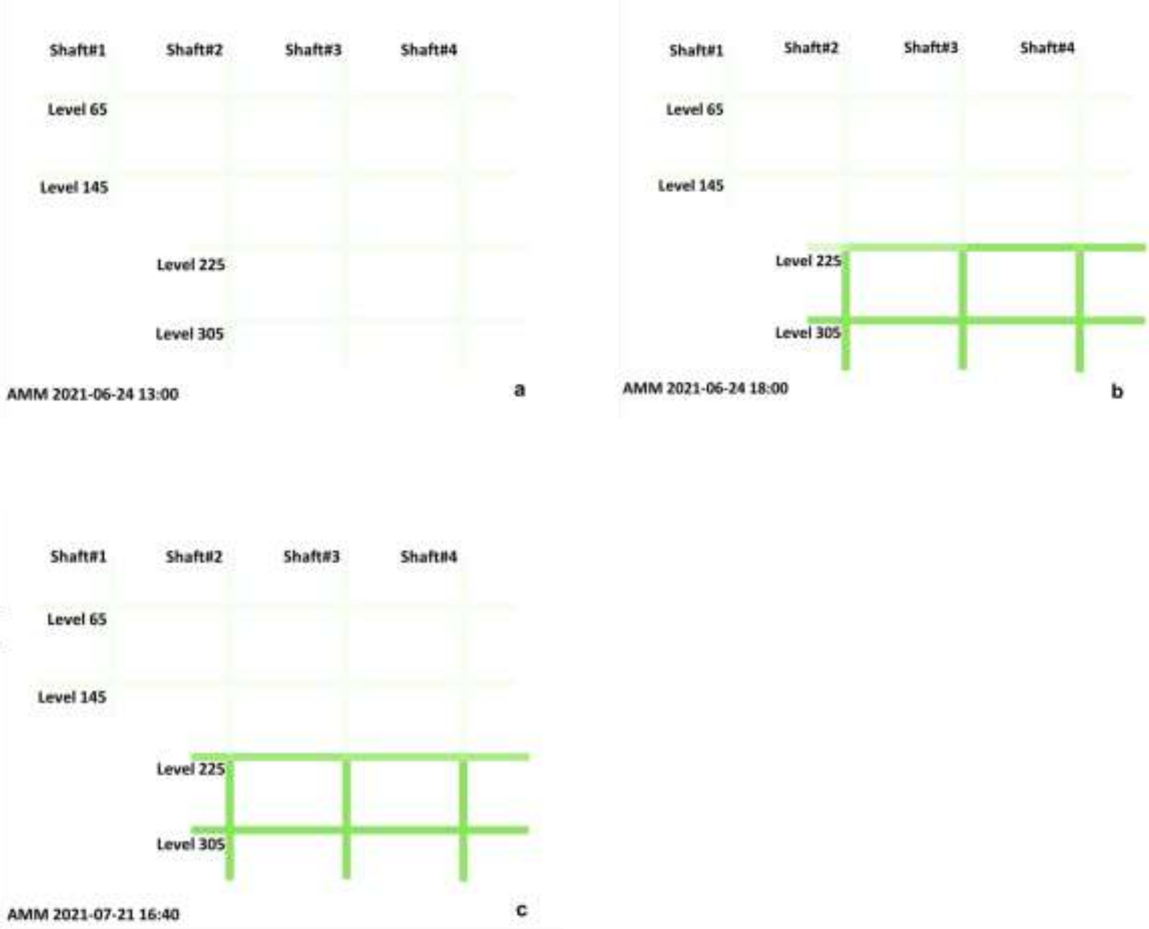

Figure 4.14: Uranine dye distribution in the AMM (a. post the flooding of the AMM with tap water to level 225, b. post the flooding of the AMM, with sodium chloride solution containing Uranine, c. 27 days (652 h) post the flooding and on the day of the flushing)

The density stratification remained stable during the duration of the first part of the experiment, thus no mixing of the CF and WM water bodies was observed. The two water bodies had different densities, the CF layer was 0.998 g cm^{-3} and the WM layer was about 1.065 g cm^{-3}, hence the observation of the stable stratification in the AMM.

Table 4.9: Uranine concentration (µg L^{-1}) in the AMM for experiment 4, depicting the averages for the tap water layer (CF) and the highly mineralised layer, containing sodium chloride (WM), C2–C5 and 2C–4C

Date	Hours	Ave CF	Ave WM	Ave C2–C5	Ave 2C–4C
2021-06-24 13:00	0	0.07	0.07	0.04	0.04
2021-06-24 18:00	5	0.19	541.07	423.07	0.21
2021-06-25 12:00	23	0.38	575.35	469.24	0.23
2021-06-28 11:15	94	0.39	585.95	494.42	0.74
2021-06-29 11:00	118	0.07	581.32	488.56	0.17
2021-06-30 13:00	144	0.06	575.66	480.35	0.14
2021-07-01 13:00	168	0.07	569.34	477.02	0.15
2021-07-02 10:30	190	0.07	574.08	477.69	0.14
2021-07-05 11:30	263	0.07	578.30	485.04	0.17
2021-07-06 10:30	286	0.09	577.39	484.02	0.17
2021-07-07 10:00	309	0.07	572.16	477.40	0.15
2021-07-08 10:00	333	0.09	571.57	477.41	0.17
2021-07-09 13:30	361	0.07	567.21	474.62	0.14
2021-07-12 12:30	432	0.06	570.55	477.67	0.14
2021-07-13 10:30	454	0.06	568.59	475.27	0.10
2021-07-14 12:00	479	0.06	564.94	472.81	0.10
2021-07-15 12:30	504	0.07	576.86	486.86	0.11
2021-07-16 13:15	528	0.09	569.70	475.47	0.16
2021-07-19 15:00	602	0.16	570.17	476.27	0.17
2021-07-20 09:00	620	0.40	571.99	475.95	0.43
2021-07-20 13:41	625	0.06	562.29	466.28	0.09
2021-07-20 15:41	627	0.04	555.62	460.64	0.09
2021-07-20 17:41	629	0.03	551.97	460.13	0.07
2021-07-20 19:41	631	0.02	567.52	473.44	0.04
2021-07-21 10:00	645	0.04	562.82	468.62	0.04
2021-07-21 12:10	647	0.03	555.76	459.64	0.05
2021-07-21 14:10	649	0.03	555.05	460.51	0.04
2021-07-21 16:40	652	0.03	553.45	455.72	0.05

4.5.4 Experiment 4: The Flushing of the AMM

The density stratification in the AMM remained stable for a week, after which Sulforhodamine B dye was injected into the CF layer of the AMM (Figure 4.15a), in preparation for the flushing of the AMM. Thereafter, the AMM was flushed with tap water from the top of shaft #4 at a flow rate of 0.33 L min^{-1}, while the WM layer contained mineralised water. The CF layer had an average concentration of 318 µg L^{-1} of Sulforhodamine B, whilst the WM layer had a concentration of 0.14 µg L^{-1}. The intermediate layer C2–C5 had negligible average concentrations and the intermediate layer 2C–4C showered an average Sulforhodamine B concentration of over 100 µg L^{-1}. Samples taken a day post the tracer injection showed a concentration averaging 296 µg L^{-1} in the CF layer. The tracer had dispersed throughout the CF layer (Figure 4.15b), however was absent in the WM layer proving the stability of the density stratification.

By the 19th day (620 h) of experiment 4, the Sulforhodamine B dye was distributed evenly (Figure 4.15c) with a concentration averaging 346 µg L^{-1} in all sections excluding 2C, which had a concentration of 19 µg L^{-1}. However, the average concentration on the intermediate layer (2C–4C) was 278 µg L^{-1}. The tracer remained undetected in the WM layer, with a concentration close to 0 µg L^{-1} of Sulforhodamine B dye. At 211 minutes post the flushing (Figure 4.15d), the CF layer had a dye concentration of 88 µg L^{-1} and showing a decrease in the Sulforhodamine B dye.

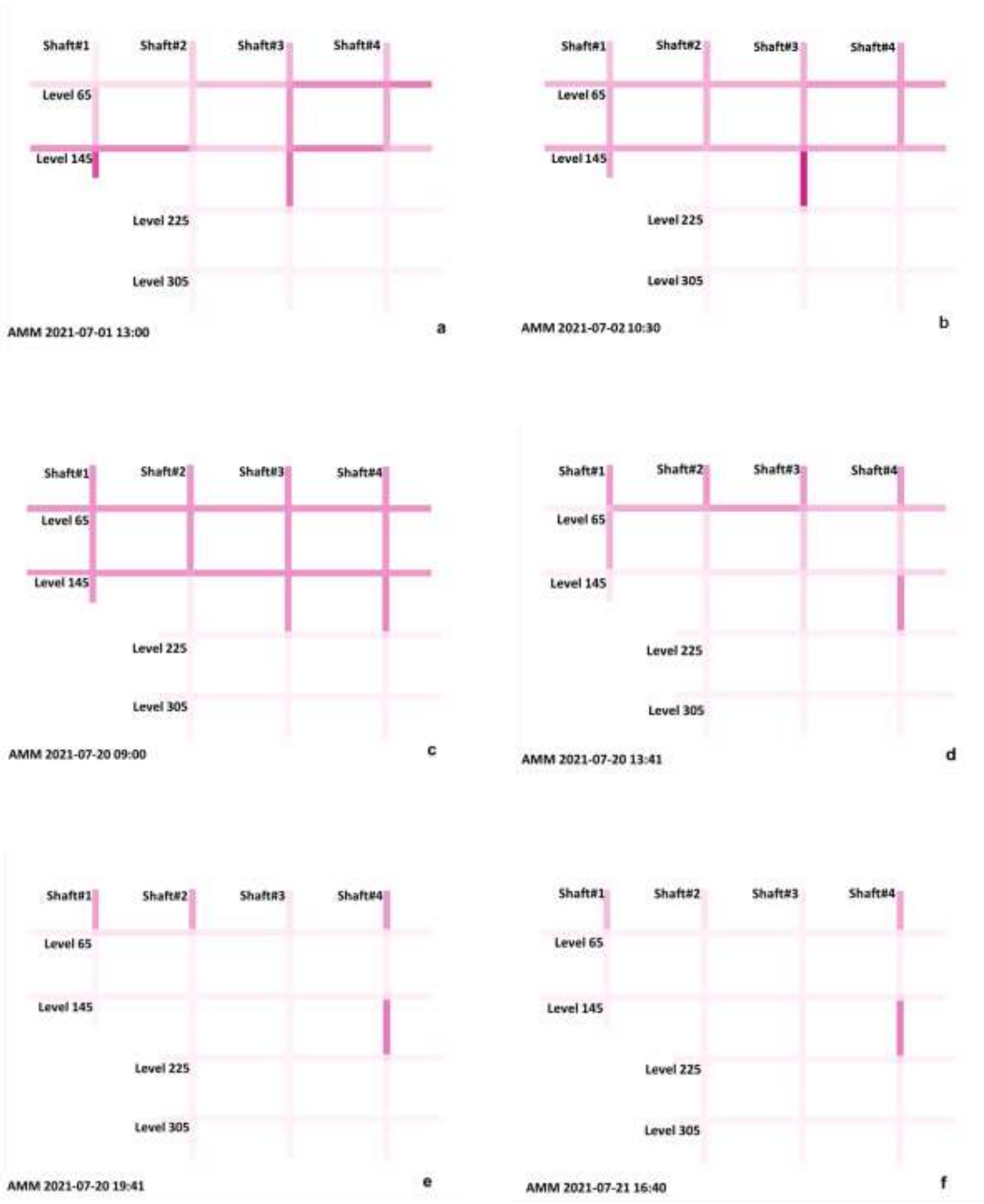

Figure 4.15: Sulforhodamine B dye distribution in the AMM (a. on the day of the injection, b. a day post the injection, c. before the flushing commenced d. 211 min after the flushing commenced, e. 571 min after the flushing commenced and f. at the end of the experiment, when the pump was switched off)

The average dye concentration in the CF layer was 56 µg L^{-1}, recorded 331 min post the commencement of experiment 4 (Figure 4.15e). Post the flushing experiment in the AMM, when the pump was turned off 571 minutes into the experiment (Figure 4.15f), the average concentration still remained at 56 µg L^{-1} for the CF layer, however still with a higher concentration at section 4C.

The AMM still had two stratified water bodies after the flushing occurred, indicating a stable stratification even after the flushing experiment. This was shown by the negligible Sulforhodamine B average concentration in the WM layer. The average for sections 2C–4C remained at 161 µg L^{-1}. At section 4C, Sulforhodamine B was still detected at a concentration of 400 µg L^{-1} regardless of the flushing process. This experiment showed that the analogue model mine flushing was included in all the sections pertaining the CF layer; except for section 4C.

The experiment's breakthrough curve represents a characteristic first flush curve, depicting the concentration of the Sulforhodamine B dye at the discharge point, showing a steady drop in concentration from 110 min to 630 min (Figure 4.16 and Figure 4.17). Nordstrom (2009) and Gzyl and Banks (2007) noticed a similar trend where the sulfate concentration increased with the initial rain and decreased with more rainfall. Cairney and Frost (1975) reported similar first flush occurrences where the sulfate concentration dropped steadily. The consistent concentration decline is interrupted by an unexpected increase between 640 to 680 min and at roughly 750 min. These concentration peaks are very likely related to the influx of Sulforhodamine B rich water flowing from section 4C and 4E. The flushing continued and eventually the concentration dropped until it reached negligible concentrations at the discharge point.

Flushing of the model's CF layer did not have an effect on the stratification in the AMM. Yet, if the discharge position were below or within the lower WM layer, the stratification would have broken down as observed by e.g. Nuttall and Younger (2004).

Figure 4.16: Sulforhodamine B samples taken at 10-minute intervals, showing the decrease in the concentration during the first flush experiment (1st 100 samples out of 114 are shown)

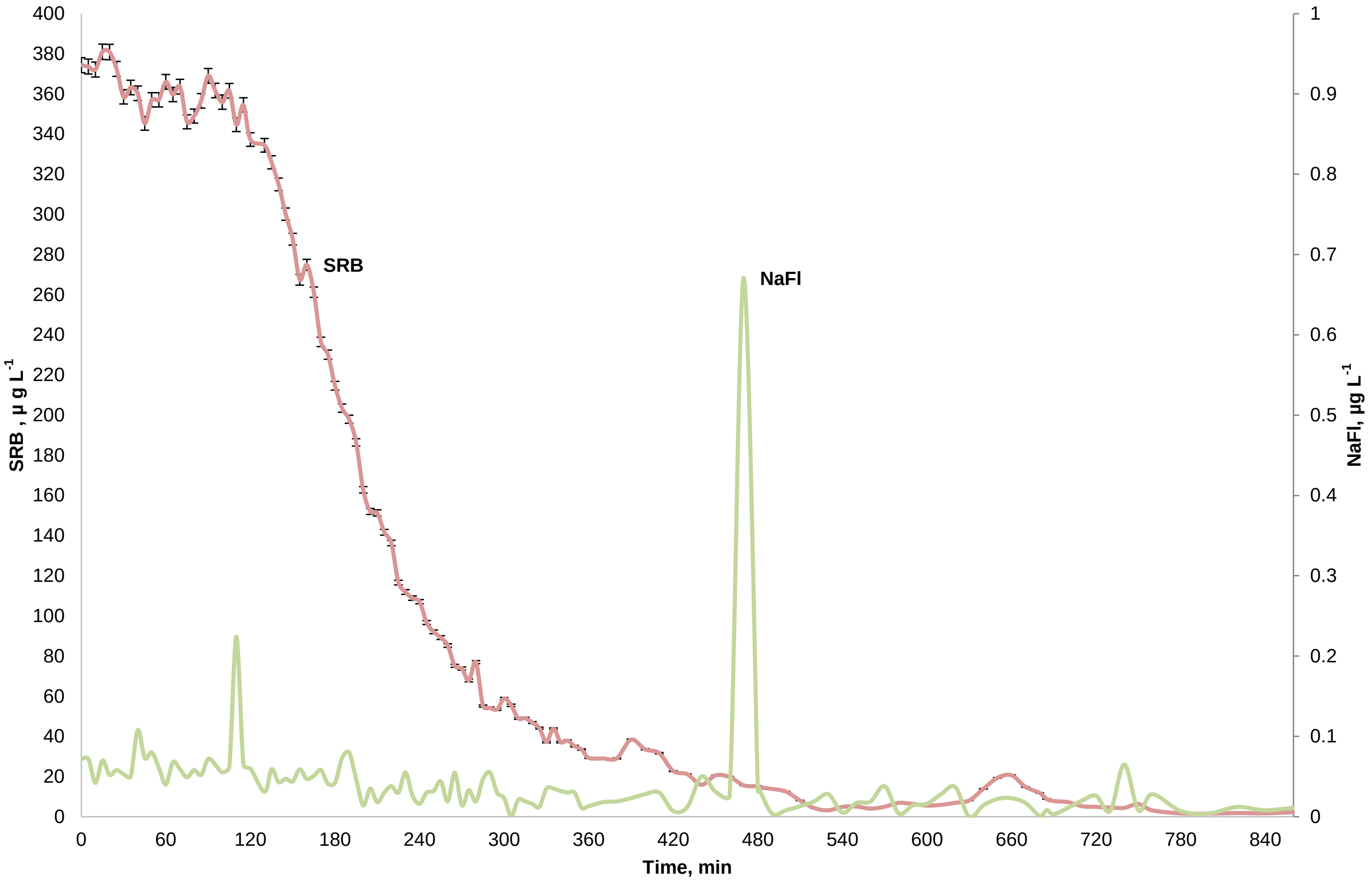

Figure 4.17: Breakthrough curve illustrating the Sulforhodamine B (SRB) and Uranine (NaFl) concentrations (μg L^{-1}) in the AMM vs time (minutes) at the discharge point (section 3E); measurement error ±1%

4.6 Stratification Breakdown due to Temperature Increase in the Analogue Model Mine

4.6.1 Experiment 5: Flow Measurement

Experiment 5 is a continuation of experiment 4 post the flushing with applying heat to the lowest sections of the AMM. Flow measurements were taken with a flow meter located vertically at leg 2B. An average flow of 0.017 m s^{-1} was measured, with a maximum flow of 0.025 m s^{-1} and a minimum flow of 0.006 m s^{-1} (Figure 4.18). At the beginning of the experiment, between 0 and 300 hours, the average flow rate was 0.013 m s^{-1}.

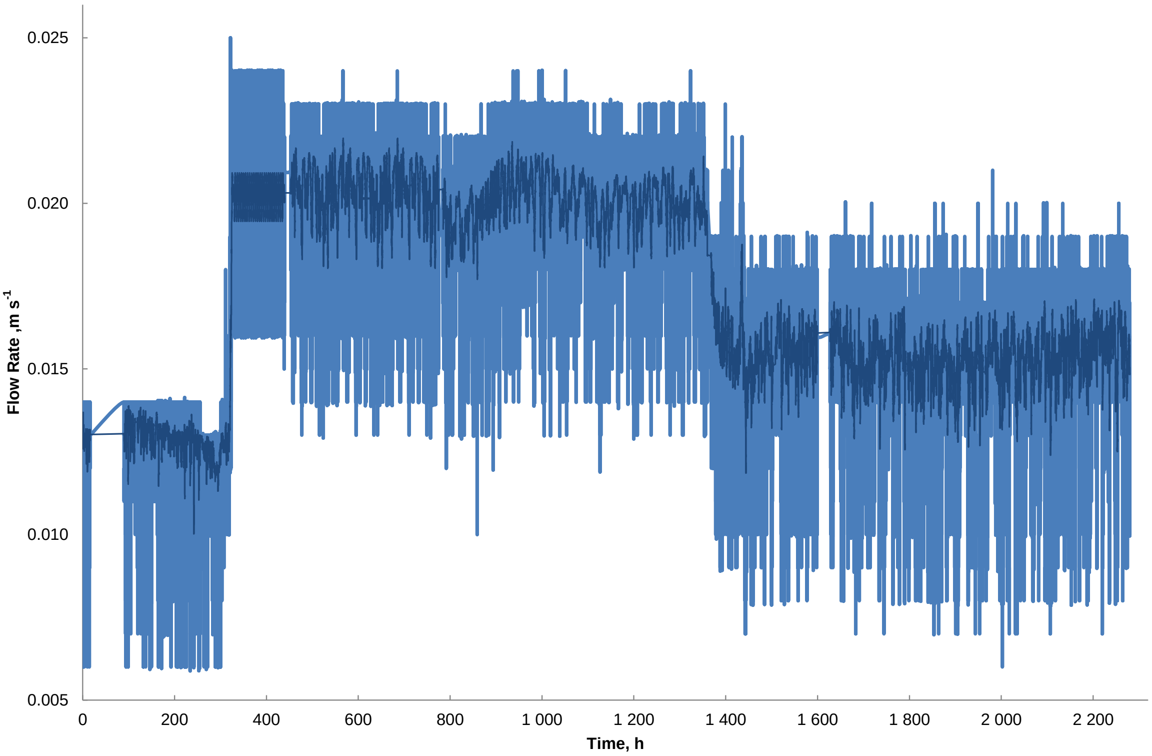

Figure 4.18: Flow rate in the AMM plotted against time; sensor located vertically at section 2B

The temperature of the heating foils was steadily increased from 19 °C by one Kelvin daily until a maximum of 44 °C was reached. A sharp increase in the flow rate from an average of 0.013 m s^{-1} to 0.020 m s^{-1} occurred 300 hours into the experiment, when the heating foil temperatures reached 39 °C. The flow stabilised between 300 and 1360 hours with an average flow of 0.020 m s^{-1}. Then, the flow decreased at 1360 hours to an average flow rate of 0.015 m s^{-1}.

The Reynolds number calculated at 20 °C equals Re = 120, at 25 °C it equals Re = 134 and at 30 °C Re = 150. As revealed by these Reynolds numbers, laminar flow conditions prevailed throughout the experiment at different temperature measurements. Regardless of laminar flow based on the Reynolds numbers, the presence of turbulent flow must not be disregarded, as obstacles in the shafts, such as tubes, cables and other point of connections inside the AMM might interfere with the flow (Wolkersdorfer, 2008; Renz *et al.*, 2009). Fluctuations in the measured flow parameters are characteristic of turbulent flow conditions.

An additional flow meter was installed horizontally at C4 four days post the commencement of the experiment. The flow measurements (Figure 4.19), varied from those taken by the vertically installed meter (Figure 4.18), with horizontal flow rates of 0.001 m s^{-1} to 0.020 m s^{-1} and an average of 0.012 m s^{-1}. This horizontal flow meter was installed while the experiment was on going. Due to the daily adjusted temperature, the heating foils were set between 21/22 °C when this particular flow meter was installed. A 0.008 m s^{-1} average flow rate was measured from 0 to 205 hours later.

Between 200 and 1300 hours, the flow rate increased and remained constant at an average of 0.015 m s^{-1}, mirroring the vertical flow rates. Thereafter, the flow rate decreased at 1300 hours, averaging 0.010 m s^{-1} and remained constant until the end of the experiment. Although the vertical meter reported higher flow rates compared to the horizontal flow meter, the patterns of both meters are very similar.

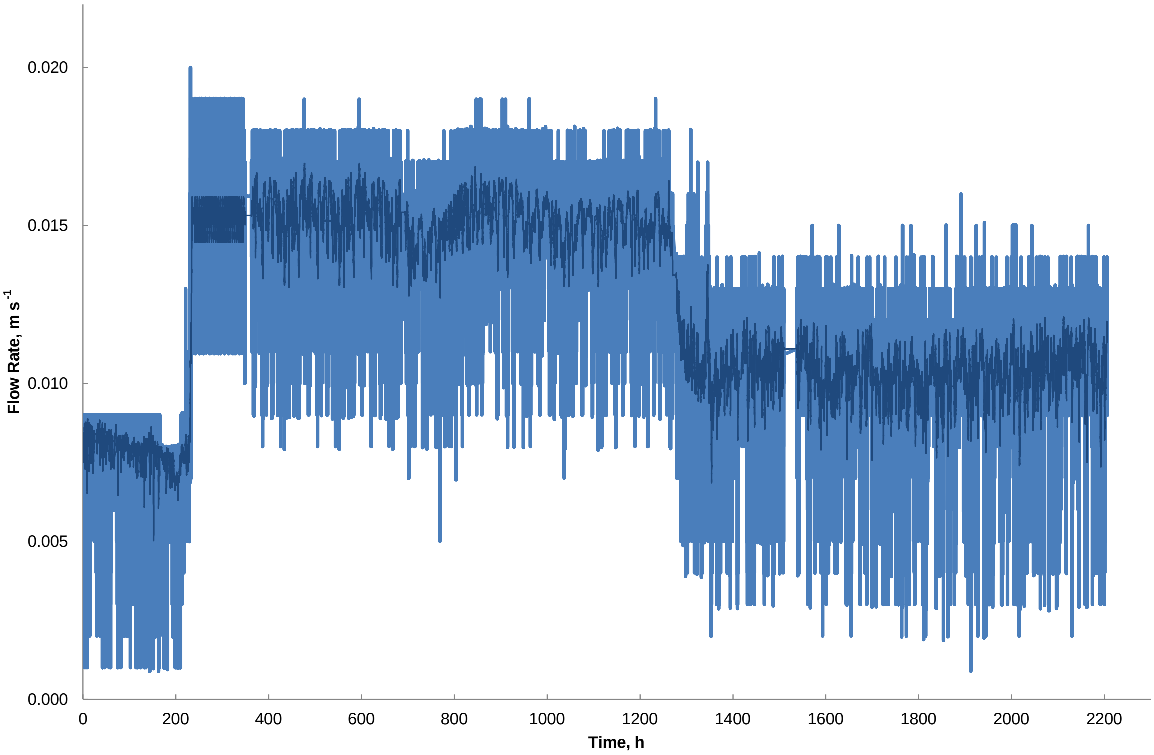

Figure 4.19: Flow rate in the AMM, plotted against time; sensor located horizontally at section C4

Reynolds numbers at 20 °C were Re = 72, at 25 °C it was Re = 86 and at 30 °C it was Re = 89. This is indicative of laminar flow in the AMM. However, as discussed before, this does not rule out the presents of turbulent flow resulting from obstacles present in the shafts and galleries and indicated by the fluctuating flow rates and temperatures.

The vertical flow rates in the shafts of the AMM seem to be higher than the horizontal flow rate in the AMM's galleries. Temperature increase and differences in density induce free convection resulting from buoyant warm water, thus resulting in heat and mass diffusion and possibly further accelerating the flow rate (Berthold & Börner, 2008). Therefore, the temperature increases, indicative for a quasi-geothermal gradient aided in increasing the average flow rate from 0.013 m s^{-1} in previous experiments at steady state conditions to 0.017 m s^{-1} in the AMM's vertical sections.

The additional flow meter to measure the horizontal flow rate was installed late in the experiment, thus there was no data to compare this with at steady state conditions.

4.6.2 Experiment 5: Temperature Measurement

For experiment 5, the heating foils were switched on, and the temperature was increased gradually (Figure 3.6) for the duration of the experiment. Furthermore, ambient temperature was measured and average temperatures calculated for AT1, AT 2 and AT3 as 22.0 °C, 21.7 °C and 21.0 °C, respectively (Table 4.10). As seen by the averages, the temperature is increasing and decreasing upward, resulting in colder temperatures at the top.

Table 4.10: Statistical values, depicting the minimum, maximum and average values for the ambient air temperatures calculated from date measured over the duration of experiment 5

Thermocouple	**AT1 (Top)**	**AT2 (Middle)**	**AT3 (Lower)**
Min	14.8	14.4	14.4
Max	29.0	28.9	28.2
Ave	22.0	21.7	21.0
Std dev	2.9	3.1	2.9
Std dev %	13.2	14.3	13.8

In shaft #1, the average temperature shows a vertical increase from the lower section 1C (23.9 °C) to the upper section 1D (25.3 °C), with a maximum of 39.4 °C at both sections (Table 4.11). This vertical temperature increase is related to the cold water sinking down to 1C, resulting from the positioning of the heating foil located at section 1D. Less dense warm water at section 1D was then moving upwards and the cold water at section 1C was too heavy to mix with the water at the top. Furthermore, the lowest minimum temperature was recorded at section 1D (3.3 °C), followed by section 1C (10.6 °C).

In shaft #2, the average temperature decreased from section 2B (31.7 °C), to 2C (30.8 °C) and lastly to 2D (26.2 °C). Therefore, the AMM was warmer at the bottom than at the top, due to the heating foils located at the lowest sections of the AMM. The maximum temperatures varied, with the highest one of 44.1 °C at 2C, followed by 41.4 °C at 2B and lastly 37.1 °C at section 2D.

Shaft #3 temperatures averaged 29.7 °C in section 3C and 22.7 °C in section 3D. Therefore, the temperature in this shaft was also increasing from the bottom of the AMM to the top, again due to the heating foils located at the bottom of the shaft. The highest maximum temperature was obtained at the lower section closer to the heating foils, and consequently the lowest minimum value was obtained on section 3D.

Two heating foils were also installed at the bottom of shaft #4, measuring warmer water of 30.7 °C at section 4B, directly above the heating foil. The uppermost temperature at section 4D had an average temperature of 25.4 °C. Section 4C had the highest maximum temperature of 42.4 °C in the shaft.

In the lowest level of the AMM (305), average temperatures were 31.9 °C (D3), 33.5 °C (D4) and 32.4 °C (D5), thus the warmest section in this level is D4. The lowest level of the AMM is overlain by level 225, showing average temperatures of 31.4 °C at C3 and 31.5 °C at C4. Therefore, the warmest conditions were observed towards the right side of the AMM. Level 145 showed temperatures of 24.3 °C (B2), 27.7 (B3) and 25.6 °C at B4. Section B3 was the warmest of the 3, followed by B4 and lastly B2.

The low *in situ* water temperature measured in B2 might be a result from the influx of cold and dense water from section 1C. Level 65 had average temperatures of 24.8 °C (A2) and 22.5 °C at A4. Warmer *in situ* water temperatures prevailed on the left side of the AMM resulting from heating foils located at section 1C. The AMM temperature is lower at the top and higher at the bottom. These temperature differences are due to the heating foils placed at the lowest parts of the AMM.

Ambient temperature ranged between 14.4 and 14.8 °C and a maximum between 28.2 and 29.0 °C (Figure 4.20). The temperature increased gradually from the day the experiment commenced and 800 hours later, when the temperature temporarily decreased abruptly, followed by a steady increase again. The temperature remained stable until days before the end of the experiment, when a gradual decrease occurred. A similar temperature trend was observed in the *in situ* water temperature, regardless of the maximum temperature, ranging between 35.7 and 45.0 °C and minimum temperatures, ranging between 2.7 and 14.7 °C.

At all the sections the temperature starts off low and increases constantly as a result of heating. In the two lower levels, 305 and 225, holding warm mineralised water, the temperature had a similar trend. This trend was characterised by a constant temperature increase followed by an abrupt decrease. A sharp temperature drop was first observed in section 4B in shaft #4 at about 800 hours after the experiment started then followed by section 2B, in shaft #2, about 1358 hours after the start. Thereafter, the temperature increased steadily then remained constant until the end of the experiment.

The temperature trend in levels 225, 145 and 65 differs from one another. In level 145, the temperature increased and then plateaued over a longer period for sections 2C, B3, 3C, B4 and 4C. This was followed by a short-lived sharp increase and another drop, which itself is succeeded by an increase in temperature and then remained constant until the end of the experiment.

Table 4.11: Temperature variation in shafts #1, #2, #3 and #4, and levels 65, 145, 225 and 305 in the AMM showing the number of samples, average, minimum, maximum, standard deviation (S.D), standard deviation % (S.D%) and temperatures in °C

	No. of samples		**Min**	**Max**	**Ave**	**S.D**	**S.D%**		**Min**	**Max**	**Ave**	**S.D**	**S.D%**		**Min**	**Max**	**Ave**	**S.D**	**S.D%**		**Min**	**Max**	**Ave**	**S.D**	**S.D%**
Shafts	137973	1D	3.3	39.4	25.3	7.0	27.7	2D	13.1	37	26.3	6.2	23.6	3D	5.8	32.3	22.7	5.4	23.8	4D	10.0	38.0	25.4	6.8	26.8
		1C	10.6	39.4	23.9	5.8	24.3	2C	14.7	44	30.8	7.6	24.7	3C	11.1	42.7	29.7	7.0	23.6	4C	11.7	42.4	30.7	8.4	27.4
								2B	10.4	41	31.7	4.7	14.8							4B	12.7	40.2	30.7	5.1	16.6
Levels		A2	2.70	35.7	24.8	6.3	25.4							A4	6.9	39.1	22.5	6.8	30.2						
		B2	10.8	37.1	24.3	5.9	24.3	B3	14.4	39.1	27.7	4.9	17.7	B4	10.6	36.1	25.6	5.2	20.3						
								C3	10.6	41.0	31.4	6.7	21.3	C4	11.1	44.6	31.5	6.3	20.0						
								D3	13.4	44.4	31.9	4.6	14.4	D4	9.8	45.0	33.5	5.1	15.2	D5	11.8	42.7	32.4	4.6	14.2

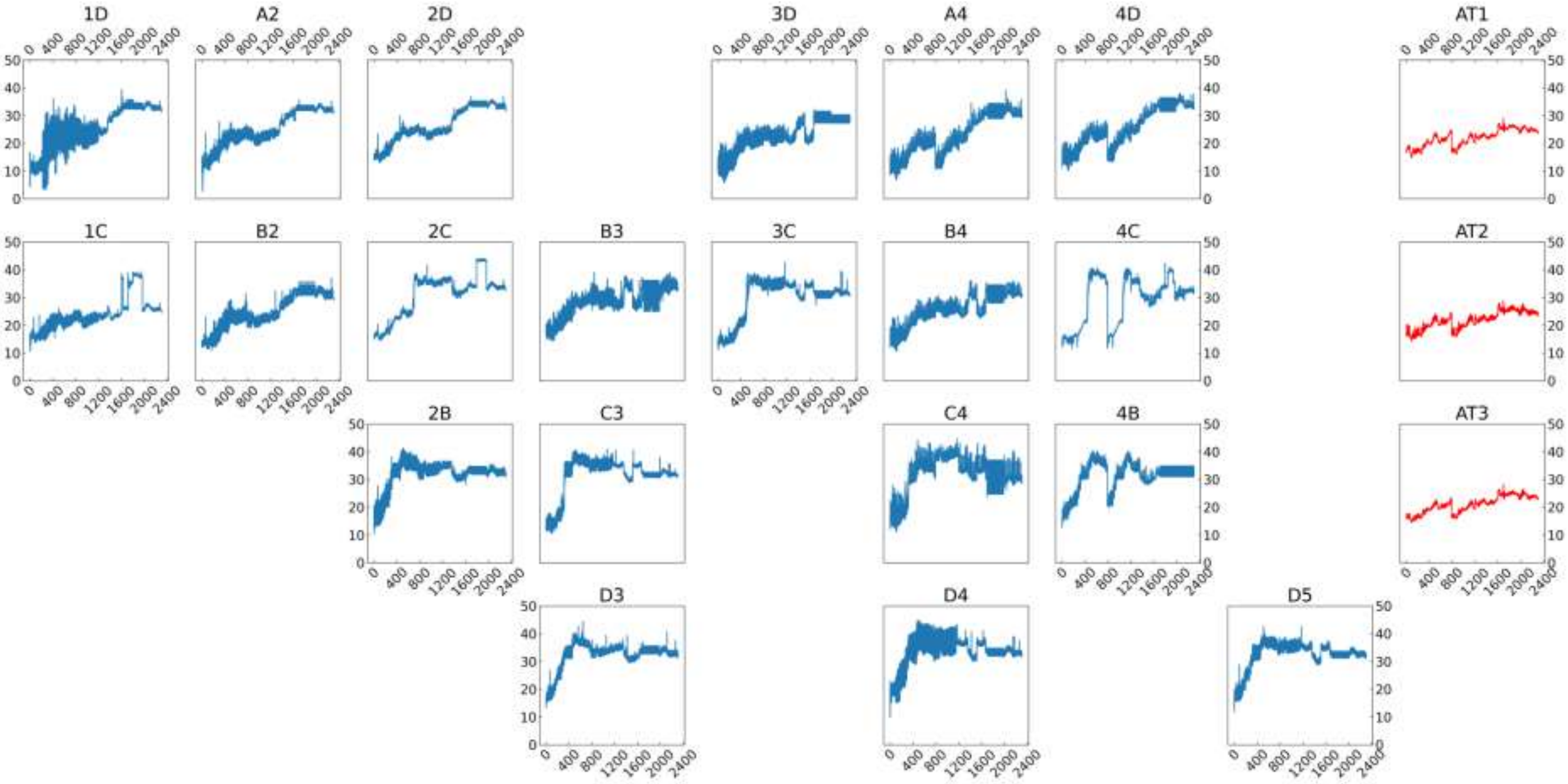

Figure 4.20: Temperature measured against time in hours for experiment 5; the blue represents the temperature inside the model and the red is the ambient air temperature in °C, with a visible stratification disintegration at 768 h in shafts #3 and #4 and a complete stratification breakdown at 1488 h in all the shafts except shaft #1, depicting typing typical sump conditions

Sections 1C and B2 in level 145 behaved differently from the other sections on the same level. Temperature increased steadily in section 1C for most part of the experiment, then 1600 hours after, the temperature increased abruptly. This may be related to the advective or diffusive flow of warm water from the above lying section 1D, where the heating foils are located. Section B2 is also an exception, as the temperature increased constantly, and then dropped gradually at around 800 hours, then started to gradually increase at around 1400 hours and thereafter it dropped again gradually. This resulted from the mixing of the water from 1C, A2 and 2C, with varying temperatures.

In the uppermost level of the AMM, the trend of the temperature at sections 1D, A2 and 2D, varied from sections 3D, A4 and 4D. In sections A2 and 2D, the temperature increased constantly and dropped slightly at 800 hours, and thereafter, it increases until the end of the experiment. A similar trend was observed at section 1D, where the heating foil was located. Furthermore, a similar trend in the temperature development was observed at sections A4 and 4D, where the temperature increased constantly with the increase in temperature from the heating foils. Roughly 800 hours later, there was a drop in temperature and thereafter a gradual increase.

Shaft #4 with sections 4D, 4C and 4B saw a drop in temperature at around 800 hours throughout. At section 3D, the temperature increased gradually and then decreased at around 1200 hours into the experiment. Later, the temperature suddenly increased and around 1450 hours later it decreased again. Shortly after, the temperature increased and stabilised, and remained constant to the end of the experiment beyond 1600 hours. This indicates that the water in the AMM at the end of the experiment had a constant temperature; the water temperature was neither increasing nor decreasing.

4.6.3 Experiment 5: Uranine Distribution

Experiment 5 is a continuation of experiment 4, and in this instance, the heating foils were operated at varying temperatures. By the end of experiment 4, two stratified water bodies were still evident in the AMM and were used in experiment 5 (Figure 4.21a). An average Uranine dye concentration of 549 µg L^{-1} was measured in the WM layer, and the CF layer averaged a negligible concentration (Figure 4.22) (Table 4.12). Intermediate layers C2–C5 had an average Uranine dye concentrations of 402 µg L^{-1}, while 2C–4C had a negligible concentration. These results proved that stratification from experiment 4 still existed, and the heating foils set at a temperature between 19 and 20 °C did not influence the stratification of the CF and WM layers.

Incremental temperature increase of the heating foils in experiment 5 initially showed no effect on the Uranine dye concentration implying that the stratification was still stable. However, when the temperature of the heating foil was increased to 43–45 °C, the average Uranine dye concentration in the intermediate layer (2C–4C), increased from 0 µg L^{-1} to 5 µg L^{-1}.

A small trace of the Uranine dye was visible in the CF layer, with a 2 µg L^{-1} average concentration. At 480 hours of the experiment, the Uranine dye concentration in the WM layer had decreased to 492 µg L^{-1}, thus resulting in the dispersion of the WM water into shaft #4 (Figure 4.21b). 457 hours post the commencement of the experiment, the Uranine concentration at section 2C increased from 0 µg L^{-1} to 11 µg L^{-1}. The average concentration increased gradually to 445 µg L^{-1} 789 hours later in the WM layer (Figure 4.21c). The average Uranine dye concentration in the

CF layer also increased steadily and decreased in the WM layer, with the standard deviation using the averages for the four layers getting smaller.

At 1030 hours, the average Uranine concentration reached 423 µg L^{-1} at section 3C resulting from the dispersion of the highly mineralised water (Figure 4.21d). Consequently, the average Uranine concentration in the CF layer increased to 55 µg L^{-1} and to 306 µg L^{-1} in the 2C–4C layer and furthermore, the standard deviation for all four layers decreased to 160 µg L^{-1}.

At 1372 hours the tracer was visible in sections B4, B5 and 1C with a concentration over 200 µg L^{-1} (Figure 4.21e). Average concentrations were increasing in both the CF and 2C–4C layers and decreasing of the WM and C2–4C layers resulting in a further decrease in the standard deviation to 107 µg L^{-1}.

On the last day (2303 h), an even distribution of the Uranine dye was observed in the AMM (Figure 4.21) with concentrations above 200 µg L^{-1} in all sections of the AMM, and the standard deviation for all the layers combined was 1 µg L^{-1}. Deterioration of stratification in the AMM was promoted by the heating in the lower sections of the model mine. Warmer solution rose to the upper parts of the AMM resulting in convective mixing of the two water bodies indicating free convection resulting from buoyancy.

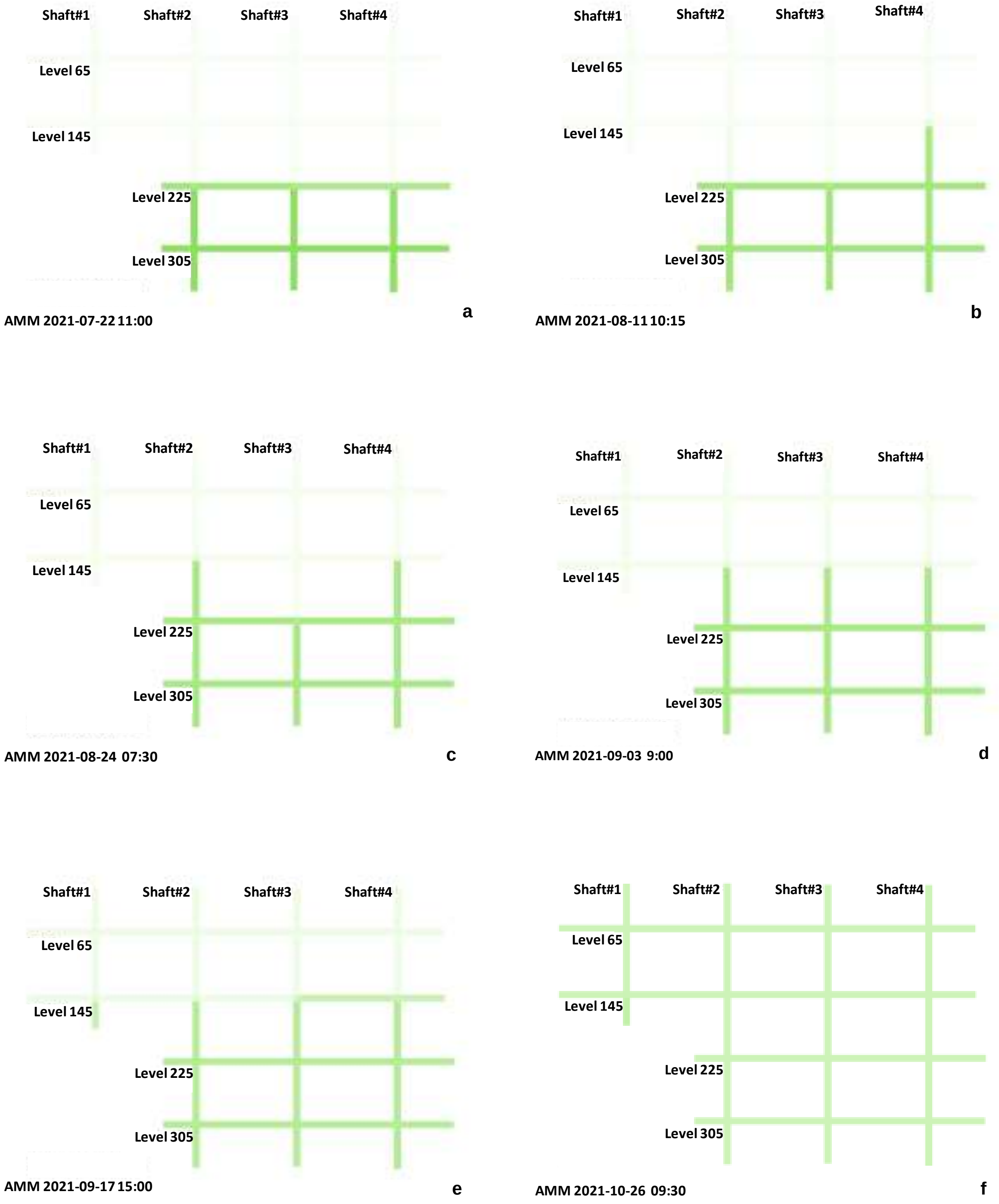

Figure 4.21: Uranine dye distribution in the AMM (a. start of experiment at 0.8 h, b. stratification breakdown in shaft #4 at 480 h, c. stratification breakdown in shaft #2 at 789 h, d. stratification breakdown in shaft #3 at 1031 h, e. stratification breakdown at 1373 h, in all shafts, except shaft #1, e. even distribution of the Uranine dye at the end of the experiment, at 2303 h)

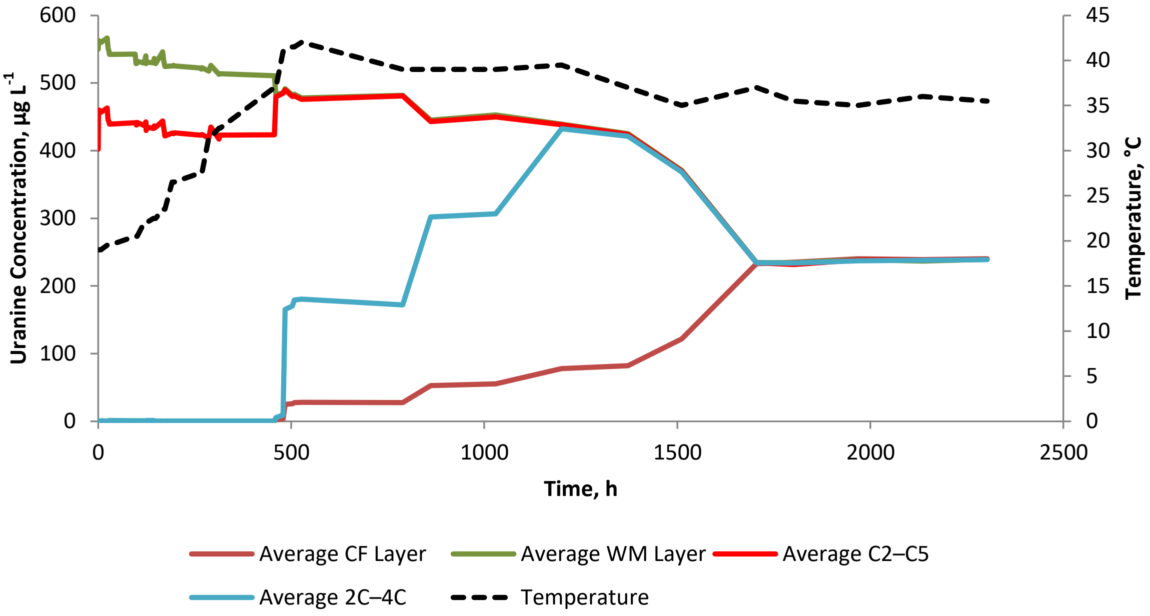

Figure 4.22: Averages for Uranine dye measurements with increase in temperature, in the CF, WM, C2–C5, 2C–4C layers in the AMM. At around 1705 h, the water in the AMM was at equilibrium concentrations

Table 4.12: Averages (for the Uranine dye measurements in the CF, WM, C2–C5, 2C–4C layers of the AMM in μg L^{-1}), standard deviation (all four layers combined) and standard deviation %

Hours	Ave CF	Ave WM	Ave C2–C5	Ave 2C–4C	Std Dev	Std Dev%
0	0.02	549.91	402.06	0.03	244	102.4
0.8	0.03	561.74	457.27	0.04	257	101.0
1.2	0.03	562.56	459.47	0.03	258	101.0
2.3	0.04	562.26	459.92	0.02	258	101.0
3.2	0.14	559.80	456.72	0.70	257	100.9
7.2	0.08	566.70	462.93	0.29	260	100.9
23.7	0.04	551.94	446.15	0.06	252	101.1
26.3	0.21	547.19	442.82	1.17	250	100.8
28.2	0.19	542.38	439.15	1.08	248	100.8
30.0	0.16	542.74	441.25	0.79	248	100.9
96.5	0.08	528.85	440.24	0.46	244	100.7
98.7	0.14	531.34	438.00	0.72	244	100.7
99.8	0.17	528.94	438.29	0.64	244	100.7
100.7	0.13	531.91	441.77	0.59	245	100.7
101.7	0.12	529.66	436.91	0.54	244	100.8
119.5	0.05	540.06	442.54	0.18	248	100.9
124.2	0.22	528.74	429.71	1.20	242	100.8
125.3	0.22	530.79	434.69	1.13	243	100.7
126.0	0.19	529.75	432.79	0.98	243	100.8
143.7	0.06	536.13	436.56	0.22	246	101.0
145.7	0.14	529.68	433.43	0.71	243	100.8
147.8	0.09	528.54	434.34	0.33	243	100.9
149.7	0.08	545.91	443.81	0.26	250	101.0
167.7	0.03	532.60	433.29	0.04	244	101.0
170.7	0.07	524.36	421.76	0.07	239	101.0
173.7	0.08	525.35	425.77	0.09	240	101.0
192.5	0.08	526.13	425.22	0.07	240	101.0
195.8	0.13	525.05	426.41	0.12	240	101.0
197.3	0.14	522.35	423.13	0.17	239	101.0
263.7	0.18	520.48	422.91	0.19	238	101.0
267.8	0.23	522.47	423.77	0.24	239	101.0
269.7	0.25	517.51	418.55	0.25	236	101.0
287.7	0.28	526.23	434.91	0.28	242	100.8
292.7	0.32	512.99	417.08	0.33	235	100.9
313.2	0.37	513.83	422.78	0.37	236	100.8
316.7	0.43	510.76	423.33	0.42	235	100.7
457.0	2.58	482.65	479.85	5.44	239	98.3
461.3	3.29	485.42	484.88	9.12	239	97.5
480.0	25.12	491.49	489.97	165.17	204	69.6
485.0	25.94	481.99	480.23	170.43	198	68.4
504.0	27.74	483.52	481.01	179.29	197	67.2
509.0	28.07	477.94	475.67	180.60	194	66.7
527.7	27.43	481.80	480.76	171.81	198	68.0
789.2	52.78	444.97	442.91	301.85	160	51.4
862.2	55.35	452.59	449.66	306.61	162	51.2
1030.7	78.02	439.27	438.22	432.53	155	44.8
1200.8	82.25	424.91	424.02	421.21	148	43.7
1372.7	121.75	371.04	369.67	368.30	107	34.9
1512.2	233.00	234.67	234.41	234.15	1	0.3
1705.7	234.96	234.05	231.68	233.83	1	0.5
1802.3	240.33	239.07	238.43	237.26	1	0.5
1968.8	238.99	236.94	238.44	238.11	1	0.3
2136.2	240.14	239.46	239.37	238.80	0	0.2
2303.3	243.08	241.97	241.92	240.07	1	0.4

4.6.4 Experiment 5: Electrical Conductivity and Temperature Measurement with CTD divers

Additional to changes in the Uranine dye concentration across the AMM, the stability and breakdown of the artificial density stratification was monitored by electrical conductivity measurements in each shaft using Van Essen CTD divers. Electrical conductivity at the start of the experiment (Figure 4.23a) was 100 mS cm^{-1} in all the shafts at 200 cm depth. Exception was shaft #1, where the electrical conductivity in the two upper CF levels containing the tap water was negligible.

Temperatures in all shafts ranged between 17 and 19.5 °C, decreasing from the sump of the shafts and reached a minimum at the intermediate layer between the CF and WM layers. This was followed by an increase towards the shaft collars. The high temperature at the bottom of the shafts was due to the heating foils, set at 19/20 °C. Three thermal stratified layers were visible, warm mineralised, cold intermediate layer and warm tap water layer. The temperature trend for the warm mineralised layer and warm tap water layer mirrored one another. This was indicative of convection, resulting in convection loops. Similar observations are reported by Mugova and Wolkersdorfer (2022) in flooded underground mines and Schmitt (1994) in oceanography.

At 24 hours, the stratification remained stable at 100 mS cm^{-1} electrical conductivity at 200 cm depth. Additionally, a similar temperature trend was observed as being high at the sump of the shafts (Figure 4.23b). However, the tap water layer’s temperature at the top had decreased slightly. This was due to the heating foil set at 20/21 °C increasing the temperature in the intermediate layer. It remained stable for a short while in all the shafts, and thereafter increased steadily to 21 °C in shaft #4.

However, at this instance, three water bodies were evident in shafts #2, #3 and #4. Convention cells (staircase like), were forming, hence the mixing of the water in the CF and WM layers due to heat and mass transfer. This phenomenon was explained by Berthold and Börner (2008), Mugova and Wolkersdorfer (2022) and Uerpmann (1980) referring to the transitional layer as boundary or intermediate layer where fluctuations in concentration and temperature are indicative of heat and mass transfer due to convection, also described as bales (Kories *et al.*, 2004). 96 hours after starting the experiment, the stratification remained stable, but still with three well defined water bodies present.

Temperature on the heating foils was set to 21/22 °C (Figure 4.23c), thus raising the temperature at the base of the AMM. Electrical conductivity remained the same as before at 100 mS cm^{-1}, at a depth of 200 cm and negligible at the two upper most levels of the AMM containing tap water.

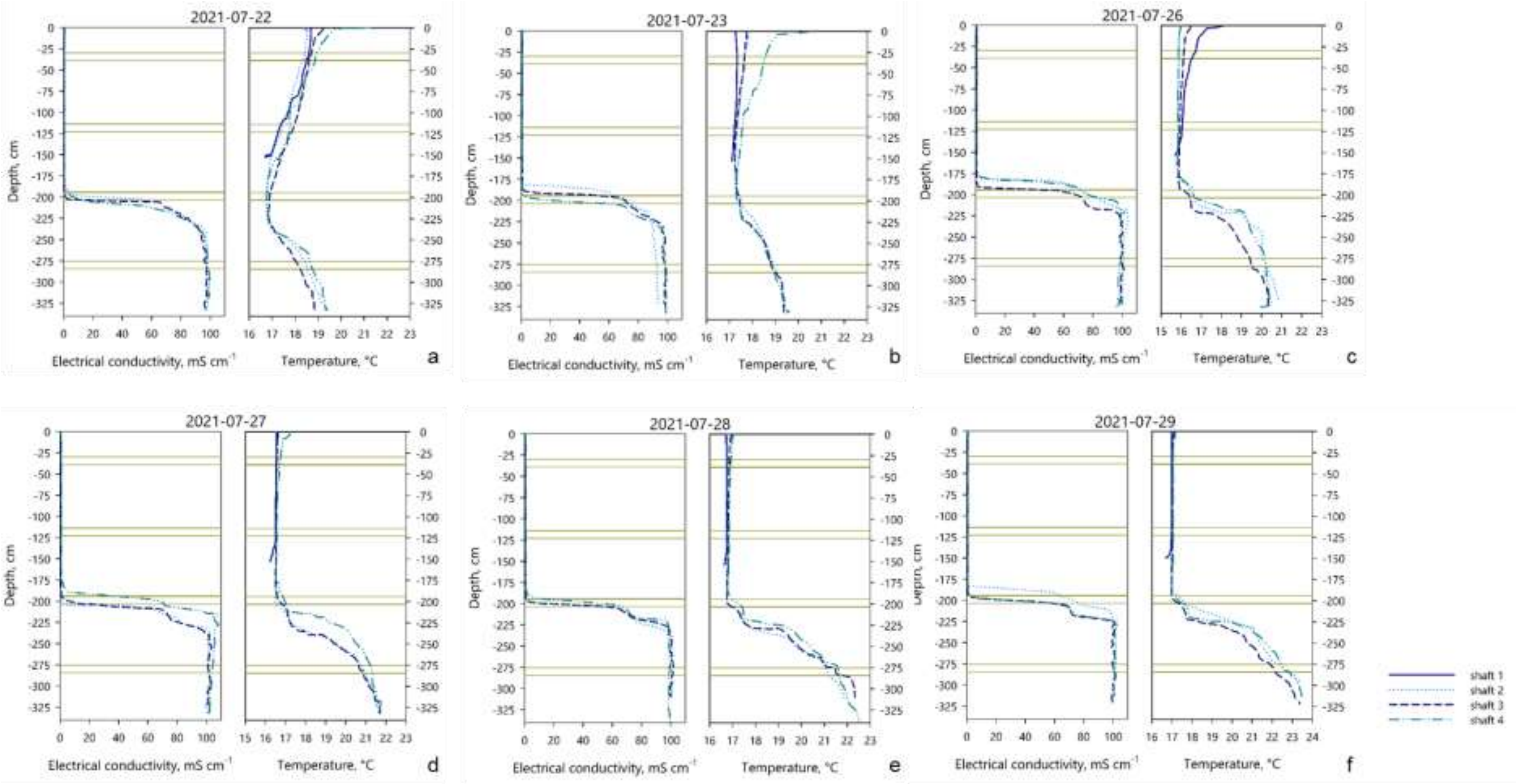

Figure 4.23: Depth dependent electrical conductivity and temperature developments, for shafts #1, #2, #3 and #4 depicting a stable stratification in all shafts, except shaft #1 (a. 0 h, b. 24 h, c. 96 h, d. 120 h, e. 144 h and f. 168 h)

Three separate stratified water bodies were visible in the AMM proven by the electrical conductivity differences. The lowermost water had an electrical conductivity of 100 mS cm^{-1} at depths greater than 200 cm (WM layer) and the upper most water body containing the tap water had negligible EC values (Figure 4.23d and e). Intermediate EC values existed in the intermediate layer that physically existed between the two water bodies, lower and upper.

The temperature at the shaft's sumps was similar to that of the heating foils. Section 1 C in shaft #4 maintained generally a lower temperature compared to other sections at similar levels. This was related to the position of the heating foils which were located at section 1D, directly above 1C. Since this water was not heated, it remained far less buoyant to induce convention cells. Hence, there was no mixing between the warm and cold water bodies.

As the temperature at the heating foils increased, the *in situ* water temperature also increased; however, the latter had lower temperatures (Figure 4.23d, e and f). Furthermore, the temperature in the AMM was decreasing from the mineralised layer towards the intermediate layer and remained constant at the CF layer. Regardless of the increase in temperature, three distinct water bodies were evident in the AMM. Moreover, section C1 remains colder than all the sections in the AMM, and the electrical conductivity remained at 100 mS cm^{-1} and 80 mS cm^{-1} at the intermediate layer. Thus, the presence of stratification was confirmed using both the electrical conductivity and temperature in the AMM.

Stratification proved robust between 192 to 456 h of the experiment (Figure 4.24a, b, c and d). Temperature on the heating foils remained higher than in the AMM;

however, the WM layer was gradually warming up, and the temperature remained around 20 °C in the CF layer. It is evident that the heating foils were effective in raising the temperature in the AMM. Although the temperature was increasing steadily, the stratification was still intact in the intermediate layer.

In the CF layer, the electrical conductivity remained at a negligible value. The WM layer, however, showed a slight EC decrease to below 100 mS cm^{-1} (Figure 4.24d) and the depth of the intermediate had risen slightly to 160 cm in shafts #3 and #4. The latter was confirmed by Uranine measurements indicating that the Uranine has dispersed to section 4C.

Thereafter, only two stratified water bodies existed, and the temperature had increased substantially in the WM layer. Furthermore, the electrical conductivity dropped to 85 mS cm^{-1} therein and increased slightly in the CF layer. Temperature at section 1C was still lower than overall in the AMM. A similar trend was observed in the CF layer (Figure 4.24f) regardless of the graphical protrusion observed in shaft #3, possibly due to a sampling error.

Electrical conductivity was at 80 mS cm^{-1} in the WM layer; however, this layer had now risen to a depth approaching 150 cm in shafts #2, #3 and #4 (Figure 4.25a, b), At this stage, the temperature was at its highest at 42 °C in the lowest levels of the AMM with section 1C temperatures increasing, yet the lowest.

At 768 h of the experiment, the WM layer began to show a further decrease in electrical conductivity to below 80 mS cm^{-1} accompanied by a temperature increase. The intermediate layer had further risen above level 145 of the AMM. The WM layer was now prevalent in the upper levels of the AMM, confirmed by the Uranine concentrations in shafts #3 and #4 (Figure 4.21c). Temperatures at the lowest sections of the AMM had decreased to 39 °C (Figure 4.25) and continued to decrease in the lower levels but increased in the upper most levels (Figure 4.25d, e). Additionally the electrical conductivity decreased to less than 60 mS cm^{-1}; however the increase was lesser at section 1C.

1488 hours into the experiment, the WM and CF layers were completely mixed (Figure 4.26a, b, c, d, e). The overall electrical conductivity for the *in situ* water was 40 mS cm^{-1}, and the temperature increased to over 35 °C in all sections except for section 1C. At this stage, experiment #5 was terminated.

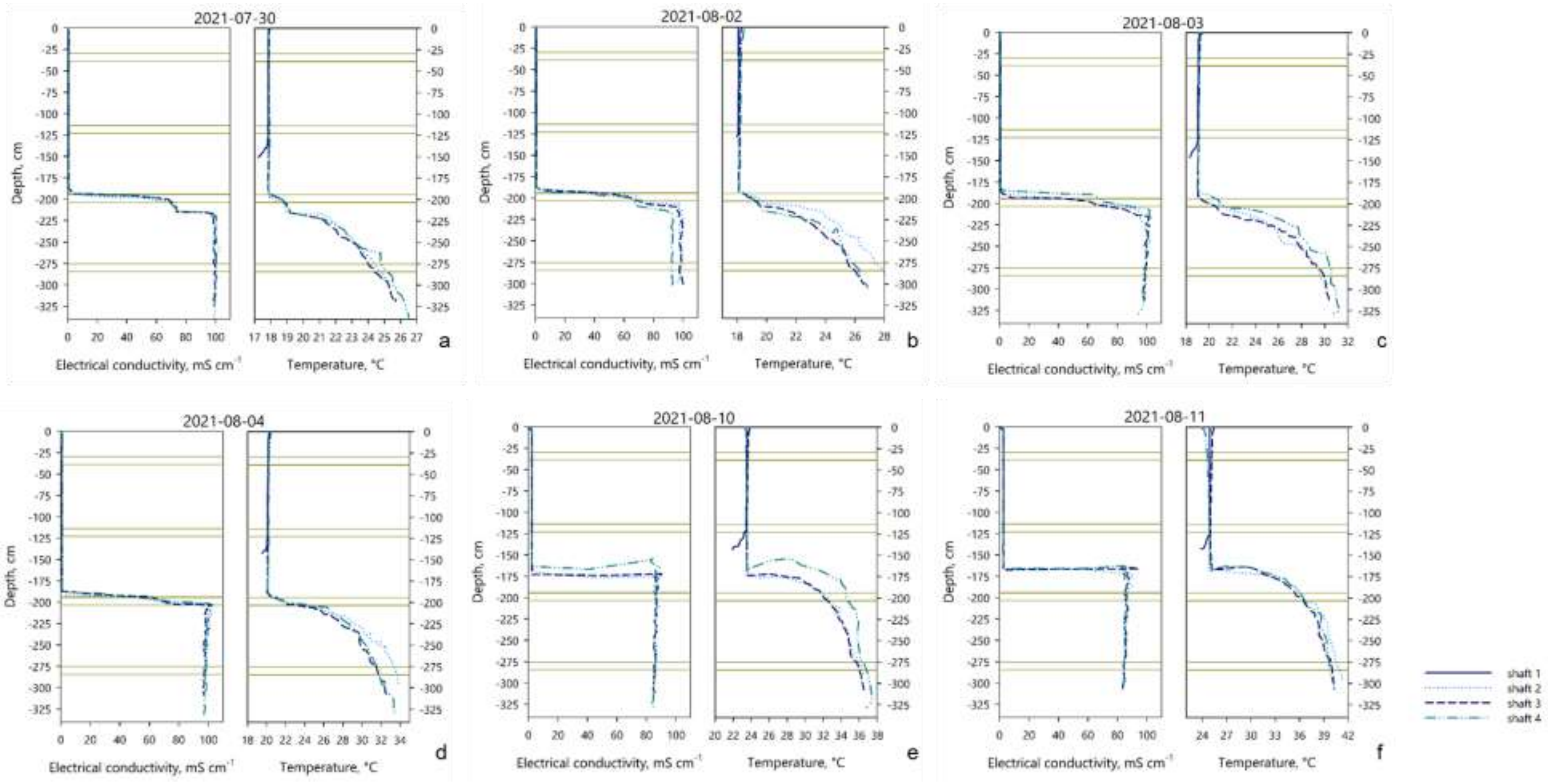

Figure 4.24: Depth dependent electrical conductivity and temperature developments, for shafts #1, #2, #3 and #4 depicting a stable stratification in all shafts, except shaft #1, (a. 192 h, b. 240 h, c. 264 h, d. 288 h, e. 432 h and f. 456 h)

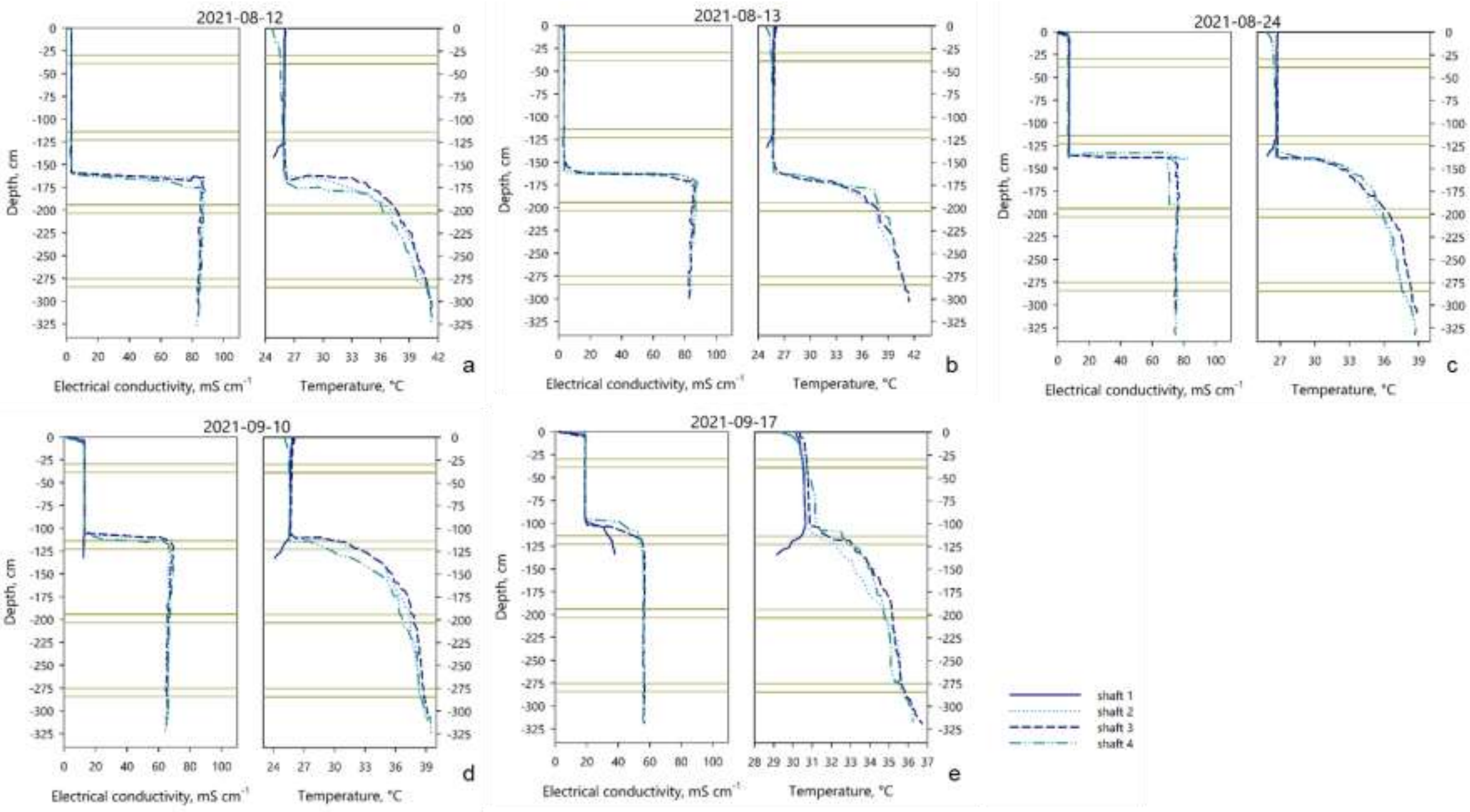

Figure 4.25: Electrical conductivity and temperature measurements, for shafts #1, #2, #3 and #4 depicting a slow stratification disintegration in all shafts, except shaft1, (a. 480 h, b. 504 h, c. 768 h, d. 1176 h and e. 1344 h)

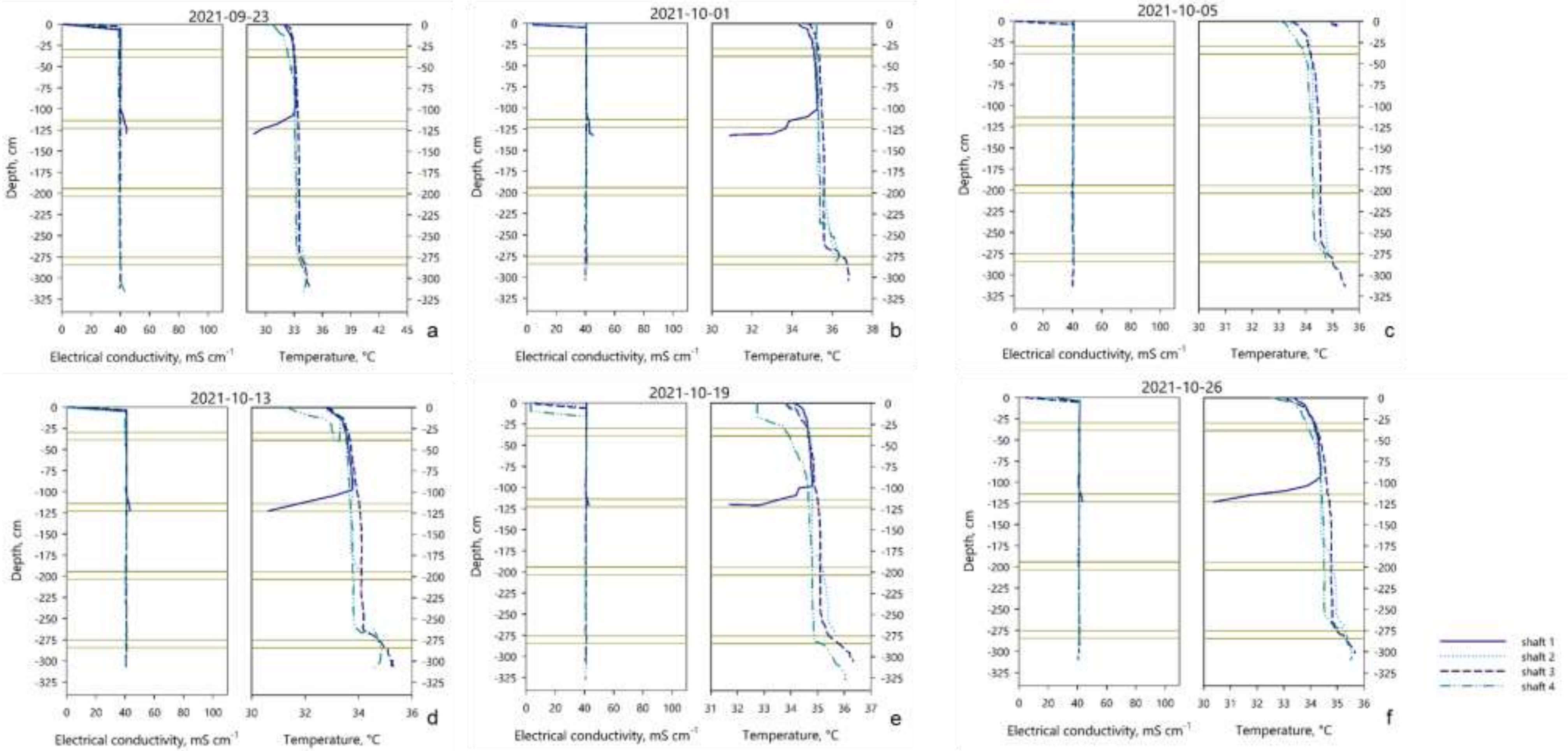

Figure 4.26: Depth dependent electrical conductivity and temperature developments, for shafts #1, #2, #3 and #4 depicting stratification breakdown in all shafts, except shaft #1, (a. 1488 h, b. 1688 h, c. 1784 h, d. 1976 h, e. 2120 h and f. 2288 h)

CHAPTER 5

5 Conclusions and Outlook

This research aimed to determine factors controlling density stratification in flooded underground mines using an analogue model mine (AMM). Results obtained from this study serve as a basis for understanding hydrodynamics of mine flooding processes, discharge pumping as well as stratification build up, stabilisation and breakdown.

The average vertical rate flow rate in the AMM was 0.013 m s^{-1} in the experiments running at steady state conditions with Reynolds numbers ranging between Re = 60 and Re = 66 for flow rates of 0.006 m s^{-1} and 0.014 m s^{-1}, respectively (Table 5.1). The individual 0.001 m s^{-1} velocity steps were due to the A/D converters' (analogue to digital converter) resolution. It can therefore be concluded that, at steady state conditions, the processes that transpired in the AMM were more or less stable. Similar flow rates existed in experiment 3 regardless of applying temperature of 23/25 °C from the heating foils. It proved that low temperatures had no measurable effect on the flow rate. It was however a different scenario with experiment 5 when the temperature was increased to a maximum of 43 °C. An average flow rate of 0.017 m s^{-1} prevailed with a minimum flow rate of 0.006 m s^{-1} and a maximum flow rate of 0.025 m s^{-1}, resulting in Reynolds numbers of Re = 120 and Re = 150 at 20 °C and 30 °C, respectively.

Laminar flow was observed throughout the duration of the experiments with Reynolds number not above Re = 150, regardless of the continuous increase in temperature. During the first two experiments, running at steady state conditions, the flow was merely driven by diffusion. However, the increase in the average flow rate

(0.013 to 0.017 m s^{-1}) in experiment 5 was attributed to convection, resulting from the temperature increase. Subsequently, the heating induced greater flow rates in the AMM. Although laminar flow persisted throughout the experiments, turbulent flow originating from the presence of obstacles in the shafts and galleries inside the AMM cannot be disregarded. Fluctuations in the measured parameters are indicative of turbulent flow conditions. The second horizontally installed flow meter measured lower flow rates. Although the vertical meter measured higher flow rates compared to the horizontal flow meter, the flow patterns of both meters are very similar. These results mirror the findings of Wolkersdorfer (2008), who found in a mine water tracer test that flow in shafts was substantially faster compared to galleries.

Table 5.1: Average flow rates and Reynolds number for experiment 1, 2, 3, 4 and 5

Experiment	Average Flow Rate m s^{-1}	Reynolds Number
1	0.013	61
2	0.013	61
3	0.013	61
4	0.013	61
5 (Vertical Flowmeter)	0.017	120 at 20 °C 134 at 25 °C 150 at 30 °C
5 (Horizontal Flowmeter)	0.012	72 at 20 °C 86 at 25 °C 89 at 30 °C

An exponential decline in the Uranine concentration occurred in experiment 3 from the point of injection 2A to the top of the AMM. Elevated dispersion rates were measured in experiment 3 and were driven by applying heat to the AMM. A 42.5 cm^3 s^{-1} dispersion rate existed 60 min post the injection and being 54 times higher than in experiment 2. At ambient conditions, the dispersion rate was however lower compared to the experiment with only tap water. Temperature increase therefore, aids in the acceleration of the tracer dispersion. However, the tracer injection had no effect on the *in situ* water flow rate.

An artificial density stratification was created in the AMM with a lower WM layer of 1.065 g cm^{-3} density and electrical conductivity (EC) of 100 mS cm^{-1}, and an upper CF layer with a density of 0.998 g cm^{-3} and EC of 0 mS cm^{-1} at the top of the AMM. Average Uranine concentrations were 0.02 µg L^{-1} in the CF layer and at about 549 µg L^{-1} in the WM layer, proving stratification in the AMM. Therefore, it can be concluded that density differences in different mine water bodies are indeed paramount to stratification development and stabilisation. At ambient conditions, the stratification remained stable, however broke down, when the AMM was heated. An 0.5 to 1 K temperature increase lead to a development of a third water body at 200 cm depth, known as intermediate layer, with the Uranine concentration increasing from 0 to 5 µg L^{-1}, indicating density and heat mass transfer between the WM and CF layers. This shows that the AMM acts as a thermosiphon, hence the development of the three water bodies hours after increasing the temperature. Increase to higher temperatures of 33/34 °C lead to stratification breakdown in all the shafts except in shaft #4 with a temperature of less than 30 °C, indicating sump conditions. The three shafts had an electrical conductivity at 40 mS cm^{-1} when the stratification broke down, but over 40 mS cm^{-1} in shaft #1. This observation was also corroborated by the Uranine concentrations that were always lower in shaft #1 than in the other shafts. This implies that the shaft #1 sump is not part of the overall convective flow, an observation made by Wolkersdorfer (1996) also in shaft 366IIb of the Niederschlema/Alberoda uranium mine. There the sump showed different conditions from the rest of the mine pool for at least 3 years.

Ambient air temperature had an influence on the *in situ* water temperature of the experiments running at steady state conditions. However, the application of heat in experiment 5 influenced the *in situ water* in the AMM. It was concluded that temperature is of paramount importance in stratification development, stabilisation and breakdown. Roughly 9606 kJ of energy was needed to heat up the water in the AMM, both the WM and CF layers.

Due to the first flush, mine water quality changes over time. This applies to both the water quality within the mine and to the discharging mine water and has profound effect on mine water management. Flushing of the AMM lead to an exponential decrease in Sulforhodamine B concentrations averaging from 34 µg L^{-1} to 56 µg L^{-1} regardless of the high concentration of over 400 µg L^{-1} at the injection point. The AMM therefore acts as a perfectly mixed chemical flow reactor. During flushing, the discharge point or the pumps should be placed above the WM layer to conserve the stratification, as could be shown in the first flush experiment. When placed in or below the WM layer, turbulent conditions or forced convection will arise, thus mixing the two water bodies resulting in stratification breakdown. The typical first flush equation is not conducive for the AMM due to the fact that only the flushing time was taken into cognisance and not the time it took to flood the AMM. An additional experiment is underway, where the flooding time is taken into consideration and the outcome will be presented in a paper at a later stage. During the planning of a mine water treatment plant, the first flush must be considered, as the changing water quality alters the demands on the plant, as shown by the AMM results. Therefore, active treatment might be necessary at first, which can later be replaced by a passive treatment system. If the water quality improves considerably over time, mine water treatment might even not be necessary at all. For each mine, a first flush curve can be estimated based on the discharging water values, although this is only a rough orientation at this point in time. Therefore, flooded stratified underground mines can be considered as an *in situ* remediation method provided the pumps on the point of discharge are positioned properly on an appropriate level in a stratified system.

This thesis conclusively proves that water stratification in flooded underground mines is due to density differences of the fluid controlled by its chemical and physical properties including but not limited to temperature and mineralisation and can be used as an *in situ* remediation method. Temperature plays a major role in mine water stratification breakdown, as it induces heat from one layer to the other through convection. Warmer solutions rise to the upper parts of the mine resulting in convective mixing of the two water bodies.

Flow measurements in flooded mine shafts are rare and only three could be found in the published literature (Žittnan *et al.*, 1990; Wolkersdorfer, 1996; Kolitsch *et al.*, 2005). The Reiche Zeche, Germany, which measured velocities of 1 – 2.5 m h^{-1} in the flooded Reiche Zeche Shaft, resulting in Re ≈ 500 – 1150. Regardless of the shaft having free and forced flow characterisation, the flow rates are still lower than that of the AMM (0.015 m s^{-1}). 80% of the world's tracer test, mostly documented in the wolkersdorfer.info website, has an average velocity of 0.014 m s^{-1} which is comparable to those in the AMM.

The "geothermal gradient" in the AMM ranged between 90 and 200 K/100 m during the experiment, however it was above 200 K/100m when the stratification broke down. This was necessary to cause the breakdown of the stratification, but it is highly unlikely to occur in nature because stratification will not only breakdown due to temperature differences but other controlling factors. As can be seen, based on the flow results, it can be concluded that findings in the AMM can be transferred to flooded underground mines in the real world.

Future studies will need to simulate different mining scenarios to understand stratification. More experiments need to be carried out on the AMM using real life mine scenarios coupled with numerical modelling. Additional temperature sensors should be installed on all section of the AMM, to monitor the processes that transpire when the sections are heated as observed in section 1C.

References

ADAMS, R. & YOUNGER, P. 2001. A strategy for modeling ground water rebound in abandoned deep mine systems. *Groundwater,* 39(2):249-261. https://doi.org/10.1111/j.1745-6584.2001.tb02306.x

ALHAMED, M. & WOHNLICH, S. 2014. Environmental impact of the abandoned coal mines on the surface water and the groundwater quality in the south of Bochum, Germany. *Environ. Earth. Sci.,* 72(9):3251-3267. https://doi.org/10.1007/s12665-014-3230-9

ALI, A., STREZOV, V. & DAVIES, P. 2017. Environmental impact of coal mining and coal seam gas production on surface water quality in the Sydney basin, Australia. *Environ. Monit. Assess.,* 189(8):408. https://doi.org/10.1007/s10661-017-6110-4

ANDERSON, M.P., WOESSNER, W.W. & HUNT, R.J. 2015. *Applied groundwater modeling: simulation of flow and advective transport.* Amsterdam: Academic press

ANDRÉS, C., ORDÓÑEZ, A. & ÁLVAREZ, R. 2017. Hydraulic and thermal modelling of an underground mining reservoir. *Mine Water Environ.,* 36(1):24-33. https://doi.org/10.1007/s10230-015-0365-1

BALSAMO, M. & MONTAGNARO, F. 2018. On the performance of continuous stirred tank reactor and plug flow reactor for chemical reactions characterised by non-elementary kinetics. *React. Kinet. Mech. Catal.,* 125(2):449-469. https://doi.org/10.1007/s11144-018-1475-0

BANKS, D., YOUNGER, P.L., ARNESEN, R.-T., IVERSEN, E.R. & BANKS, S.B. 1997. Mine-water chemistry: the good, the bad and the ugly. *Environ. Geol.,* 32(3):157-174. https://doi.org/10.1007/s002540050204

BAO, T., LIU, Z., MELDRUM, J., GREEN, C., XUE, P. & VITTON, S. 2018. Field tests and multiphysics analysis of a flooded shaft for geothermal applications with mine water. *Energy Convers. Manag.,* 169:174-185. https://doi.org/10.1016/j.enconman.2018.05.065

BAU, H.H. & TORRANCE, K.E. 1981a. On the stability and flow reversal of an asymmetrically heated open convection loop. *J. Fluid Mech.,* 109:417-433. https://doi.org/10.1017/S0022112081001146

BAU, H.H. & TORRANCE, K.E. 1981b. Transient and steady behavior of an open, symmetrically-heated, free convection loop. *Int. J. Heat Mass Transf.,* 24(4):597-609. https://doi.org/10.1016/0017-9310(81)90004-1

BERTHOLD, S. & BÖRNER, F. 2008. Detection of free vertical convection and double-diffusion in groundwater monitoring wells with geophysical borehole measurements. *Environ. Geol.,* 54(7):1547-1566. https://doi.org/10.1007/s00254-007-0936-y

BOEHRER, B. & SCHULTZE, M. 2008. Stratification of lakes. *Rev. Geophys.,* 46(2):1-27. https://doi.org/10.1029/2006RG000210

BOZAU, E., LICHA, T. & LIESSMANN, W. 2017. Hydrogeochemical characteristics of mine water in the Harz Mountains, Germany. *Chemie der Erde.,* 77(4):614-624. https://doi.org/10.1016/j.chemer.2017.10.001

BREDEHOEFT, J.D. & KONIKOW, L.F. 2012. Reflections on our Model Validation editorial. *Ground Water,* 50(4):493-495. https://doi.org/10.1111/j.1745-6584.2012.00951

BROWN, K. & TROTT, S. 2014. Groundwater flow models in open pit mining: can we do better? *Mine Water Environ.,* 33(2):187-190. https://doi.org/10.1007/s10230-014-0270

BRUSSEAU, M.L. 1996. Evaluation of simple methods for estimating contaminant removal by flushing. *Groundwater,* 34(1):19-22. https://doi.org/10.1111/j.1745-6584.1996.tb01860.x

CAIRNEY, T. & FROST, R. 1975. A case study of mine water quality deterioration, Mainsforth Colliery, County Durham. *J. Hydrol.,* 25(3):275-293. https://doi.org/10.1016/0022-1694(75)90026-8

CHEONG, Y.W., YIM, G.-J., JI, S.W., KANG, S.S. & SKOUSEN, J. 2012. Water quality changes of a closed underground coal mine in Korea. *Environ. Monit. Assess.,* 184(1):503-513. https://doi.org/10.1007/s10661-011-1983-0

DAVIS, S.N., THOMPSON, G.M., BENTLEY, H.W. & STILES, G. 1980. Ground-water tracers—A short review. *Groundwater,* 18(1):14-23. https://doi.org/10.1111/j.1745-6584.1980.tb03366.x

DEMCHAK, J., SKOUSEN, J. & MCDONALD, L. 2004. Longevity of acid discharges from underground mines located above the regional water table. *J. Environ. Qual.,* 33(2):656-668. https://doi.org/10.2134/jeq2004.6560

DENIMAL, S., BERTRAND, C., MUDRY, J., PAQUETTE, Y., HOCHART, M. & STEINMANN, M. 2005. Evolution of the aqueous geochemistry of mine pit lakes–Blanzy–Montceau-les-Mines coal basin (Massif Central, France): origin of sulfate contents; effects of stratification on water quality. *Appl. Geochem.,* 20(5):825-839. https://doi.org/10.1016/j.apgeochem.2004.11.015

DIERSCH, H.-J.G. 2013. *FEFLOW: finite element modeling of flow, mass and heat transport in porous and fractured media.* Heidelberg: Springer. https://doi.org/10.1007/978-3-642-38739-5_11

DIVINE, C.E. & MCDONNELL, J.J. 2005. The future of applied tracers in hydrogeology. *Hydrogeol. J.,* 13(1):255-258. https://doi.org/10.1007/s10040-004-0416-3

DUNNE, T. 1990. Hydrology, mechanics, and geomorphic implications of erosion by subsurface flow. *Groundwater geomorphology: The role of subsurface water in earth-surface processes and landforms,* 252:1-28. https://doi.org/10.1130/SPE252-p1

ELLIOT, T. & YOUNGER, P. 2007. Hydrochemical and isotopic tracing of mixing dynamics and water quality evolution under pumping conditions in the mine shaft of the abandoned Frances Colliery, Scotland. *Appl. Geochem.,* 22(12):2834-2860. https://doi.org/010.1016/j.apgeochem.2007.07.007

ELLIOT, T. & YOUNGER, P.L. 2014. Detection of mixing dynamics during pumping of a flooded coal mine. *Groundwater,* 52(2):251-263. https://doi.org/10.1111/gwat.12057

FORSTER, H. & POTSDAM, H. 2005. Mineralogy of the U-Se-polymetallic deposit Niederschlema-Alberoda, Erzgebirge, Germany. IV. The continuous clausthalite-galena solid-solution series. *Neu. Jb. Mineral. Abh.,* 181(2):125-134. https://doi.org/10.1127/0077-7757/2005/0011

FROST, R. 1979. Evaluation of the rate of decrease in the iron content of water pumped from a flooded shaft mine in County Durham, England. *J. Hydrol.,* 40(1-2):101-111. https://doi.org/10.1016/0022-1694(79)90090-8

GABARRÓN, M., ZORNOZA, R., ACOSTA, J., FAZ, Á. & MARTÍNEZ-MARTÍNEZ, S. 2019. Mining environments. In: Pereira, P. (ed.). *Advances in Chemical Pollution, Environmental Management and Protection*. Vol. 4. Cartagena Colombia: Elsevier:157-205. https://doi.org/10.1016/bs.apmp.2019.07.003

GEBHART, B., JALURIA, Y., MAHAJAN, R.L. & SAMMAKIA, B. 1988. *Buoyancy-Induced Flows and Transport.* Washington: Hemisphere. https://doi.org/10.1115/1.3226555

GONZÁLEZ-QUIRÓS, A. & FERNÁNDEZ-ÁLVAREZ, J.P. 2019. Conceptualization and finite element groundwater flow modeling of a flooded underground mine reservoir in the Asturian Coal Basin, Spain. *J. Hydrol.,* 578:124036. https://doi.org/10.1016/j.jhydrol.2019.124036

GZYL, G. & BANKS, D. 2007. Verification of the “first flush” phenomenon in mine water from coal mines in the Upper Silesian Coal Basin, Poland. *J. Contam. Hydrol.,* 92(1-2):66-86. https://doi.org/10.1016/j.jconhyd.2006.12.001

HENKEL, L. & MELCHERS, C. 2017. Hydrochemical and isotopegeochemical evaluation of density stratification in mine water bodies of the Ruhr coalfield. In: Wolkersdorfer, C., Sartz, L., Sillanpää, M. & Hakkinen, A. (eds.). *IMWA 2017 - Mine Water and Circular Economy*. International Mine Water Association:430-436

HOOVER, H. & HOOVER, L.H. 1950. *De re metallica.* London: Courier Corporation

IVEY, G., WINTERS, K. & KOSEFF, J. 2008. Density stratification, turbulence, but how much mixing? *Annu. Rev. Fluid Mech.,* 40(1):169-184. https://doi.org/10.1146/annurev.fluid.39.050905.110314

JÄGER, B., OBERMANN, P. & WILKE, F. 1990. Studie zur Eignung von Steinkohlebergwerken im rechtsrheinischen Ruhrkohlenbezirkzur Untertageverbringung von Abfall- und Reststoffen. 4 Text-, 1 Anlagenband, unveröffentl. Machbarkeitsstudie im Auftrag des Landesamt für Wasser und Abfall NRW.

JENK, U., ZIMMERMANN, U., UHLIG, U., SCHÖPKE, R. & PAUL, M. 2014. In Situ Mine Water Treatment: Field Experiment at the Flooded Königstein Uranium Mine (Germany). *Mine Water Environ.,* 33(1):39-47. https://doi.org/10.1007/s10230-013-0241-9

KARAKAS, G., BROOKLAND, I. & BOEHRER, B. 2003. Physical characteristics of acidic mining lake 111. *Aqua Sci.,* 65(3):297-307. https://doi.org/10.1007/s00027-003-0651-z

KGARI, T., VAN WYK, Y., COETZEE, H. & DIPPENAAR, M. 2016. Mine Water approach using Tracers in South African abandoned Coal Mines. In: Drebenstedt, C. & Paul, M. (eds.). *IMWA 2016 – Mining Meets Water-Conflicts and Solutions*. International Mine Water Association:410-416

KOLITSCH, S., JUNGHANS, M., KLEMM, W., DEGNER, T. & BAACKE, D. 2005. Hydrochemical monitoring (1970–2003), depth profile and flow measurements in partly flooded underground workings of the central polymetallic vein ore deposit of Freiberg/Germany. *Z. geol. Wiss.,* 5(1):51-78

KORIES, H., RÜTERKAMP, P. & SIPPEL, M. 2004. Field and numerical studies of water stratification in flooded shafts. In: *International Mine Water Association Symposium 2004*.149-159

LEIBUNDGUT, A., MALOSZEWSKI, P. & KÜLLS, C. 2009. *Tracers in hydrology.* Chichester: Wiley-Blackwell. https://doi.org/10.1002/9780470747148

LEVENSPIEL, O. 1998. *Chemical reaction engineering.* New York: Wiley

LUO, J., DIERSCH, H.-J.G. & MONNINKHOFF, L.M. 2012. 3D modeling of saline groundwater flow and transport in a flooded salt mine in Stassfurt, Germany. *Mine Water Environ,* 31(2):104-111. https://doi.org/10.1007/s10230-012-0181-9

MACK, B. & SKOUSEN, J. 2008. Acidity decay curves of 40 above drainage mines in West Virginia. *Proceedings, 2008 American Society of Mining and Reclamation*:612-627. https://doi.org/10.21000/JASMR08010613

MEINRATH, A., SCHNEIDER, P. & MEINRATH, G. 2003. Uranium ores and depleted uranium in the environment, with a reference to uranium in the biosphere from the Erzgebirge/Sachsen, Germany. *J. Environ. Radioact.,* 64(2-3):175-193. https://doi.org/10.1016/S0265-931X(02)00048-6

MERRITT, P. & POWER, C. 2022. Assessing the long-term evolution of mine water quality in abandoned underground mine workings using first-flush based models. *Sci. Total Environ.,* 846:157390. https://doi.org/10.1016/j.scitotenv.2022.157390

MUGOVA, E. & WOLKERSDORFER, C. 2019. Stratification in Flooded Underground Mines – State of Knowledge and Further Research Ideas. In: Khayrulina, E., Wolkersdorfer, C., Polyakova, S. & Bogush, A. (eds.). *IMWA 2019 – Mine Water: Technological and Ecological Challenges*. Perm, Russia: Perm State University:40–44

MUGOVA, E. & WOLKERSDORFER, C. 2022. Density Stratification and Double - Diffusive Convection in Mine Pools of Flooded Underground Mines – A Review. *Water Res.*:118033. https://doi.org/10.1016/j.watres.2021.118033

NAICKER, K., CUKROWSKA, E. & MCCARTHY, T. 2003. Acid mine drainage arising from gold mining activity in Johannesburg, South Africa and environs. *Environ. Pollut.,* 122(1):29-40. https://doi.org/10.1016/S0269-7491(02)00281-6

NORDSTROM, D.K. 2009. Acid rock drainage and climate change. *J. Geochem. Explor.,* 100(2-3):97-104. https://doi.org/10.1016/j.gexplo.2008.08.002

NORTHEY, S., MUDD, G., WERNER, T., HAQUE, N. & YELLISHETTY, M. 2019. Sustainable water management and improved corporate reporting in mining. *Water Resour. Ind,* 21:1-20. https://doi.org/10.1016/j.wri.2018.100104

NORTON, D. & KNAPP, R. 1977. Transport phenomena in hydrothermal systems: the nature of porosity. *Am. J. Sci.,* 277(8):913-936. https://doi.org/10.2475/ajs.277.8.913

NUTTALL, C., ADAMS, R. & YOUNGER, P. 2002. Integrated hydraulic-hydrogeochemical assessment of flooded deep mine voids by test pumping at the Deerplay (Lancashire) and Frances (Fife) Collieries. *Geol. Soc. Spec. Publ.,* 198(1):315-326. https://doi.org/10.1144/GSL.SP.2002.198.01.21

NUTTALL, C.A. & YOUNGER, P.L. 2004. Hydrochemical stratification in flooded underground mines: an overlooked pitfall. *J. Contam. Hydrol.,* 69(1):101-114. https://doi.org/10.1016/S0169-7722(03)00152-9

PAUL, M., METSCHIES, T., FRENZEL, M. & MEYER, J. 2011. The Mean Hydraulic Residence Time and its Use for Assessing the Longevity of Mine Water Pollution from Flooded Underground Mines. In: *The New Uranium Mining Boom*. Berlin: Springer:689-699. https://doi.org/10.1007/978-3-642-22122-4_79

PAVELYEV, A., RESHMIN, A., TEPLOVODSKII, S. & FEDOSEEV, S. 2003. On the lower critical Reynolds number for flow in a circular pipe. *Fluid Dyn.,* 38(4):545-551. https://doi.org/10.1023/A:1026369727130

PERRY, E.F. & RAUCH, H. 2013. Estimating water quality trends in abandoned coal mine-pools. In: *WV Mine Drain. Task Force Meet*.1-11

PETKOVSKA, M., NIKOLIĆ, D. & SEIDEL-MORGENSTERN, A. 2018. Nonlinear frequency response method for evaluating forced periodic operations of chemical reactors. *Isr. J. Chem.,* 58(6-7):663-681. https://doi.org/10.1002/ijch.201700132

RAPANTOVÁ, N., LICBINSKA, M., BABKA, O., GRMELA, A. & POSPISIL, P. 2013. Impact of uranium mines closure and abandonment on groundwater quality. *Environ. Sci. Pollut. Res.,* 20(11):7590-7602. https://doi.org/10.1007/s11356-012-1340-z

RENZ, A., RÜHAAK, W., SCHÄTZL, P. & DIERSCH, H.-J. 2009. Numerical modeling of geothermal use of mine water: challenges and examples. *Mine Water Environ.,* 28(1):2-14. https://doi.org/10.1007/s10230-008-0063-3

REYNOLDS, O. 1883. XXIX. An experimental investigation of the circumstances which determine whether the motion of water shall be direct or sinuous, and of the law of resistance in parallel channels. *Philosophical Transactions of the Royal society of London*(174):935-982. https://doi.org/10.1098/rstl.1883.0029

RUBIN, J. 1966. Theory of rainfall uptake by soils initially drier than their field capacity and its applications. *Water Resour. Res.,* 2(4):739-749. https://doi.org/10.1029/WR002i004p00739

RYAN, N. & JOHNSON, M. 1959. Transistion from laminar to turbulent flow in pipes. *AIChE J.,* 5(4):433-435. https://doi.org/10.1002/aic.690050407

SAKO, A., BAMBA, O. & GORDIO, A. 2016. Hydrogeochemical processes controlling groundwater quality around Bomboré gold mineralized zone, Central Burkina Faso. *J. Geochem. Explor.,* 170:58-71. https://doi.org/10.1016/j.gexplo.2016.08.009

SANDERS, C. & HOLMAN, J. 1972. Franz Grashof and the Grashof number. *International Journal of Heat and Mass Transfer,* 15(3):562-563

SCHMITT, R.W. 1994. Double diffusion in oceanography. *J. Fluid Mech.,* 26(1):255-285. https://doi.org/10.1146/annurev.fl.26.010194.001351

SHERWOOD, J.M. 1997. Modelling minewater flow and quality changes after coalfield closure. (Doctoral dissertation, Newcastle University).

SNYDER, W. & CASTRO, I. 2002. The critical Reynolds number for rough-wall boundary layers. *J. Wind. Eng. Ind. Aerodyn.,* 90(1):41-54. https://doi.org/10.1016/S0167-6105(01)00114-3

SOLODOV, I., MALKOVSKY, V., PEK, A. & BENSON, S. 2002. New evidence for the combined influence of vapor condensation and thermal convection on groundwater monitoring wells. *Environ. Geol.,* 42(2):145-150. https://doi.org/10.1007/s00254-001-0484-9

STUART, W. & SIMPSON, T. 1961. Variations of pH with depth in anthracite mine-water pools in Pennsylvania: US Geological Survey Prof. In: *Synopsis of Geologic and Hydrologic Results*. Washington Geologic Survey Research:B82-B84

TAYLOR, G.I. 1931. Effect of variation in density on the stability of superposed streams of fluid. *Proc. R. soc. Lond. Ser. A-Contain. Pap. Math. Phys. Character,* 132(820):499-523. https://doi.org/10.1098/rspa.1931.0115

UERPMANN, E.P. 1980. Hydrogeologische Fragen bei der Endlagerung radioaktiver Abfälle. (Doctoral dissertation., Ges. für Strahlen- u. Umweltforschung)

V. HÜNEFELD-MUGOVA, E. & WOLKERSDORFER, C. 2018. A Review of Mine Water Stratification. In: Meier, G., Benndorf, J., Löbel, K.-H., Butscher, C., Tondera, D., Busch, W., Dziurzynski, W. & Sroka, A. (eds.). *18. Altbergbau-Kolloquium – Tagungsband.* Wagner:125-132

WIEBER, G., STEMKE, M., WONIK, T., ENZMANN, F. & KERSTEN, M. 2019. Stratification dynamics and geothermal potential of a deep shaft in the flooded Wolf Mine, Siegerland/Germany. *Mine Water Environ.,* 38(2):325-334. https://doi.org/10.1007/s10230-019-00602-8

WOLKERSDORFER, C. 1996. Hydrogeochemical investigations of an abandoned uranium mine in the Erzgebirge/Germany. *J. Appl. Geochem.,* 11(1):237-241. https://doi.org/10.1016/0883-2927(95)00060-7

WOLKERSDORFER, C. 2001. Tracer Tests in flooded underground mines. *New Approaches Characterizing Groundwater Flow. Proceedings of the 31st International Association of Hydrogeologists Congress 10-14 September 2001, Munich, Germany.*229-233

WOLKERSDORFER, C. 2008. *Water Management at Abandoned Flooded Underground Mines – Fundamentals, Tracer Tests, Modelling, Water Treatment.* Heidelberg: Springer. https://doi.org/10.1007/978-3-540-77331-3

WOLKERSDORFER, C. & HASCHE, A. 2001. Tracer test in the abandoned fluorspar mine Straßberg/Harz Mountains, Germany. *Wissensch Mitt,* 16:57-67

WOLKERSDORFER, C., KOMISCHKE, H., PESTER, S. & HASCHE-BERGER, A. 2013. Hydrodynamics in a flooded underground limestone mine. In: Brown, A., Figueroa, L. & Wolkersdorfer, C. (eds.). *Reliable Mine Water Technology*. International Mine Water Association:1165-1172

WOLKERSDORFER, C. & MERKEL, B.J. 2005. The flooded Freiberg/Sachsen Mining District – Hydrogeochemistry, Hydrodynamics and Environmental Impacts. In: Loredo, J. & Pendás, F. (eds.). *Mine Water 2005 – Mine Closure.* University of Oviedo:185-187

WOLKERSDORFER, C., SHONGWE, L. & SCHMIDT, C. 2016. Can natural Stratification prevent Pollution by Acid Mine Drainage? In: Drebenstedt, C. & Paul, M. (eds.). *International Mine Water Association 2016 Mining Meets Water Conflicts and Solutions*. Freiberg: TU Bergakademie Freiberg:115-121

YOUNGER, P. 1997. The Longevity of Mine Water Pollution–A Basis for Decision Making. *Sci. Total Environ.,* 24(194-195):457-466. https://doi.org/10.1016/s0048-9697(96)05383-1

YOUNGER, P. 2002. Coalfield closure and the water environment in Europe. *Int. J. Min. Sci Technol.,* 111(3):201-209. https://doi.org/10.1179/mnt.2002.111.3.201

YOUNGER, P.L. 2000a. Nature and practical implications of heterogeneities in the geochemistry of zinc-rich, alkaline mine waters in an underground F–Pb mine in the UK. *J. Appl. Geochem.,* 15(9):1383-1397. https://doi.org/10.1016/S0883-2927(00)00010-X

YOUNGER, P.L. 2000b. Predicting temporal changes in total iron concentrations in groundwaters flowing from abandoned deep mines: a first approximation. *J. Contam. Hydrol.,* 44(1):47-69. https://doi.org/10.1016/S0169-7722(00)00090-5

ZALDÍVAR, J., CANO, J., ALÓS, M., SEMPERE, J., NOMEN, R., LISTER, D., MASCHIO, G., OBERTOPP, T., GILLES, E. & BOSCH, J. 2003. A general criterion to define runaway limits in chemical reactors. *J. Loss Prev. Process Ind.,* 16(3):187-200. https://doi.org/10.1016/S0950-4230(03)00003-2

ZEMAN, J., ŠUPÍKOVÁ, I. & ČERNÍK, M. 2008. Mine Water Stratification at Abandoned Mines and its Geochemical Model. In: *Proceedings of the 10th International Mine Water Association Congress 2008, Karlsbad, Czech Republic*.2-5

ŽITTNAN, P., RAVINGER, R. & KOVÁC, L. 1990. Radioaktive Tracer-Meßgeräte und ihre Anwendung unter extremen Bedingungen. *Freiberger Forsch.-H.,* C 442:97-104